

# Modeling of Coolant Leakage in Two-Phase Cooling Systems within the CMS Experiment

MSc Thesis

Daniel Balbuena Silvestre



# Modeling of Coolant Leakage in Two-Phase Cooling Systems within the CMS Experiment

by

Daniel Balbuena Silvestre

to attain the degree of Master of Science in Aerospace Engineering  
at the Delft University of Technology,  
to be defended publicly on Friday 27 September 2024 at 12:00 h.

Student number:	5723701	
Project duration:	January 22, 2024 – September 27, 2024	
TU Delft supervisor:	Dr. Alessandra Menicucci	
CERN supervisor:	Ir. Francesco Dragoni	
Thesis committee:	Dr. A. Cervone,	TU Delft, Chairman
	Dr. A. Menicucci,	TU Delft, Supervisor
	Dr. D. Modesti,	TU Delft, External
	Ir. F. Dragoni,	CERN, supervisor

Cover: CMS gets a "heart transplant" - The pixel detector.  
By Maximilien Brice (CERN)

An electronic version of this thesis is available at <http://repository.tudelft.nl/>.





# Preface

With this work, I finish my stage as a master student in Aerospace Engineering at the Technical University of Delft, becoming an Engineer, after a path full of adventures, opportunities, decisions and above all, big changes. Having gone through 5 countries and 5 cities during my higher education, I can only be grateful for having been able to live an experience as unique and enriching as this one. This master's degree will undoubtedly be marked by the incredible people I met along the way, who have affected my way of understanding, as well as by the opportunity I have had to experience a long research stay at CERN.

CERN is far from what is expected in the field of aerospace engineering. This worried me from the beginning. However, today I can say that I was not wrong to take advantage of this opportunity. CERN, located on the French-Swiss border, is a world center of cutting-edge technology, and operates the largest physics laboratory we have ever known.

My stay has made me realize that, through scientific and engineering collaboration in multiple disciplines, excellent technological achievements can be made, not only for research, but also for the improvement of everyday life.

In this sense, I would like to thank all the EN-CV team and the CFD team for their warm welcome, especially Francesco for his tireless supervision and teachings, as well as Íñigo and Levente for so many conversations and advice in the office.

I would also like to thank Alessandra, for her unconditional support since the first thesis proposal, when the ideas were not yet clear, and for her help in guiding what is now my final master thesis. In Delft, I will never forget my Spanish family from the Spaceflight track, nor the many philosophical conversations with Marc (to PhD or not to PhD), at any time of the day or night.

Of course I have fallen short, as many more people have marked these last two years. I would like to extend thanks to all those with whom I had the pleasure of conversing both at CERN and in Delft. You can be sure that, if I had the possibility to talk to you, I learned something from you, which is written today in this thesis.

I would also like to thank my other small families, both in Munich and in Madrid, for being so often an inspiration. You are also in this thesis.

Back home in Benalmádena, there is not a day that goes by that I do not think of you: Álvaro, Enrique, Joan and Miguel. You are the friends that anyone would dream of having, I admire you.

And finally, to my family, who even though it has not been the easiest year, have supported me from day one, unconditionally, to follow my own path, since I decided to leave home, 6 years ago. If I am here today, it is thanks to you. And Ainhoa, for daring to take a leap of faith of an unimaginable caliber.

This chapter is closed, although the story has only just begun.

*Daniel Balbuena Silvestre  
Geneva, August 2024*



# Summary

The management of toxic leaks in confined environments, such as the experimental caverns present at CERN, or future space habitats, is a subject of imperative analysis, due to the ability to drastically threaten the lives of workers, visitors or inhabitants.

In this thesis, an exhaustive study is made of different cases of aggressive carbon dioxide releases, coming from the two-phase cooling system patented at CERN and currently used in numerous experiments both terrestrial (CMS, ATLAS, LHCb) and extraterrestrial (AMS).

This system, the 2PACL (2-Phase Accumulator Controlled Loop), presents different failure cases that have been previously studied by the CMS and ATLAS Safety teams, as well as by the Detector Technology section, within the Experimental Physics department at CERN.

To assess the severity of the different failure modes, computational fluid dynamics (CFD) simulations were performed using the CERN supercomputing cluster, modeling the different thermal and air quality control systems present in the cavern.

First, the study involved a two-dimensional analysis at the immediate location of the failure point (section 5.1). Here, the leak is extremely aggressive, producing a shock expansion due to the cryogenic conditions of the carbon dioxide prior to its release. Through this analysis, it is concluded that the shock wave travels, in the worst case, about 30 centimeters from the point of failure. This study, in general, remains valid for the different types of leakage of the 2PACL system regardless of the experiment or detector. In addition, this study allows to obtain the behavior of the leakage beyond the shock wave, conditions that will be the starting point for the three-dimensional simulations to be conducted in the experimental cavern of the CMS detector.

After the two-dimensional study, a matrix of the different failure cases and their strategic positions was designed hand in hand with CMS Safety team for the correct assessment of the threats. Subsequently, the 3D model of the CMS experimental cavern (UXC55) was developed and different simplifications were analyzed to facilitate the meshing and numerical resolution of the CFD equations (section 5.2). Finally, CFD simulations were carried out, studying the different cases that were detailed.

It is concluded that the cases relating to the main part of the cavern (floors X1 to X5) present an excellent protection against this type of leakage, mainly due to the ventilation system used in the cavern, as well as the large number of evacuation pathways. However, the cases related to the lower part of the cavern (floors X0 and X0.5), due to their semi-confined situation in the basement of the cavern, present a high danger for any worker in the area. Specific safety measures are presented, concerning the use of oxygen deficiency monitoring devices as well as the use of self-rescue masks and the exhaustive knowledge of the different evacuation plans.



# Contents

<b>Preface</b>	<b>iii</b>
<b>Summary</b>	<b>v</b>
<b>Nomenclature</b>	<b>xv</b>
<b>1 Introduction</b>	<b>1</b>
1.1 Context and Background	1
1.2 Problem Statement	1
1.3 Research Objectives	5
1.4 Significance of the Study	5
<b>2 Literature Review</b>	<b>7</b>
2.1 Two-phase Cooling Systems	7
2.1.1 Fundamentals and Principles	7
2.1.2 The 2PACL System at CERN	7
2.1.3 Technological Developments	7
2.1.4 Applications in High-Energy Physics	8
2.2 Leakage Risks and Their Impacts	8
2.2.1 Incidence and Causes	8
2.2.2 Consequences of Leakages	8
2.2.3 Mitigation Strategies	8
2.3 CFD Simulations in Leakage Analysis	9
2.3.1 CFD Studies on Coolant Leakages	9
2.3.2 Gaps in Current Research	9
2.4 Two-phase Cooling in Space Applications	9
2.4.1 Adaptation of Two-Phase Cooling for Space	9
2.4.2 Research Needs and Opportunities	9
2.5 Summary and Research Gap Identification	10
<b>3 Research Questions and Hypotheses</b>	<b>11</b>
<b>4 Methodology</b>	<b>15</b>
4.1 Overview of the CFD Simulation Process	15
4.1.1 Navier-Stokes equations	15
4.1.2 RANS equations for a mixture of species	16
4.1.3 Closure of the RANS equations	16
4.2 2D Simulation of Shock Expansion	16
4.3 3D Transient Simulation	17
4.4 Data Analysis Plan	17
4.5 Verification and Validation Framework	17
4.5.1 Verification	17
4.5.2 Validation	17
<b>5 Results</b>	<b>19</b>
5.1 Shock expansion behavior	19
5.1.1 Geometry, discretization and setup	19
5.1.2 Case 1: Maintenance	20
5.1.3 Case 2: Overpressure	24
5.1.4 Case 3: Fitting leak	31
5.2 CMS experimental cavern 3D model	35
5.2.1 Simplification of the geometry	35
5.2.2 Complete 3D CAD model	36
5.2.3 Summary of simulation cases	38
5.2.4 Discretization of the 3D model	38
5.3 Results of the 3D CFD simulations	39
5.3.1 2D profiles adapted to the 3D simulations	39

---

5.3.2	Sim. 1: Fitting leak at Vacuum Tank . . . . .	44
5.3.3	Sim. 2: Cold overpressure at X5 . . . . .	44
5.3.4	Sim. 3: Warm overpressure at X0 . . . . .	47
5.3.5	Sim. 4: Warm overpressure at X0.5 . . . . .	51
5.3.6	Sim. 5: Maintenance at X0 . . . . .	54
<b>6</b>	<b>Discussion</b>	<b>57</b>
6.1	Recommendations and Future Work . . . . .	58
	<b>References</b>	<b>61</b>
<b>A</b>	<b>Source Code User-Defined Functions</b>	<b>63</b>

# List of Figures

1.1	Schematic of the CERN accelerator complex. The starting point for proton-proton collisions (pp) are hydrogen ions being accelerated at LINAC 4 (Linear Accelerator 4). Subsequently, the Booster, PS (Proton Synchrotron) and SPS (Super PS) increase the energy of the particles up to the point when they can be injected into the LHC (Large Hadron Collider). On the way to LHC, proton bunches get diverted from the LHC beam to the multitude of experiments at lower energies being carried out at different experimental points in the complex. Credits: CERN. . . . .	2
1.2	Photography of the cavern that hosts the CMS experiment, named UXC55 (Underground eXperimental Cavern 55) in CERN documents. There are 5 different levels in the cavern, plus 2 smaller underground floors under the detector. Besides, a service cavern contains necessary machinery for the proper functioning of the detector. Credits: Maximilien Brice, CERN. . . . .	3
1.3	The Integrated 2-Phase Accumulator Controlled Loop (2PACL) is a modification of the existing 2PACL system developed for the AMS-Tracker and LHCb-VELO CO <sub>2</sub> cooling systems. The integrated 2PACL method is a different way of operating and control the original 2PACL concept (Here the accumulator cooling is integrated with the internal heat exchanger. The only remaining control of the system is a simple heater control in the accumulator). The modification makes the system simpler, more reliable, better to control and cheaper. Credits: CERN. . . . .	4
5.1	Geometry, discretization and setup for the 2D local simulations in the leak point vicinity. . . . .	20
5.2	Maintenance case: Output profiles of axial velocity, temperature and carbon dioxide mass fraction for the five different discretizations of the geometry used in the grid independence study. M1, the finest mesh, shows numerical error, specially noticeable when looking at the macroscopic behavior. M2 to M5 show a very similar behavior in terms of output profiles for the 3D simulation. . . . .	21
5.3	Contours of axial velocity, temperature and carbon dioxide mass fraction computed using mesh M5 in the maintenance leakage situation. . . . .	22
5.4	Profiles extracted for the 3D simulation as equivalently representing initial conditions proposed by CMS safety team in the maintenance leakage situation. Conditions are verified being within 1% margin of the mass-flow condition given. . . . .	23
5.5	Warm overpressure case: Output profiles of axial velocity, temperature and carbon dioxide mass fraction for the five different discretizations of the geometry used in the grid independence study. M1, the finest mesh, shows numerical error, specially noticeable when looking at the macroscopic behavior. M4 and M5, the courser meshes, cannot properly resolve the 2D inlet as they used equal or less than 10 cells on the characteristic dimension. M2 and M3 show a very similar behavior in terms of output profiles for the 3D simulation. . . . .	25
5.6	Contours of axial velocity, temperature and carbon dioxide mass fraction computed using mesh M3 in the warm overpressure leakage situation. . . . .	26
5.7	Profiles extracted for the 3D simulation as equivalently representing initial conditions proposed by CMS safety team in the warm overpressure leakage situation. Conditions are verified being within 1% margin of the mass-flow condition given. . . . .	27
5.8	Cold overpressure case: Output profiles of axial velocity, temperature and carbon dioxide mass fraction for the five different discretizations of the geometry used in the grid independence study. M1, the finest mesh, shows numerical error, specially noticeable when looking at the macroscopic behavior. M4 and M5, the courser meshes, cannot properly resolve the 2D inlet as they used equal or less than 10 cells on the characteristic dimension. M2 and M3 show a very similar behavior in terms of output profiles for the 3D simulation. . . . .	28
5.9	Contours of axial velocity, temperature and carbon dioxide mass fraction computed using mesh M3 in the cold overpressure leakage situation. . . . .	29
5.10	Profiles extracted for the 3D simulation as equivalently representing initial conditions proposed by CMS safety team in the cold overpressure leakage situation. Conditions are verified being within 1% margin of the mass-flow condition given. . . . .	30
5.11	Geometry, discretization and setup for the 2D local simulations in the leak point vicinity for the case of the fitting leak. . . . .	31

5.12 Fitting leak case: Output profiles of axial velocity, temperature and carbon dioxide mass fraction for the five different discretizations of the geometry used in the grid independence study. Every mesh resolves the 2D inlet, with the two finer meshes, M0.2 and M0.4 leading to numerical instabilities. M1.0 to M0.6 show a similar behavior in terms of output profiles for the 3D simulation.	32
5.13 Contours of axial velocity, temperature and carbon dioxide mass fraction computed using mesh M1 in the fitting leak leakage situation.	33
5.14 Profiles extracted for the 3D simulation as equivalently representing initial conditions proposed by CMS safety team in the cold overpressure leakage situation. Conditions are verified being within 1% margin of the mass-flow condition given.	34
5.15 Major geometry simplifications on the CMS experimental cavern.	35
5.16 Complete 3D CAD geometrical models of the CMS experimental cavern, separating the X0 and X0.5 floors (beneath the detector) from the main UXC55 model.	36
5.17 Boundaries configuration on the underground floors model, floors X0 and X0.5.	37
5.18 Boundaries configuration on the experimental cavern, floors X1 to X5.	37
5.19 Boundaries configuration for the fitting leak leakage scenario.	37
5.20 Discretization of the 3D CAD model using ANSYS Meshing applied to the main area of the experimental cavern.	38
5.21 Discretization of the 3D CAD model using ANSYS Meshing applied to the basement of the experimental cavern.	39
5.22 Fitted 2D profiles via minimum squared method for the fitting leak case.	40
5.23 Fitted 2D profiles via minimum squared method for the cold overpressure case.	41
5.24 Fitted 2D profiles via minimum squared method for the warm overpressure case.	42
5.25 Fitted 2D profiles via minimum squared method for the maintenance case.	43
5.26 Contour of carbon dioxide concentration in the vicinity of the vacuum tank of CMS in its open configuration (fitting leak case). There is no threat to workers in the cavern, with the leakage spreading about a meter from the leakage point.	44
5.27 Carbon dioxide concentration contour in the CMS underground cavern: 1 s after the leak is initiated (cold overpressure case). Plume reaches about 2 meters height.	45
5.28 Carbon dioxide concentration contour in the CMS underground cavern: 5 s after the leak is initiated (cold overpressure case). Plume spreads up to ceiling of the cavern.	45
5.29 Carbon dioxide concentration contour in the CMS underground cavern: Steady-state behavior after the leak is initiated (cold overpressure case). Plume is spread up to ceiling of the cavern.	46
5.30 Carbon dioxide concentration contour in the CMS underground cavern: 1 s after the closure of the leak point (142 s) (cold overpressure case). Vicinity of the leak point is quickly dissipated.	46
5.31 Carbon dioxide concentration contour in the CMS underground cavern: 5 s after the closure of the leak point (146 s) (cold overpressure case). Carbon dioxide has been appropriately dissipated from the cavern thanks to the ventilation system.	46
5.32 Contour of carbon dioxide concentration in the underground floors of the CMS cavern (X0 and X0.5): 5 s after the leak is initiated in the X0 floor (warm overpressure case). Carbon dioxide spreads over the central space.	48
5.33 Contour of carbon dioxide concentration in the underground floors of the CMS cavern (X0 and X0.5): 30 s after the leak is initiated in the X0 floor (warm overpressure case). Carbon dioxide is fully spread over the central space.	48
5.34 Contour of carbon dioxide concentration in the underground floors of the CMS cavern (X0 and X0.5): 1 s after the leak is closed in the X0 floor (warm overpressure case). Worst event, carbon dioxide reaches life-threatening concentrations in the entire central area.	49
5.35 Contour of carbon dioxide concentration in the underground floors of the CMS cavern (X0 and X0.5): 30 s after the leak is closed in the X0 floor (warm overpressure case). Carbon dioxide has dissipated but the concentrations remain dangerous.	49
5.36 Contour of carbon dioxide concentration in the underground floors of the CMS cavern (X0 and X0.5): 60 s after the leak is closed in the X0 floor (warm overpressure case). Carbon dioxide dissipation occurs at a low rate, the concentrations remain dangerous.	50
5.37 Contour of carbon dioxide concentration in the underground floors of the CMS cavern (X0 and X0.5): 5 s after the leak is initiated in the X0.5 floor (warm overpressure case). Carbon dioxide spreads over the central space.	51
5.38 Contour of carbon dioxide concentration in the underground floors of the CMS cavern (X0 and X0.5): 30 s after the leak is initiated in the X0.5 floor (warm overpressure case). Carbon dioxide is fully spread over the central space.	52
5.39 Contour of carbon dioxide concentration in the underground floors of the CMS cavern (X0 and X0.5): 1 s after the leak is closed in the X0.5 floor (warm overpressure case). Worst event, carbon dioxide reaches life-threatening concentrations in the entire central area.	52

---

5.40	Contour of carbon dioxide concentration in the underground floors of the CMS cavern (X0 and X0.5): 30 s after the leak is closed in the X0.5 floor (warm overpressure case). Carbon dioxide has dissipated but the concentrations remain dangerous. . . . .	53
5.41	Contour of carbon dioxide concentration in the underground floors of the CMS cavern (X0 and X0.5): 60 s after the leak is closed in the X0.5 floor (warm overpressure case). Carbon dioxide dissipation occurs at a low rate, the concentrations remain dangerous. . . . .	53
5.42	Contour of carbon dioxide concentration in the underground floors of the CMS cavern (X0 and X0.5): 1 s after the leak is initiated in the X0 floor (maintenance case). Carbon dioxide aggressively spreads. . . . .	54
5.43	Contour of carbon dioxide concentration in the underground floors of the CMS cavern (X0 and X0.5): 3 s after the leak is initiated in the X0 floor (maintenance case). Carbon dioxide reaches its maximum spread. . . . .	55
5.44	Contour of carbon dioxide concentration in the underground floors of the CMS cavern (X0 and X0.5): 2 s after the leak is closed in the X0 floor (maintenance case). Concentrations diminish quickly from the peak event. . . . .	55
5.45	Contour of carbon dioxide concentration in the underground floors of the CMS cavern (X0 and X0.5): 10 s after the leak is closed in the X0 floor (maintenance case). Carbon dioxide has dissipated and the concentrations are less dangerous. . . . .	56
5.46	Contour of carbon dioxide concentration in the underground floors of the CMS cavern (X0 and X0.5): 30 s after the leak is closed in the X0 floor (maintenance case). Carbon dioxide is almost fully dissipated and there is no danger in the area. . . . .	56



# List of Tables

3.1	Research Questions Derived from High-Level Questions. . . . .	12
3.2	Research Questions and Corresponding Hypotheses. . . . .	13
5.1	Boundary conditions for the under-expanded choked flow in the maintenance leakage condition, as provided by CMS safety team. . . . .	20
5.2	Boundary conditions for the under-expanded choked flow in the warm overpressure leakage condition, as provided by CMS safety team. . . . .	24
5.3	Boundary conditions for the under-expanded choked flow in the cold overpressure leakage condition, as provided by CMS safety team. . . . .	24
5.4	Boundary conditions for the under-expanded choked flow in the fitting leak leakage condition, as provided by CMS safety team. . . . .	31
5.5	Coefficients defining the fitted porous-jump in the 2D plates resembling the grided platforms and baffles within the CMS experimental cavern. Thickness of the medium is taken as 1 mm. Error on pressure drop is kept within less than 1%. . . . .	36
5.6	Summary of the different cases to be resolved and their location and type of simulation. . . . .	38
6.1	Recommendations and future work to be performed on the line of this study. . . . .	59



# Nomenclature

## Abbreviations

Abbreviation	Definition
2PACL	2-Phase Accumulator Controlled Loop
ANSYS	Analysis System (Commercial Software)
AMS	Alpha Magnetic Spectrometer
ATLAS	A Toroidal LHC Apparatus
CAD	Computer Aided Design
CERN	European Organization for Nuclear Research
CFD	Computational Fluid Dynamics
CMS	Compact Muon Solenoid
GWP	Global Warming Potential
H	Hypothesis
HLQ	High Level Question
ISS	International Space Station
LHC	Large Hadron Collider
LHC-b	LHC-beauty
ODH	Oxygen Deficiency Hazard
PS	Proton Synchrotron
RQ	Research Question
RANS	Reynolds-Averaged Navier-Stokes
SPS	Super Proton Synchrotron
UDF	User-Defined Function
UNOOSA	United Nations Office for Outer Space Affairs

## Symbols

Symbol	Definition	Unit
$C_2$	Pressure-jump coefficient	[1/m]
$\dot{m}$	Mass flow	[kg/s]
$p$	Pressure	[Pa]
$T$	Temperature	[°C]
$V$	Velocity	[m/s]
$\alpha$	Face permeability	[m <sup>2</sup> ]
$\mu$	Laminar fluid viscosity	[Pa s]
$\rho$	Density	[kg/m <sup>3</sup> ]



# 1

## Introduction

The introductory chapter sets the stage for the entire thesis, providing the reader with a comprehensive background on the significance of two-phase cooling systems, particularly focusing on their critical application within the CMS experiment at CERN and potential implications for space habitats. It outlines the motivation behind exploring the dynamics of coolant leakage, the health and safety risks associated, and the broader relevance of these systems in space exploration. The chapter is structured into sections covering the context and background of the study, the problem statement highlighting the research's motivation, the objectives framing the study's goals, and the significance of the study, elucidating the expected contributions to the fields of thermal management in high-energy physics and space technology.

### 1.1. Context and Background

The Compact Muon Solenoid (CMS) experiment, hosted by the European Organization for Nuclear Research (CERN), represents a cornerstone in the field of particle physics. A schematic of CERN's accelerator complex is depicted in Figure 1.1. As one of the largest international scientific collaborations, its primary objective is to investigate a wide range of physics phenomena, including the search for the Higgs boson, extra dimensions, and particles that could make up dark matter. Central to the CMS experiment's success is its sophisticated detector system, designed to observe particles produced by the Large Hadron Collider's (LHC) high-energy proton-proton collisions. A photography of the CMS cavern (around 100 m under the ground level), is shown in Figure 1.2. Ensuring the operational integrity and efficiency of these detectors is paramount, necessitating advanced cooling solutions to manage the substantial heat generated during operation.

Among these solutions, the Two-Phase Accumulator Controlled Loop (2PACL) system plays a crucial role. The 2PACL system employs a two-phase cooling methodology, leveraging the latent heat of vaporization to efficiently remove heat from critical components. This method is particularly suited to the demanding environment of high-energy physics experiments due to its ability to provide high cooling capacity while maintaining precise temperature control across the detectors and electronic systems. A schematic of the loop is shown in Figure 1.3.

Two-phase cooling systems, characterized by their utilization of both liquid and vapor phases of a coolant to absorb and transport heat, offer significant advantages over traditional single-phase systems. These include enhanced thermal performance, reduced system size and weight due to higher heat transfer coefficients, and the ability to passively manage heat loads by exploiting the natural circulation of the coolant. Such features are not only vital for the CMS experiment but also hold potential for applications beyond particle physics, including space exploration missions where reliability, efficiency, and thermal management are of the utmost importance.

The application of two-phase cooling systems in space habitats, for example, could revolutionize thermal management solutions in extraterrestrial environments. The unique challenges of space, such as extreme temperature fluctuations, limited resources, and the necessity for systems to operate autonomously, demand innovative approaches to cooling. The study and optimization of systems like the 2PACL within the context of the CMS experiment thus provide valuable insights into their potential adaptability and resilience in space habitats, where they could support life-support systems, electronic equipment, and scientific instruments.

### 1.2. Problem Statement

The 2PACL system, integral to the operational efficiency of the CMS experiment, presents a unique set of challenges and concerns, particularly regarding the potential for coolant leakage. Such a leakage not only

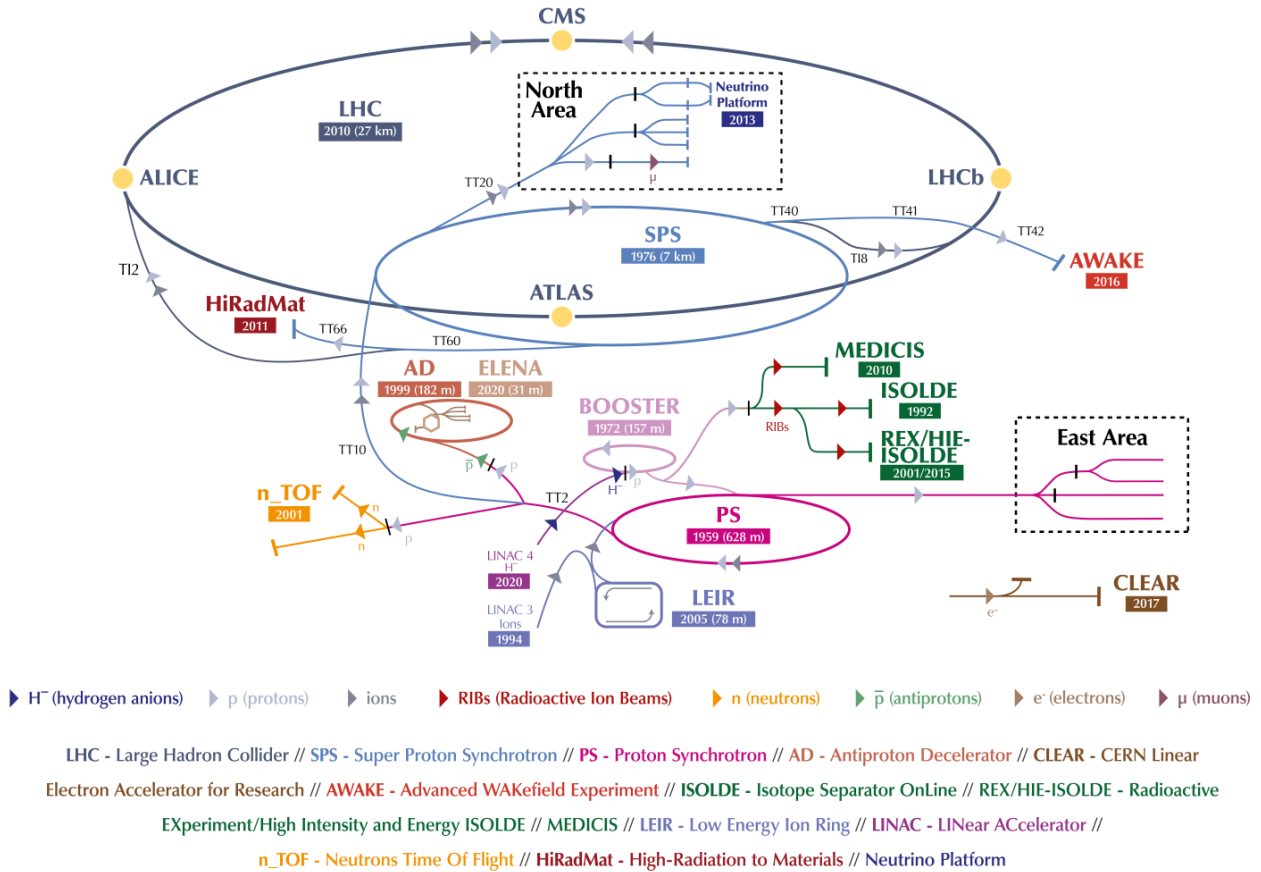


**Figure 1.1:** Schematic of the CERN accelerator complex. The starting point for proton-proton collisions (pp) are hydrogen ions being accelerated at LINAC 4 (Linear Accelerator 4). Subsequently, the Booster, PS (Proton Synchrotron) and SPS (Super PS) increase the energy of the particles up to the point when they can be injected into the LHC (Large Hadron Collider). On the way to LHC, proton bunches get diverted from the LHC beam to the multitude of experiments at lower energies being carried out at different experimental points in the complex. Credits: CERN.

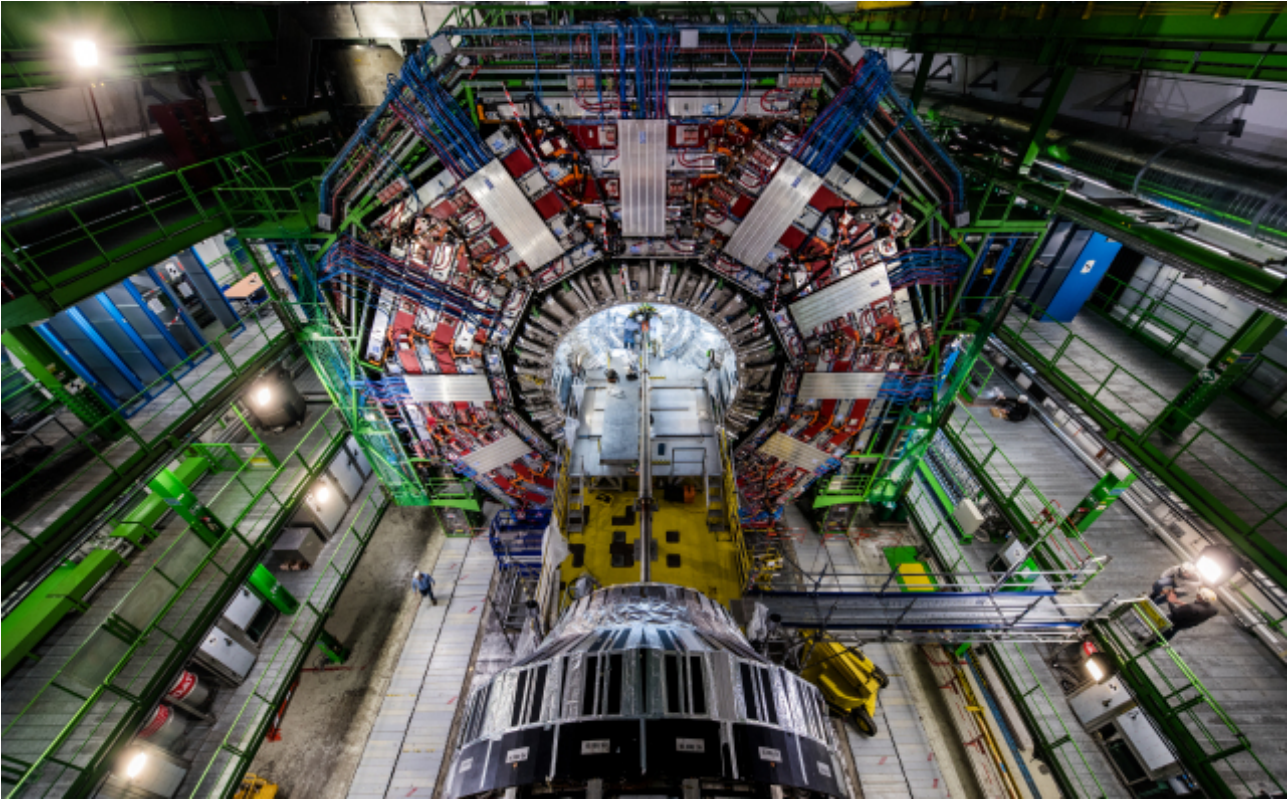


**Figure 1.2:** Photography of the cavern that hosts the CMS experiment, named UXC55 (Underground eXperimental Cavern 55) in CERN documents. There are 5 different levels in the cavern, plus 2 smaller underground floors under the detector. Besides, a service cavern contains necessary machinery for the proper functioning of the detector. Credits: Maximilien Brice, CERN.

poses a risk to the CMS detector's operational integrity but also carries significant health and safety implications for personnel and the environment surrounding the CERN facility. The critical nature of the CMS experiment, combined with the high-energy environment it operates within, amplifies the potential consequences of any leakage, making the mitigation and understanding of these risks a priority.

Coolant leakage in the 2PACL system can result from a variety of factors, including mechanical failure, system overpressure, or degradation of components over time. The escape of coolant, especially in a two-phase system, can lead to a rapid phase change and expansion, potentially causing a shock wave or explosive dispersion that could damage the CMS infrastructure or injure personnel. Furthermore, the release of certain coolants into the CMS cavern could introduce toxic or asphyxiating conditions, posing an immediate health risk to researchers and staff on-site.

The situation is compounded by the complexity and scale of the CMS experiment's infrastructure. The dense arrangement of detectors, electronics, and cooling systems within the CMS cavern makes it difficult to predict the precise behavior of leaked coolant, complicating efforts to design effective containment and ventilation strategies. Moreover, the potential for a leak to disrupt the experiment's data collection and processing capabilities raises concerns about the long-term impact on research outcomes and the experiment's overall scientific objectives.

In addition to the immediate risks associated with the CMS experiment, there is a broader concern regarding the application of two-phase cooling systems in space habitats. The extreme and isolated conditions of space exacerbate the consequences of a coolant leakage, where the failure of thermal management systems can jeopardize mission success and crew safety. The absence of a natural atmosphere for dispersal and the reliance on closed-loop life support systems in space habitats introduce unique challenges in managing and mitigating leakage risks. Understanding the behavior of two-phase cooling systems under such conditions is crucial for designing resilient and reliable thermal management solutions for future lunar or Martian habitats.

This research aims to address these gaps in knowledge and practice. Conducting comprehensive Computational Fluid Dynamics (CFD) simulations, the study will explore the dynamics of coolant leakage within the CMS cavern, assessing the effectiveness of current ventilation systems in mitigating health and safety risks.

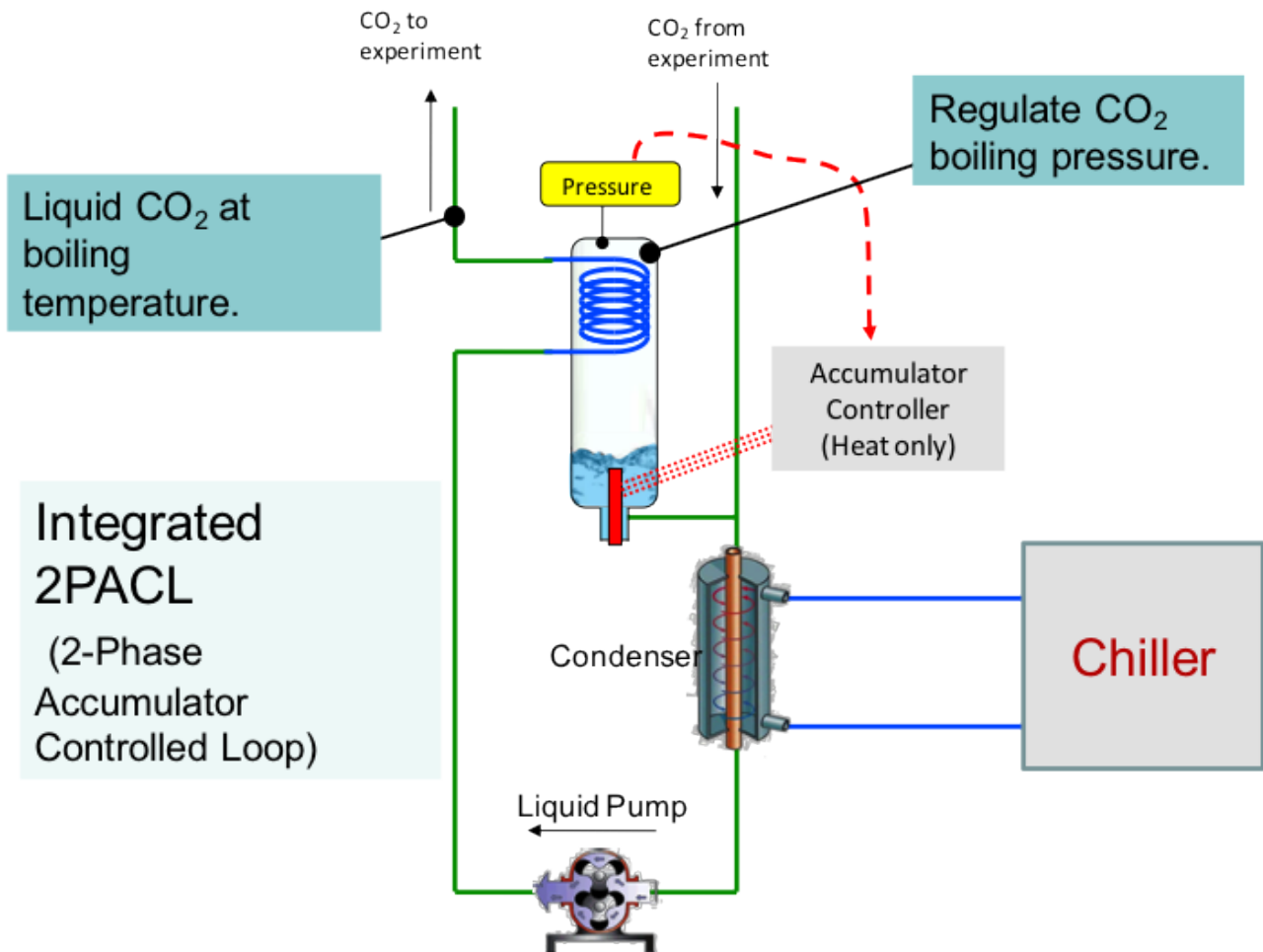


**Figure 1.3:** The Integrated 2-Phase Accumulator Controlled Loop (2PACL) is a modification of the existing 2PACL system developed for the AMS-Tracker and LHCb-VELO CO<sub>2</sub> cooling systems. The integrated 2PACL method is a different way of operating and control the original 2PACL concept (Here the accumulator cooling is integrated with the internal heat exchanger. The only remaining control of the system is a simple heater control in the accumulator). The modification makes the system simpler, more reliable, better to control and cheaper. Credits: CERN.

### 1.3. Research Objectives

The primary aim of this research is to conduct an in-depth analysis of the potential leakage scenarios within the 2PACL system at the CMS experiment and to evaluate the subsequent behavior of such leaks within the CMS cavern environment. This investigation is motivated by the need to enhance our understanding of the health and safety risks associated with coolant leakage and to assess the effectiveness of existing ventilation systems in mitigating these risks. Furthermore, the study seeks to extend the applicability of its findings to the design and safety considerations of two-phase cooling systems in space habitats, thereby contributing valuable insights to the field of thermal management in extraterrestrial environments. The specific research objectives are as follows:

- **To Model and Simulate the Initial Leakage and Shock Expansion:** Utilize CFD to create a detailed 2D simulation of the initial leakage event, focusing on the shock expansion phase. This simulation aims to capture the rapid phase change and expansion of the coolant upon leakage, providing a foundational understanding of the initial dynamics involved.
- **To Conduct a Comprehensive 3D CFD Simulation of the CMS Cavern:** Develop and execute a 3D transient CFD model of the entire CMS cavern, incorporating the initial conditions derived from the 2D shock expansion simulation. This model will simulate the dispersion of the leaked coolant within the cavern, evaluating the effectiveness of current ventilation systems in controlling the spread and concentration of potentially hazardous substances.
- **To Assess Health and Safety Risks:** Analyze the simulation data to identify areas within the CMS cavern that may present health and safety risks due to elevated concentrations of coolant or reduced oxygen levels. This objective includes evaluating the potential for toxic exposure or asphyxiation hazards to personnel within the cavern.
- **To Develop Recommendations for Mitigation and Design Improvements:** Based on the outcomes of the CFD simulations and theoretical analysis, provide recommendations for enhancing the safety and reliability of two-phase cooling systems. These recommendations will be applicable to both the CMS experiment and potential future applications in space habitats, focusing on improvements to system design, leakage detection, and emergency ventilation strategies.

### 1.4. Significance of the Study

This research holds significant implications across multiple domains, from enhancing the operational safety of high-energy physics experiments like the CMS at CERN, to advancing the reliability and safety of thermal management systems. The study's findings are poised to contribute valuable insights into the design, operation, and emergency response strategies associated with two-phase cooling systems. The significance of this study can be delineated across several key areas:

- **Enhancing Safety and Operational Integrity at CERN:** Providing a detailed analysis of coolant leakage scenarios within the CMS experiment, this research will directly contribute to improving the safety protocols and operational strategies of one of the world's leading particle physics research facilities. Understanding the dynamics of such leakages and their impact on the CMS cavern environment is crucial for minimizing health and safety risks to personnel, as well as for preventing disruptions to critical research activities.
- **Advancements in Thermal Management Systems for Particle Physics Experiments:** The study's focus on the 2PACL system and its behavior under leakage conditions will yield insights that are broadly applicable to the design and operation of cooling systems in similar high-energy physics experiments. The development of more reliable and safer two-phase cooling solutions will be instrumental in supporting the future progression of particle physics research, enabling experiments to operate at higher energies and with greater efficiency.
- **Informing Policy and Best Practices:** Beyond its academic contributions, the study's outcomes have the potential to inform policy and best practices related to safety and environmental management in research facilities and space habitats. Recommendations for system design improvements, leakage detection technologies, and emergency response protocols will be valuable resources for policymakers, facility managers, and design engineers seeking to mitigate the risks associated with two-phase cooling systems.



# 2

## Literature Review

In the literature review chapter, an extensive survey of existing research related to two-phase cooling systems, coolant leakage risks, and the application of Computational Fluid Dynamics (CFD) simulations in such contexts is presented. This chapter is organized into sections that discuss the principles and technological advancements in two-phase cooling systems, the risks and impacts associated with coolant leakages, the role of CFD simulations in understanding and mitigating these risks, and the specific challenges and opportunities in adapting these systems for space environments. It concludes with an analysis of the gaps in current research, setting the groundwork for the study's research questions and hypotheses.

### 2.1. Two-phase Cooling Systems

#### 2.1.1. Fundamentals and Principles

Two-phase cooling systems utilize the latent heat of vaporization to achieve highly efficient heat removal from hot surfaces. This process involves a working fluid absorbing heat and transitioning from a liquid to a vapor phase at a constant temperature. The efficiency of these systems is markedly superior to single-phase systems due to the significant amount of heat absorbed during the phase change, which occurs with minimal temperature increase in the fluid [1].

The cycle of a two-phase cooling system begins with the liquid coolant being pumped over hot components. Upon absorbing heat, the coolant evaporates, and this vapor is then transported to a condenser where it releases its heat and condenses back into a liquid. This liquid is recirculated back to the components, completing the cooling cycle. The design of the system, including the selection of coolant and the configuration of the heat exchanger and condenser, is critical for its efficiency and effectiveness.

#### 2.1.2. The 2PACL System at CERN

The Two-Phase Accumulator Controlled Loop (2PACL) system [2], a patented innovation by CERN, exemplifies the application of two-phase cooling in high-demand environments. The 2PACL system is distinguished by its inclusion of an accumulator, a key component that regulates the pressure within the cooling loop. This accumulator not only acts as a reservoir for the liquid and vapor phases of the coolant but also plays a crucial role in maintaining a stable operating pressure across varying heat loads. By absorbing pressure fluctuations, the accumulator ensures consistent cooling performance, an essential feature for applications requiring precise temperature control.

The uniqueness of the 2PACL system lies in its ability to provide efficient cooling while being compact and lightweight. The accumulator's design allows for the mitigation of the system's sensitivity to changes in heat load, making it particularly suitable for applications where space and weight are critical constraints. This system represents a significant advancement in two-phase cooling technology, demonstrating CERN's commitment to innovation in thermal management. A more technical explanation of the 2PACL system is given in [2].

#### 2.1.3. Technological Developments

Recent technological advancements in two-phase cooling systems have shown significant development in the context of space applications. In particular, recent studies highlight the suitability of pump-assisted two-phase flow cooling systems for future spacecraft thermal control systems [3]. Besides, the development of a two-phase flow cooling system for space systems under the Baridi-Sana Project, sponsored by the United Nations Office for Outer Space Affairs (UNOOSA), indicates a significant interest in utilizing two-phase cooling for the

miniaturization of space systems and satellites [4].

#### 2.1.4. Applications in High-Energy Physics

Originally developed for the Alpha Magnetic Spectrometer (AMS) onboard the International Space Station (ISS), the 2PACL system was designed to meet the stringent requirements for a thermal control device that was both compact and lightweight. The success of the 2PACL system in this application highlighted its potential for broader use in high-energy physics experiments.

Following its deployment in the AMS, the 2PACL system has been utilized in other major detectors, including CMS, ATLAS and LHC-b at CERN [5, 6]. These applications underscore the system's versatility and effectiveness in managing the thermal loads of complex experimental setups. The integration of two-phase cooling systems like the 2PACL in these environments not only enhances the performance and reliability of detectors but also contributes to the advancement of particle physics research by enabling experiments to operate at higher energies and with greater precision.

## 2.2. Leakage Risks and Their Impacts

### 2.2.1. Incidence and Causes

The operational reliability of two-phase cooling systems, while generally high, is occasionally threatened by the risk of coolant leakage. Such incidents can arise from a multitude of causes, including mechanical failure (e.g., wear and tear of components), system overpressure, manufacturing defects, and corrosion, among others [7, 8, 9, 10, 11, 12]. The complexity of these systems, especially in high-demand applications like high-energy physics experiments and space missions, exacerbates the risk, making the understanding and prevention of leaks a critical area of concern. The incidence of leakage not only disrupts the thermal management process but also poses significant safety and operational risks.

### 2.2.2. Consequences of Leakages

The potential consequences of coolant leakage in two-phase cooling systems extend far beyond the immediate disruption to cooling efficiency. Firstly, there is the risk of direct physical damage to the system's components, particularly in environments where the leaked coolant may come into contact with sensitive electronics or other vulnerable materials. Additionally, the sudden release of coolant can lead to rapid changes in pressure and temperature, potentially causing physical harm to personnel through exposure to toxic substances or extreme cold [13, 14, 7].

From a health and safety perspective, the leakage of certain coolants, depending on their chemical properties, may introduce toxic or flammable hazards into the workplace [15]. For instance, refrigerants commonly used in two-phase cooling systems can pose asphyxiation risks or contribute to fire hazards under certain conditions [16]. In confined spaces, such as the CMS cavern or space habitats, the rapid accumulation of leaked coolant could displace oxygen, creating an asphyxiation risk for individuals present [17]. Studies have demonstrated the severe poisonous effect of concentrations of carbon dioxide in human health, with values as low as 4% rapidly causing the loss of consciousness [18].

Moreover, the environmental impact of coolant leaks, particularly those involving substances with high global warming potential (GWP) or ozone-depleting characteristics, cannot be overlooked. The release of such substances into the atmosphere contributes to climate change and stratospheric ozone depletion, making the containment and prevention of leaks a concern of environmental stewardship as well [19, 20].

### 2.2.3. Mitigation Strategies

Efforts to mitigate the risks associated with coolant leakage in two-phase cooling systems encompass a range of strategies, from design improvements to operational protocols. At the design level, the incorporation of redundant safety features, such as double-walled tubing and leak detection sensors, can significantly reduce the risk of unintended coolant release. Material selection also plays a crucial role, with an emphasis on corrosion-resistant and durable components to withstand the rigors of operation in challenging environments.

Operational strategies include regular maintenance and inspection routines to identify and rectify potential weak points before failure occurs. Advanced monitoring systems, capable of real-time detection of pressure or temperature anomalies, offer an additional layer of safety, enabling swift response to prevent leaks from escalating into more serious incidents.

Training and preparedness are equally important, ensuring that personnel are equipped with the knowledge and tools to respond effectively to leakage events. This includes emergency response plans tailored to the specific hazards associated with the coolant used in the system, as well as drills to ensure that response protocols are well understood and can be executed efficiently.

## 2.3. CFD Simulations in Leakage Analysis

### 2.3.1. CFD Studies on Coolant Leakages

The application of CFD to study coolant leakages in two-phase cooling systems has yielded valuable insights into the mechanisms and consequences of such events. These studies typically involve the simulation of leak scenarios to assess the dispersion of coolant within a given environment, the impact on surrounding temperatures and pressures, and the effectiveness of containment and ventilation strategies [21]. For instance, CFD simulations can model the rapid expansion and phase change of coolant as it escapes from a system, predicting the resultant shock waves and their potential impact on nearby equipment and personnel [13].

CFD studies have also been instrumental in evaluating the performance of safety measures, such as leak detection systems and emergency ventilation, in mitigating the risks posed by coolant leaks. By simulating different leakage rates and locations, researchers can identify vulnerabilities in system design and operation that may not be apparent through traditional analysis methods. This includes assessing the distribution of leaked coolant in confined spaces, such as the CMS cavern or spacecraft modules, where inadequate ventilation can lead to hazardous concentrations of coolant accumulating.

### 2.3.2. Gaps in Current Research

Despite the advancements in CFD simulations for leakage analysis, several gaps remain in current research, particularly concerning specific applications and conditions. One such gap is the detailed simulation of shock expansion phenomena resulting from high-pressure coolant leaks in two-phase systems, a scenario that is critically relevant to high-energy physics experiments and space habitats. Additionally, the extrapolation of terrestrial CFD findings to the unique conditions of space—where microgravity and vacuum environments present entirely different fluid dynamics and heat transfer challenges—requires further exploration.

Another area where existing research could be expanded is in the integration of CFD simulations with real-world operational data from two-phase cooling systems. Such integration could enhance the predictive accuracy of simulations and provide more actionable insights for the design and management of these systems. Moreover, there is a need for more comprehensive studies on the environmental impact of coolant leaks, particularly those involving substances with significant global warming potential, to inform safer and more sustainable cooling solutions.

## 2.4. Two-phase Cooling in Space Applications

### 2.4.1. Adaptation of Two-Phase Cooling for Space

Two-phase cooling systems offer several advantages for space applications, primarily due to their high heat transfer efficiency and the ability to manage significant heat loads over long distances with minimal temperature drop. The latent heat of vaporization inherent in two-phase systems enables the removal of large amounts of heat with relatively small volumes of coolant, an essential feature for minimizing weight and space onboard spacecraft.

Research and development efforts have focused on adapting two-phase cooling technologies for space, overcoming challenges such as ensuring consistent fluid flow and phase change in microgravity [4, 22]. Innovations in system design, such as the use of capillary action in heat pipes and loop heat pipes, have shown promise in facilitating effective liquid-vapor phase cycling [23]. These systems have been successfully deployed in space missions such as AMS, demonstrating their viability for cooling high-power electronics, propulsion systems, and scientific instruments.

Furthermore, the integration of advanced materials and manufacturing techniques has led to the development of more efficient, lightweight, and durable two-phase cooling components. These advancements enhance the overall performance and reliability of space thermal management systems, contributing to the success of long-duration missions and the safety of crewed space habitats.

### 2.4.2. Research Needs and Opportunities

Despite the progress made in adapting two-phase cooling systems for space, several research needs and opportunities remain. A key area of focus is the optimization of system performance in microgravity and vacuum conditions, including the improvement of phase separation devices and the control of flow instabilities. Addressing these challenges requires innovative approaches to system design and an in-depth understanding of fluid dynamics and heat transfer in space environments.

Another significant research avenue is the exploration of environmentally benign coolants that can meet the stringent safety and performance requirements of space missions. The development of such coolants would mitigate potential risks to crew health and the environment, aligning with broader sustainability goals in space

exploration.

Moreover, the potential for two-phase cooling systems to support human habitation on the Moon, Mars, and beyond presents a compelling research opportunity. The ability of these systems to efficiently manage the thermal loads of life support, habitat conditioning, and scientific research facilities will be critical to the success of future crewed missions. Investigating the scalability, modularity, and integration of two-phase cooling technologies within the broader ecosystem of space habitat engineering will be essential in meeting the diverse and evolving thermal management needs of these endeavors.

## 2.5. Summary and Research Gap Identification

The literature review has systematically explored the fundamental principles, technological advancements, and diverse applications of two-phase cooling systems, highlighting their significance in high-energy physics experiments and space applications. Through this exploration, it became evident that two-phase cooling systems offer superior efficiency and performance compared to traditional cooling methods, particularly in managing high heat loads across various demanding environments. The review also delved into the risks associated with coolant leakage in these systems, outlining the potential operational, safety, and environmental impacts. CFD simulations emerged as a powerful tool for analyzing coolant leakages, offering insights into the dynamics of such events and informing mitigation strategies.

Despite the wealth of knowledge available, several critical gaps remain in the literature, particularly concerning the detailed analysis of leakage phenomena in two-phase cooling systems and the extrapolation of terrestrial findings to space environments. These gaps underscore the need for focused research efforts to advance the safety, reliability, and efficiency of two-phase cooling technologies.

The literature review has identified prominent research gaps that this study aims to address, specifically:

- **Detailed Leakage Dynamics:** There is a scarcity of research focusing on the detailed dynamics of coolant leakage in two-phase cooling systems, especially regarding the initial shock expansion phase and its implications for system integrity and safety. This gap highlights the need for comprehensive CFD simulations that can capture the complex fluid dynamics involved in leakage scenarios.
- **Effectiveness of Mitigation Strategies:** While existing studies discuss various mitigation strategies for coolant leakages, there is limited quantitative analysis on the effectiveness of these strategies in real-world scenarios. This gap calls for empirical research and advanced simulations to evaluate and optimize containment and ventilation solutions.

# 3

## Research Questions and Hypotheses

This chapter delineates the specific research questions derived from the identified gaps in the literature, segmented into four main areas: the dynamics of coolant leakage, the effectiveness of ventilation systems, and health & safety risks. First, Table 3.1 presents high-level questions from the main topics accompanied by more detailed, measurable questions aiming to focus the research. Then, Table 3.2 presents the corresponding hypotheses for each question, proposing expected outcomes based on the theoretical foundation laid in the previous chapters. This approach aims to clarify the research's direction and the basis for the subsequent methodology.

**Table 3.1:** Research Questions Derived from High-Level Questions.

Category	High-Level Questions (HLQs)	Research Questions (RQs)
<b>Leakage Dynamics in Two-Phase Cooling Systems</b>	<b>HLQ1:</b> What are the detailed dynamics of coolant leakage in a two-phase cooling system?	<p><b>RQ1:</b> How does the shock expansion phase manifest and what are the immediate physical effects on the surrounding environment?</p> <p><b>RQ2:</b> How do the initial conditions of leaked coolant correlate with the distance traveled by the vapor cloud within the first few seconds of a leakage event?</p> <p><b>RQ3:</b> What is the rate and pattern of coolant dispersion following a simulated leakage event?</p>
<b>Effectiveness of Ventilation Systems</b>	<b>HLQ2:</b> How effective are current ventilation systems in mitigating the dispersion of leaked coolant within the CMS cavern?	<p><b>RQ4:</b> What percentage of leaked coolant can be evacuated by the current ventilation system within X minutes after detection of a leak?</p> <p><b>RQ5:</b> How does the concentration of coolant in the air change spatially across the CMS cavern with the existing ventilation setup during a leak?</p> <p><b>RQ6:</b> How does the location and initial conditions of the leak influence the effectiveness of the ventilation?</p> <p><b>RQ7:</b> Which specific modifications to the CMS cavern's ventilation design can reduce the time required to disperse leaked coolant concentrations to safe levels?</p>
<b>Health and Safety Risks</b>	<b>HLQ3:</b> What specific health and safety risks are associated with coolant leakage in the CMS experiment's two-phase cooling system?	<p><b>RQ8:</b> What are the peak concentrations of toxic substances released during a coolant leak, and how do these concentrations compare to occupational safety thresholds?</p> <p><b>RQ9:</b> How quickly do hazardous conditions develop in terms of oxygen displacement and toxic substance accumulation in different locations within the CMS cavern?</p> <p><b>RQ10:</b> Which areas within the CMS cavern are most susceptible to health and safety risks due to coolant accumulation, and how do these areas correlate with human occupancy and sensitive equipment locations?</p> <p><b>RQ11:</b> What is the estimated time frame for safe evacuation of personnel from different locations within the CMS cavern following a coolant leak?</p>

**Table 3.2:** Research Questions and Corresponding Hypotheses.

<b>Research Question (RQ)</b>	<b>Hypothesis (H)</b>
<b>RQ1:</b> How does the shock expansion phase manifest and what are the immediate physical effects on the surrounding environment?	<b>H1:</b> The shock expansion phase will manifest as a rapid increase in local pressure and temperature, potentially causing structural stresses and thermal effects on nearby sensitive equipment.
<b>RQ2:</b> How do the initial conditions of leaked coolant correlate with the distance traveled by the vapor cloud within the first few seconds of a leakage event?	<b>H2:</b> The distance traveled by the vapor cloud in the initial seconds post-leakage is directly proportional to the mass-flow rate of leaked coolant, following a predictable pattern that can be modeled through CFD simulations.
<b>RQ3:</b> What is the rate and pattern of coolant dispersion following a simulated leakage event?	<b>H3:</b> Coolant dispersion rate and pattern will be influenced by the cavern's ventilation system design and the initial leak conditions.
<b>RQ4:</b> What percentage of leaked coolant can be evacuated by the current ventilation system within X minutes after detection of a leak?	<b>H4:</b> The current ventilation system can evacuate a significantly higher percentage of leaked coolant within the first minute, with diminishing efficiency observed in subsequent minutes due to airflow dynamics and system capacity limitations.
<b>RQ5:</b> How does the concentration of coolant in the air change spatially across the CMS cavern with the existing ventilation setup during a leak?	<b>H5:</b> Coolant concentration will vary spatially across the CMS cavern, with higher concentrations persisting in areas further from ventilation outlets due to inadequate airflow distribution.
<b>RQ6:</b> How does the location and initial conditions of the leak influence the effectiveness of the ventilation?	<b>H6:</b> The effectiveness of the ventilation system in mitigating coolant dispersion is significantly influenced by the leak's location and initial conditions, with leaks closer to ventilation outlets being more efficiently mitigated.
<b>RQ7:</b> Which specific modifications to the CMS cavern's ventilation design can reduce the time required to disperse leaked coolant concentrations to safe levels?	<b>H7:</b> Implementing targeted modifications, such as increasing airflow rates or optimizing air distribution pathways, can reduce the time required to disperse leaked coolant concentrations.
<b>RQ8:</b> What are the peak concentrations of toxic substances released during a coolant leak, and how do these concentrations compare to occupational safety thresholds?	<b>H8:</b> Peak concentrations of toxic substances during a coolant leak will exceed occupational safety thresholds, necessitating immediate evacuation and containment measures.
<b>RQ9:</b> How quickly do hazardous conditions develop in terms of oxygen displacement and toxic substance accumulation in various parts of the CMS cavern?	<b>H9:</b> Hazardous conditions due to oxygen displacement and toxic substance accumulation will develop within minutes in enclosed areas of the CMS cavern, posing immediate risks to personnel.
<b>RQ10:</b> Which areas within the CMS cavern are most susceptible to health and safety risks due to coolant accumulation, and how do these areas correlate with human occupancy and sensitive equipment locations?	<b>H10:</b> Areas with poor ventilation and high occupancy or sensitive equipment concentration will be most susceptible to health and safety risks, highlighting the need for strategic safety measures and evacuation planning.
<b>RQ11:</b> What is the estimated time frame for safe evacuation of personnel from different locations within the CMS cavern following a coolant leak?	<b>H11:</b> The estimated time frame for safe evacuation will vary significantly across different cavern locations, with areas closer to exits or well-ventilated spaces requiring less time for evacuation.



# 4

## Methodology

The methodology chapter details the approach employed to investigate the research questions, emphasizing the use of CFD simulations to model coolant leakage and its consequences. It is divided into sections that explain the overview of the CFD simulation process, the specifics of conducting 2D and 3D simulations, and the plan for data analysis. Additionally, the chapter addresses the expected challenges and limitations of the research methodology, setting realistic expectations for the study's outcomes.

### 4.1. Overview of the CFD Simulation Process

Computational Fluid Dynamics (CFD) is a numerical analysis tool used to simulate fluid flow, heat transfer, and associated phenomena. Its applicability to this research lies in its ability to model the complex interactions and dynamics of coolant leakage and dispersion within engineered environments, providing insights into both immediate and longer-term effects of such events.

For this study, ANSYS Fluent is selected due to its comprehensive modeling capabilities, which include advanced turbulence models, multiphase flow simulations, and user-friendly interface for complex geometries [24]. This choice is justified by ANSYS Fluent's proven track record in accurately simulating fluid dynamics and thermal phenomena in both academic and industrial applications. In particular, Fluent has been used in the literature to accurately simulate shock expansions and gas mixture dispersion, in similar situations to the problem at hand [13, 25, 14, 26, 27, 28]. Therefore, following best practice guidelines to select the appropriate models to resolve the equations will ensure high fidelity results.

#### 4.1.1. Navier-Stokes equations

The Navier-Stokes equations are the fundamental equations governing the motion of fluid flow, capturing the balance of forces acting on fluid elements. They are derived from Newton's second law applied to fluid motion, taking into account viscosity, pressure, and external forces. There are three fundamental equations that need to be coupled to a equation of state (such as ideal or real gas law for gases). Additionally, the continuity equation can be extended to account for species transport. The extended Navier-Stokes equations are presented in Equation 4.1.

$$\begin{aligned}\frac{\partial(\rho Y_k)}{\partial t} + \nabla \cdot (\rho Y_k \mathbf{u}) &= -\nabla \cdot \mathbf{J}_k + \dot{\omega}_k \\ \frac{\partial(\rho \mathbf{u})}{\partial t} + \nabla \cdot (\rho \mathbf{u} \otimes \mathbf{u}) &= -\nabla p + \nabla \cdot \boldsymbol{\tau} + \mathbf{f} \\ \text{with: } \boldsymbol{\tau} &= \mu (\nabla \mathbf{u} + (\nabla \mathbf{u})^T) - \frac{2}{3} \mu (\nabla \cdot \mathbf{u}) \mathbf{I} \\ \frac{\partial(\rho E)}{\partial t} + \nabla \cdot [\mathbf{u}(\rho E + p)] &= \nabla \cdot (\kappa \nabla T) + \Phi + \mathbf{u} \cdot \mathbf{f}\end{aligned}\tag{4.1}$$

Where  $\rho$  is the fluid density,  $Y_k$  is the mass fraction of species  $k$ ,  $\mathbf{J}_k$  is the diffusive flux of species  $k$ ,  $\dot{\omega}_k$  is the rate of production/depletion of a reactive species  $k$ ,  $\mathbf{u}$  is the velocity vector,  $p$  is the pressure,  $\boldsymbol{\tau}$  is the stress tensor accounting for viscous forces,  $\mathbf{f}$  are external body forces such as gravity,  $\mu$  is the dynamic viscosity,  $\mathbf{I}$  is the identity matrix,  $E$  is the total energy per unit mass,  $T$  is the temperature,  $\kappa$  is the thermal conductivity, and  $\Phi$  is the viscous dissipation term.

### 4.1.2. RANS equations for a mixture of species

The Navier-Stokes equations fully describe the dynamics of fluid flow, but for turbulent flows, they become extremely challenging to solve directly due to the wide range of scales involved. Turbulent flows are characterized by chaotic and random fluctuations in velocity, pressure, and other flow variables, requiring a very fine resolution in both space and time to capture all details.

To make the problem more tractable, the Reynolds-Averaged Navier-Stokes (RANS) approach is employed. The idea is to decompose the instantaneous flow variables into mean (time-averaged) and fluctuating components. By substituting these decompositions into the Navier-Stokes equations and averaging, the RANS equations are obtained, describing the time-averaged behavior of the flow variables, including velocity, pressure, temperature, and species concentration. The RANS equations are presented in Equation 4.2.

$$\begin{aligned}
\frac{\partial(\overline{\rho Y_k})}{\partial t} + \frac{\partial(\overline{\rho Y_k U_j})}{\partial x_j} &= \frac{\partial}{\partial x_j} \left( \overline{J_k} + \frac{\mu_t}{Sc_t} \frac{\partial \overline{Y_k}}{\partial x_j} \right) + \overline{\dot{\omega}_k} \\
\frac{\partial(\overline{\rho U_i})}{\partial t} + \frac{\partial(\overline{\rho U_i U_j})}{\partial x_j} &= -\frac{\partial \overline{p}}{\partial x_i} + \frac{\partial}{\partial x_j} \left[ \mu \left( \frac{\partial \overline{U_i}}{\partial x_j} + \frac{\partial \overline{U_j}}{\partial x_i} \right) - \overline{\rho u'_i u'_j} \right] + \overline{\rho f_i} \\
\text{with: } -\overline{\rho u'_i u'_j} &= \mu_t \left( \frac{\partial \overline{U_i}}{\partial x_j} + \frac{\partial \overline{U_j}}{\partial x_i} \right) - \frac{2}{3} \overline{\rho k} \delta_{ij} \\
\frac{\partial(\overline{\rho E})}{\partial t} + \frac{\partial(\overline{\rho E U_j})}{\partial x_j} &= \frac{\partial}{\partial x_j} \left[ \overline{U_i} \left( \mu_t \left( \frac{\partial \overline{U_i}}{\partial x_j} + \frac{\partial \overline{U_j}}{\partial x_i} \right) \right) - \overline{\rho u'_i u'_j} \right] + \frac{\partial}{\partial x_j} \left( \kappa_t \frac{\partial \overline{T}}{\partial x_j} \right) + \overline{\rho f_i U_i} + \Phi
\end{aligned} \tag{4.2}$$

Where the overline represents time-averaged values and  $\overline{u'_i u'_j}$  is the Reynolds stress tensor, representing the effect of turbulence,  $\mu_t$  is the turbulent viscosity,  $\kappa_t$  is the turbulent thermal conductivity, and  $Sc_t$  is the Schmidt turbulent number, quotient of turbulent viscosity and turbulent diffusivity.

### 4.1.3. Closure of the RANS equations

Turbulence significantly affects the flow characteristics, such as velocity, pressure, and heat transfer, by introducing complex, chaotic, and fluctuating patterns. For the purpose of this thesis, a  $k - \epsilon$  turbulence model is used, being one of the most widely used models for simulating turbulent flows in Computational Fluid Dynamics. It belongs to the class of Reynolds-Averaged Navier-Stokes (RANS) models and is used to approximate the effects of turbulence by introducing two additional transport equations—one for the turbulent kinetic energy  $k$  and one for the turbulent dissipation rate  $\epsilon$ . The equations of the model are presented in Equation 4.3.

$$\begin{aligned}
\frac{\partial k}{\partial t} + \overline{U_j} \frac{\partial k}{\partial x_j} &= \frac{\partial}{\partial x_j} \left[ \left( \nu + \frac{\nu_t}{\sigma_k} \right) \frac{\partial k}{\partial x_j} \right] + P_k - \epsilon \\
\frac{\partial \epsilon}{\partial t} + \overline{U_j} \frac{\partial \epsilon}{\partial x_j} &= \frac{\partial}{\partial x_j} \left[ \left( \nu + \frac{\nu_t}{\sigma_\epsilon} \right) \frac{\partial \epsilon}{\partial x_j} \right] + C_{1\epsilon} \frac{\epsilon}{k} P_k - C_{2\epsilon} \frac{\epsilon^2}{k} \\
\text{with: } \nu_t &= C_\mu \frac{k^2}{\epsilon}, \quad P_k = \nu_t \left( \frac{\partial \overline{U_i}}{\partial x_j} \frac{\partial \overline{U_i}}{\partial x_j} \right)
\end{aligned} \tag{4.3}$$

Where  $k$  is the turbulent kinetic energy,  $\epsilon$  is the turbulent dissipation rate,  $\nu_t$  is the turbulent viscosity, and  $P_k$  is the production of turbulent kinetic energy.

In this manner, the  $k - \epsilon$  model provides a way to calculate the turbulent viscosity, which is used to model the Reynolds stresses and close the RANS equations, in conjunction with simpler models for the turbulent diffusion and the turbulent thermal conductivity.

## 4.2. 2D Simulation of Shock Expansion

The initial 2D simulation focuses on the shock expansion phase immediately following a coolant leak. The model setup includes defining the physical properties of the coolant (e.g., density, viscosity, and phase change characteristics) and creating a simplified geometry to represent the leak source and immediate surroundings. The fluids involved will be treated as real gases due to the presence in the flow of very high gradients in pressure, temperature, velocity and density.

Key parameters such as mesh size, time step, and convergence criteria are selected based on preliminary sensitivity analyses to ensure the simulation's accuracy and computational efficiency. A fine mesh is employed in areas expected to experience rapid changes in fluid properties, ensuring detailed capture of the shock expansion phenomena.

The 2D simulation is expected to elucidate the initial expansion velocity of the coolant vapor, pressure waves generated by the rapid phase change, and initial dispersion patterns. These outcomes will inform the development of mitigation strategies and guide the setup of the more comprehensive 3D simulations.

### 4.3. 3D Transient Simulation

Building on the 2D simulation results, a 3D model of the CMS cavern is developed. This model incorporates the cavern's geometry, including ventilation systems, obstacles, and equipment, to simulate the dispersion of coolant in a more realistic environment. In this case, the conditions after the shock expansion are milder, and now an ideal gas model can be used to accurately represent the behavior of the flow.

The 3D model accurately represents the CMS cavern's physical layout and environmental conditions. Ventilation system representations include inlet and outlet positions and capacities, reflecting the current ventilation design and potential modifications for analysis.

Various leak scenarios, including different locations, volumes, and rates of coolant release, are simulated to assess the ventilation system's effectiveness. Scenarios are chosen based on likely failure points and historical data on system vulnerabilities.

The analysis focuses on identifying dispersion patterns, areas of high coolant concentration, and the effectiveness of the ventilation system under different scenarios. The outcomes will inform the design of improved safety measures and emergency response strategies.

### 4.4. Data Analysis Plan

Statistical methods, including regression analysis and variance analysis, are used to quantify the relationships between leak parameters and dispersion outcomes. Data analysis is performed using Python, leveraging libraries such as NumPy and pandas for data manipulation and SciPy for statistical analysis, as well as the ANSYS software provided for post-processing purposes, CFD-Post.

Qualitative assessments are made regarding the effectiveness of ventilation modifications and their potential applicability to space habitats. This includes evaluating the feasibility and potential impact of design changes based on simulation results and existing engineering practices.

A risk analysis framework is applied to quantify health and safety risks, using simulation data to model exposure scenarios and compare them against occupational safety standards. This analysis helps prioritize mitigation strategies based on their potential to reduce risk.

### 4.5. Verification and Validation Framework

A verification and validation plan is mandatory to ensure that the computational models used and the assumptions made, accurately represent the physical phenomena at hand. Therefore, a verification and validation plan has been developed. The time and resources constraints on this project are acknowledged however, leaving steps of the validation process as future work that could address these areas.

#### 4.5.1. Verification

The goal of the verification process is to ensure that the CFD tool correctly solves the governing equations. It contains two main areas:

- Code Verification: Correctness of the numerical algorithms and their implementation in the software. Already performed by the software vendor (ANSYS).
- Solution Verification: Ensure that the mesh is adequately refined, and numerical errors like discretization, convergence, and round-off errors are minimized. For this purpose, a grid independence study will be conducted.

#### 4.5.2. Validation

The goal of the validation process is to ensure that the CFD model accurately represents the physical reality. Given the complexity of the geometries and phenomena, benchmarking against analytical solutions is difficult. Performing comparative studies is complex as well, as the CMS cavern results in a unique environment with very few analogues. Thus, the best way of validating the CFD results is the comparison with experimental data from experiments performed in the CMS cavern.

Validation will be left for future work, as performing experiments of this caliber in the underground experimental cavern is extremely restricted. It could only be performed when the beam is off. However, when the beam is off, maintenance takes places, therefore being hazardous to perform such experiments with toxic gas releases.

A scaled model could be constructed to solve this problem and perform validation studies expending lower resources.

# 5

## Results

In this chapter, the main results obtained through the proposed methodology are presented. On the first section, the shock expansion produced after the opening of the leakage point on the carbon dioxide saturated cooling line is studied for each leakage condition. Leakage conditions are provided directly from the CMS safety team. On the second section, the 3D model of the experimental cavern for its use in the final CFD simulations is presented along its boundary conditions related to thermal and air management. After that, a summary of the different simulations to be performed is given. Just before analyzing, the mesh discretization is proposed. Finally, on section three, the results of each and every case is presented independently.

The CMS safety team, in collaboration with the detector technologies section from the experimental physics department studied the possible failure cases of the 2PACL system, arriving to the conclusion that there are only three types of leakage that can occur. Therefore, these are the cases to be studied in the following simulations:

- Fitting leak: Extremely small leak occurring on the vacuum tank due to bad fitting.
- Maintenance leak: Leak that occurs due to accidental manipulation of a worker.
- Overpressure leak: Leak due to overpressure in the cryogenic lines, it can be of two types:
  - Warm overpressure: Occurring on the warmer pipe.
  - Cold overpressure: Occurring on the colder pipe.

### 5.1. Shock expansion behavior

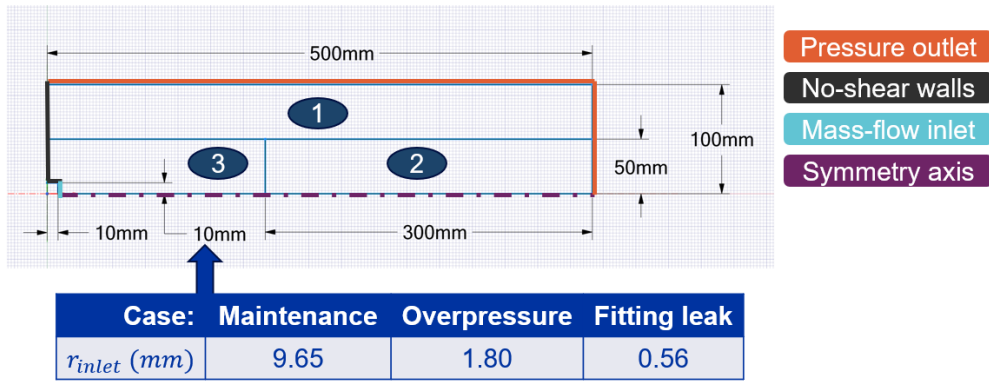
In this section, the 2D model for the execution of simulations to study the shock expansion phase is presented along with the results from the simulations.

#### 5.1.1. Geometry, discretization and setup

The geometry consist on an axi-symmetric tube with an inlet in the center of one of the circular faces. This geometry is divided into three different discretization zones to facilitate the computations, with greater refinement on the zones closest to the inlet, where it is expected to have a shock expansion wave. The radius of the inlet varies depending on the type of leak condition being considered, and the values are computed from the leak area which was provided by CMS safety team. There are three different conditions: first the "maintenance" which has the biggest leak area as it is supposed to be caused by a worker in the local vicinity, the radius of the inlet in this case is 9.65 mm; second the "overpressure" which is supposed to be caused by an overpressure in the system, later on it will diverge in two different cases, a warm and a cold overpressure, depending on the point of the saturated line in which the fluid is released, the radius of the inlet in this case is 1.80 mm; finally the third condition is a "fitting leak" which is a particular leak condition coming from the Vacuum Tank on the inner part of the CMS detector, the radius for the inlet in this case is 0.56 mm.

For the discretization part, there is a nominal mesh which characterizes the length of the cell in the coarser area of the domain, being reduced geometrically for the more refined zones. A sensitivity study will be run for five different values of this nominal mesh to perform a grid independence assessment for verification of the solution obtained. The detailed dimensions of the geometry, discretization and boundary conditions setup is presented in Figure 5.1. It should be noted that, in order to properly characterize the flow, a minimum of ten cells is required on the inlet dimension. This requirement on the minimum grid resolution was set following best practice guidelines according to literature on the topic [29, 30]. This presumably means that for the case of

the fitting leak, a more local geometry will be needed closer to the inlet, allowing for more refinement without increasing dramatically the computational time of the simulations.



Discretization zones

Zone:	1	2	3
Element size	Nominal	0.2 * Nominal	0.1 * Nominal

Sensitivity study for mesh dependence around five nominal values: 1, 2, 3, 4 and 5 mm.

\* Growth rate 1.1 at zone boundary

Figure 5.1: Geometry, discretization and setup for the 2D local simulations in the leak point vicinity.

The goal of the 2D simulations is to provide equivalent boundary conditions for a virtual inlet close to the leakage point after the shock wave, providing a computationally simpler inlet for the 3D simulations. For this purpose, three key variables are selected for the 3D CFD simulations that will properly define the inlet condition. These variables are the axial velocity, the temperature, and the carbon dioxide mass fraction, and they will be extracted from the end of the model domain.

5.1.2. Case 1: Maintenance

The maintenance case is presented by CMS safety team with the conditions given in Table 5.1, which represent under-expanded choked flow.

Table 5.1: Boundary conditions for the under-expanded choked flow in the maintenance leakage condition, as provided by CMS safety team.

A (mm <sup>2</sup> )	$\dot{m}$ (g/s)	T (°C)	P (bar)
292.55	500	-55.8	3

After computing the CFD simulations, the axial velocity, temperature and carbon dioxide mass fraction are computed on the end of the domain for each of the discretizations on the study, showing the behavior depicted in Figure 5.2. On this leakage scenario, every mesh resolves the 2D inlet (meaning it uses more than 10 elements). It can be seen how M1, the finest mesh, leads to numerical instabilities. On the other hand, the rest of the discretizations show a similar behavior. Output for the 3D simulation will be taken from the coarser mesh, M5. For M5, the contours of the three variables of interest can be computed and are presented in Figure 5.3, where also a black line at the end of the domain is shown, depicting where the conditions for the 3D simulations are taken. These conditions are presented in Figure 5.4 and will be further studied in the next section for its transition into boundary conditions to the 3D CFD model.

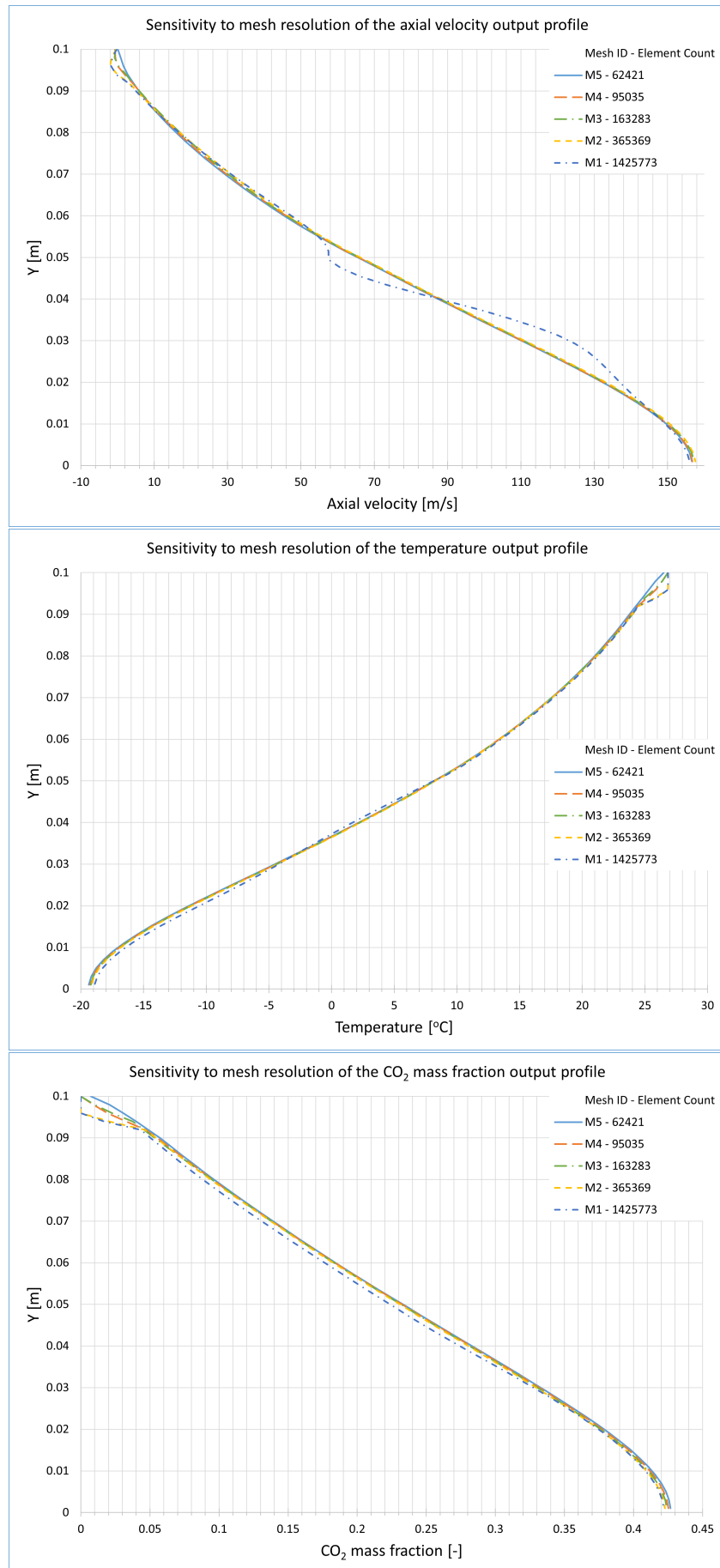


**Figure 5.2:** Maintenance case: Output profiles of axial velocity, temperature and carbon dioxide mass fraction for the five different discretizations of the geometry used in the grid independence study. M1, the finest mesh, shows numerical error, specially noticeable when looking at the macroscopic behavior. M2 to M5 show a very similar behavior in terms of output profiles for the 3D simulation.

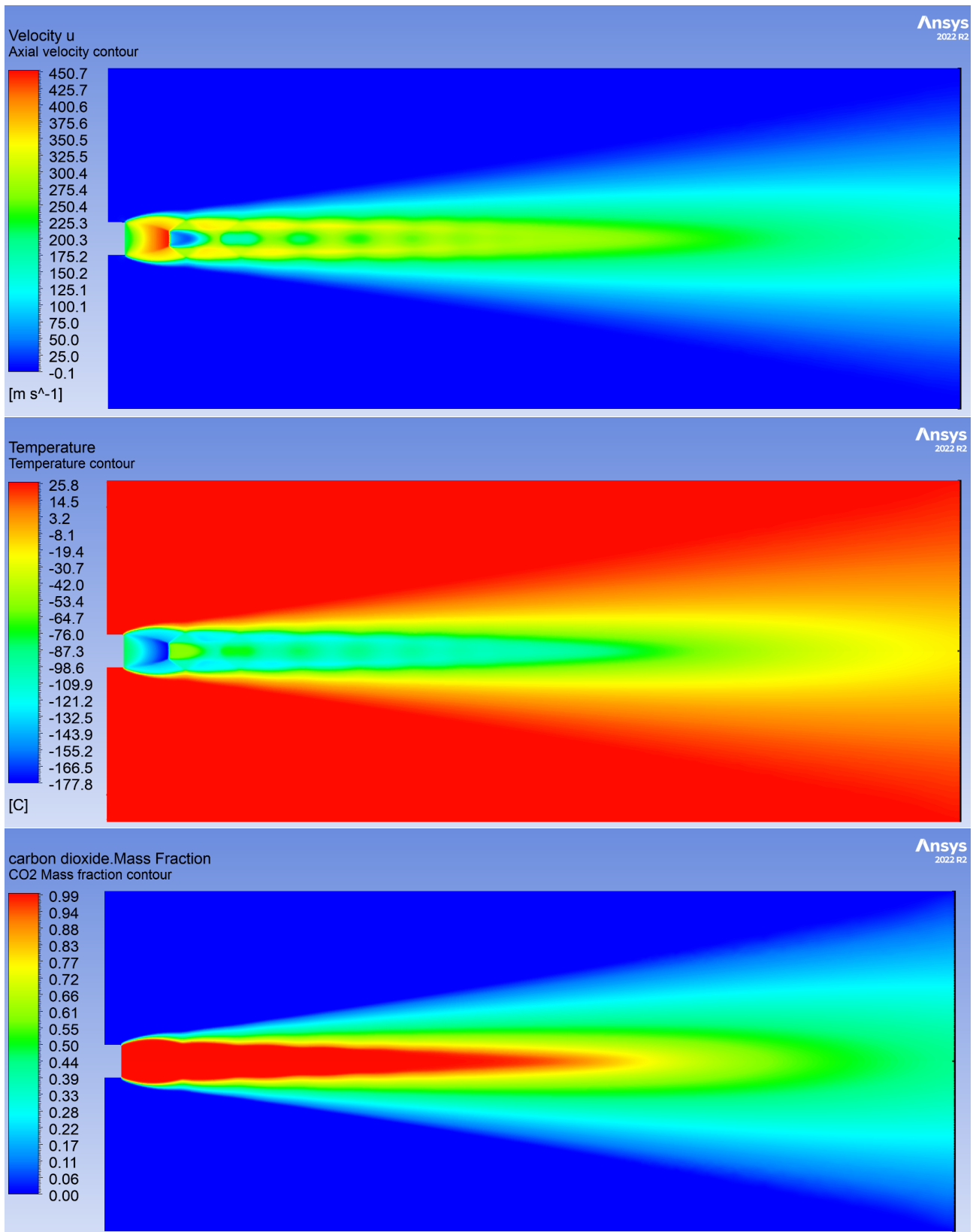


**Figure 5.3:** Contours of axial velocity, temperature and carbon dioxide mass fraction computed using mesh M5 in the maintenance leakage situation.

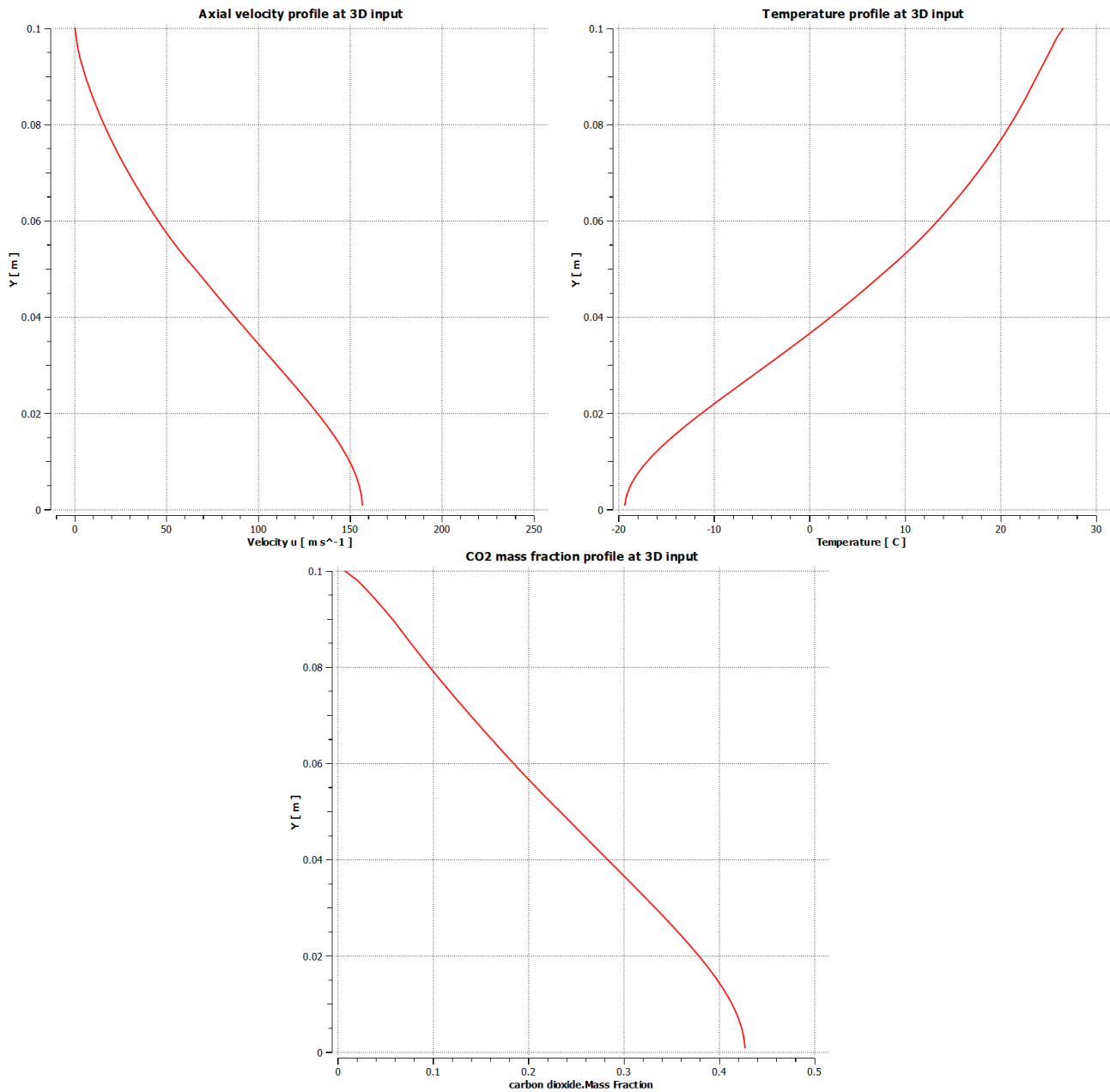


**Figure 5.4:** Profiles extracted for the 3D simulation as equivalently representing initial conditions proposed by CMS safety team in the maintenance leakage situation. Conditions are verified being within 1% margin of the mass-flow condition given.

### 5.1.3. Case 2: Overpressure

The overpressure case is presented with two different subcases by CMS safety team. A warm overpressure case with the conditions given in Table 5.2, and a cold overpressure case with the conditions given by Table 5.3.

Again, the CFD cases are resolved, showing in Figure 5.5 and in Figure 5.8 respectively, the profiles of the key variables at the end of the domain for each of the discretizations on the study. On this leakage scenario, M5 and M4, the courser meshes, cannot properly resolve the 2D inlet (using equal or less than 10 cells), therefore the results cannot be reliably used. Once again, M1, the finest mesh, leads to numerical instabilities, as it will be the case as long as the same geometry is used. On the other hand, M3 and M2 show a similar behavior. Output for the 3D simulation will be taken from the coarser mesh, M3. For M3, the contours of the three variables of interest can be computed and are presented in Figure 5.6 and in Figure 5.9 respectively, where again a black line at the end of the domain is shown, depicting where the conditions for the 3D simulations are taken. These conditions are presented in Figure 5.7 and in Figure 5.10 respectively, and will be further studied in the next section for its transition into boundary conditions to the 3D CFD model.

#### Case 2.1: Warm Overpressure

**Table 5.2:** Boundary conditions for the under-expanded choked flow in the warm overpressure leakage condition, as provided by CMS safety team.

A (mm <sup>2</sup> )	$\dot{m}$ (g/s)	T (°C)	P (bar)
10.18	280	3.5	38

#### Case 2.2: Cold Overpressure

**Table 5.3:** Boundary conditions for the under-expanded choked flow in the cold overpressure leakage condition, as provided by CMS safety team.

A (mm <sup>2</sup> )	$\dot{m}$ (g/s)	T (°C)	P (bar)
10.18	164	-40	10.1

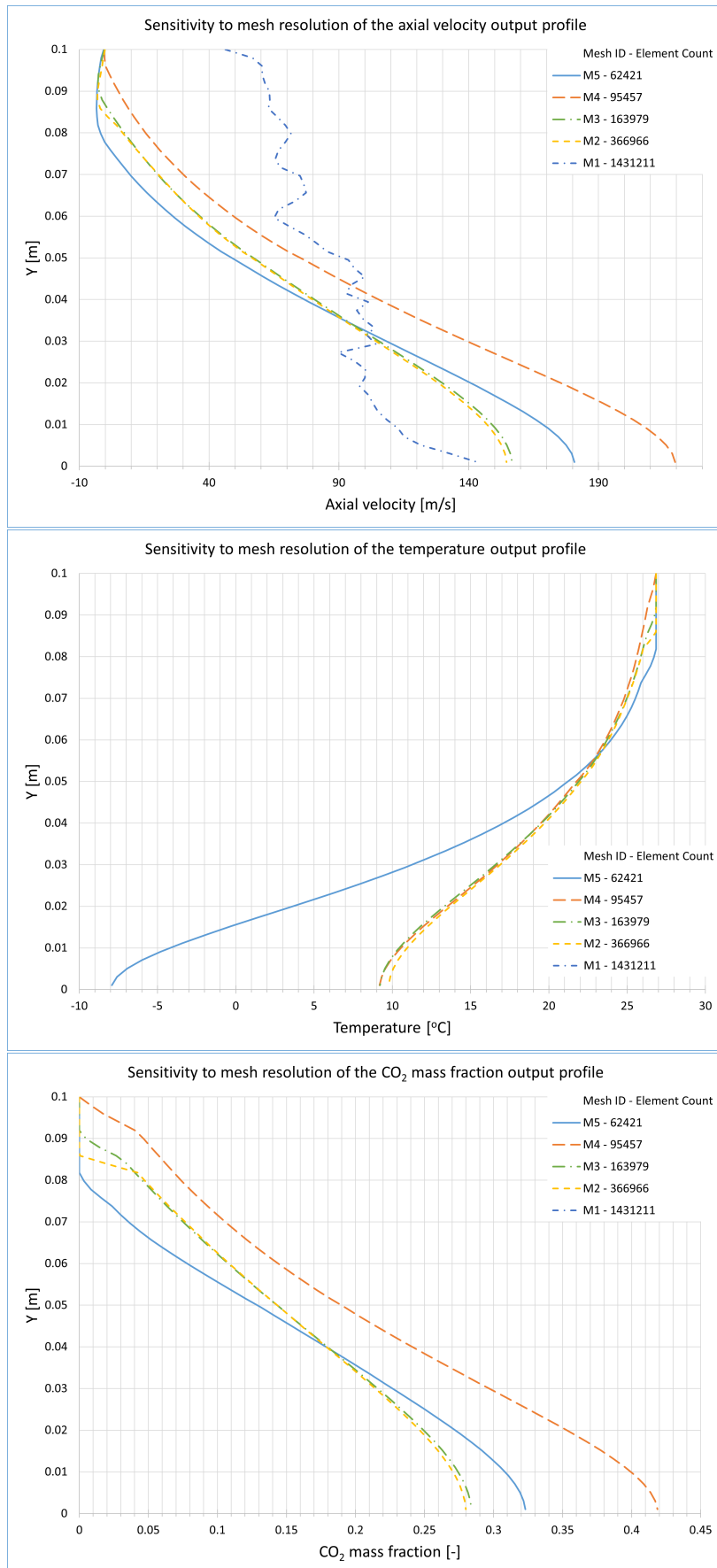


**Figure 5.5:** Warm overpressure case: Output profiles of axial velocity, temperature and carbon dioxide mass fraction for the five different discretizations of the geometry used in the grid independence study. M1, the finest mesh, shows numerical error, specially noticeable when looking at the macroscopic behavior. M4 and M5, the coarser meshes, cannot properly resolve the 2D inlet as they used equal or less than 10 cells on the characteristic dimension. M2 and M3 show a very similar behavior in terms of output profiles for the 3D simulation.

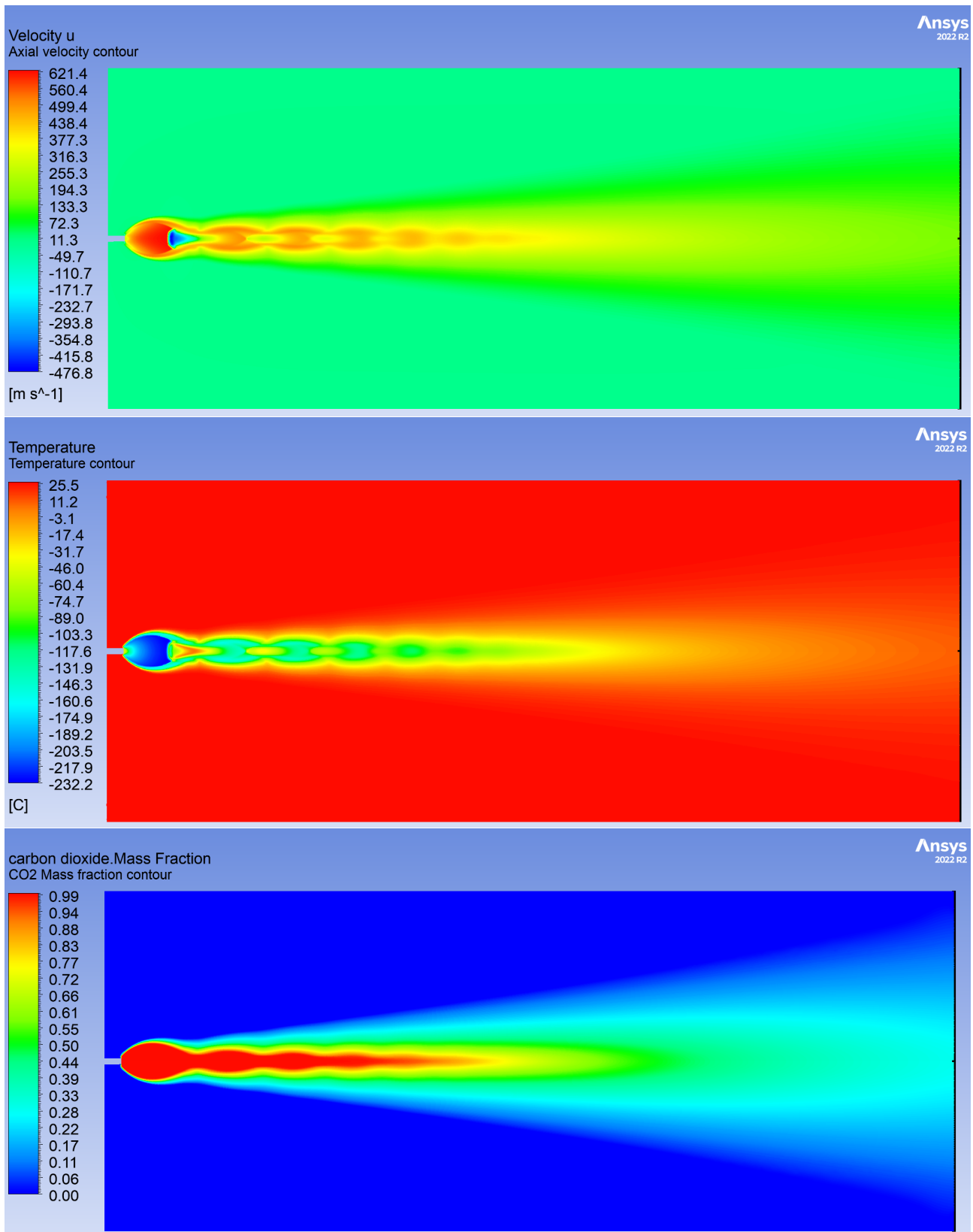


**Figure 5.6:** Contours of axial velocity, temperature and carbon dioxide mass fraction computed using mesh M3 in the warm overpressure leakage situation.

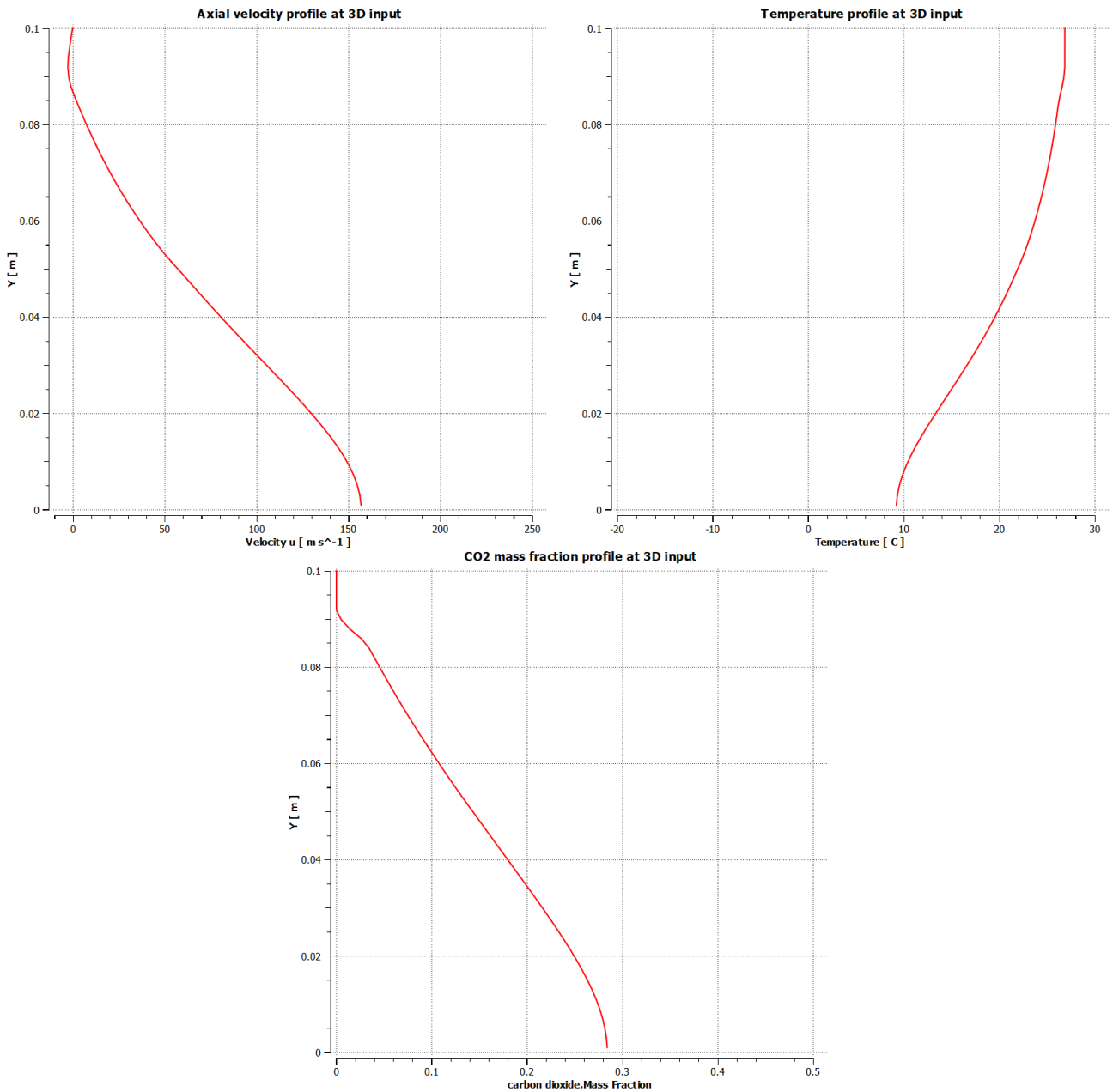


**Figure 5.7:** Profiles extracted for the 3D simulation as equivalently representing initial conditions proposed by CMS safety team in the warm overpressure leakage situation. Conditions are verified being within 1% margin of the mass-flow condition given.

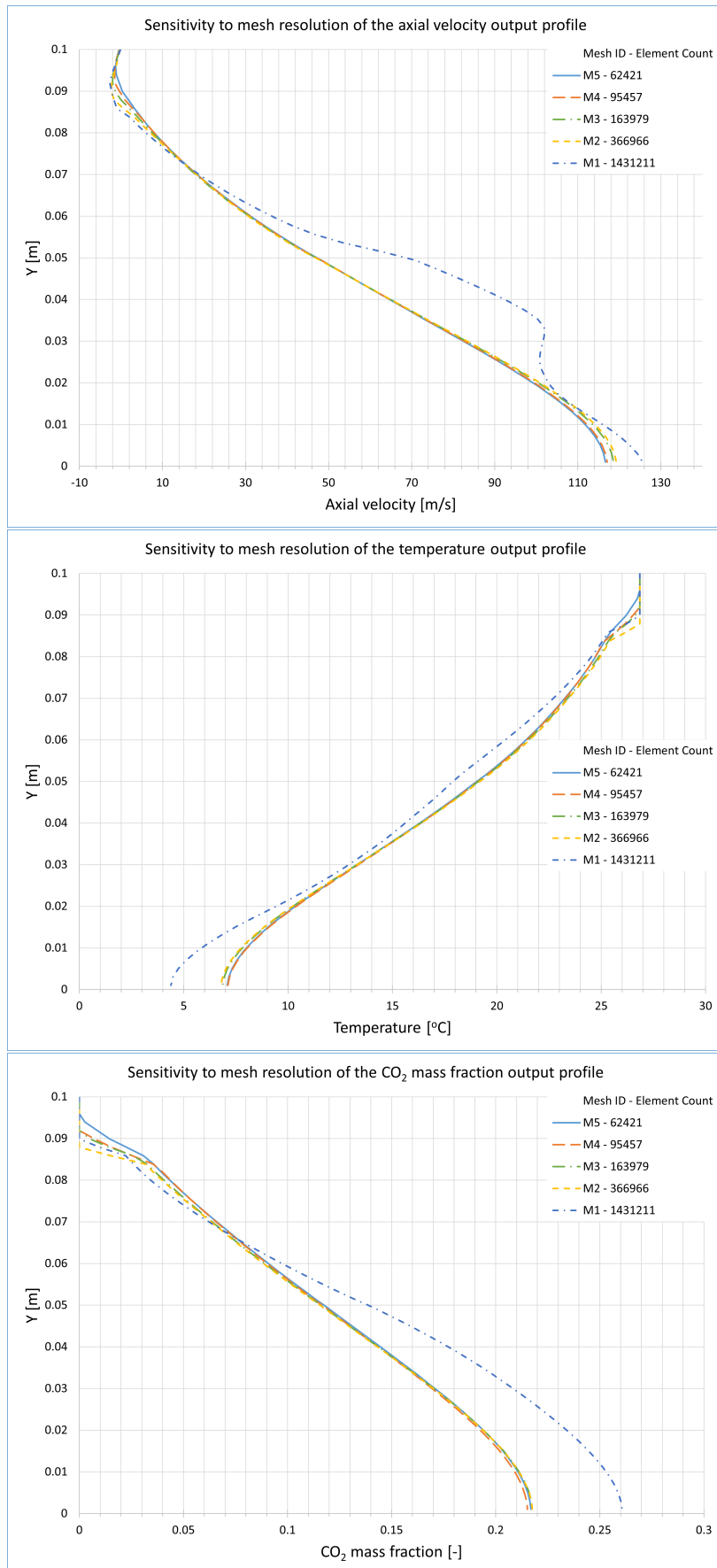


**Figure 5.8:** Cold overpressure case: Output profiles of axial velocity, temperature and carbon dioxide mass fraction for the five different discretizations of the geometry used in the grid independence study. M1, the finest mesh, shows numerical error, specially noticeable when looking at the macroscopic behavior. M4 and M5, the coarser meshes, cannot properly resolve the 2D inlet as they used equal or less than 10 cells on the characteristic dimension. M2 and M3 show a very similar behavior in terms of output profiles for the 3D simulation.

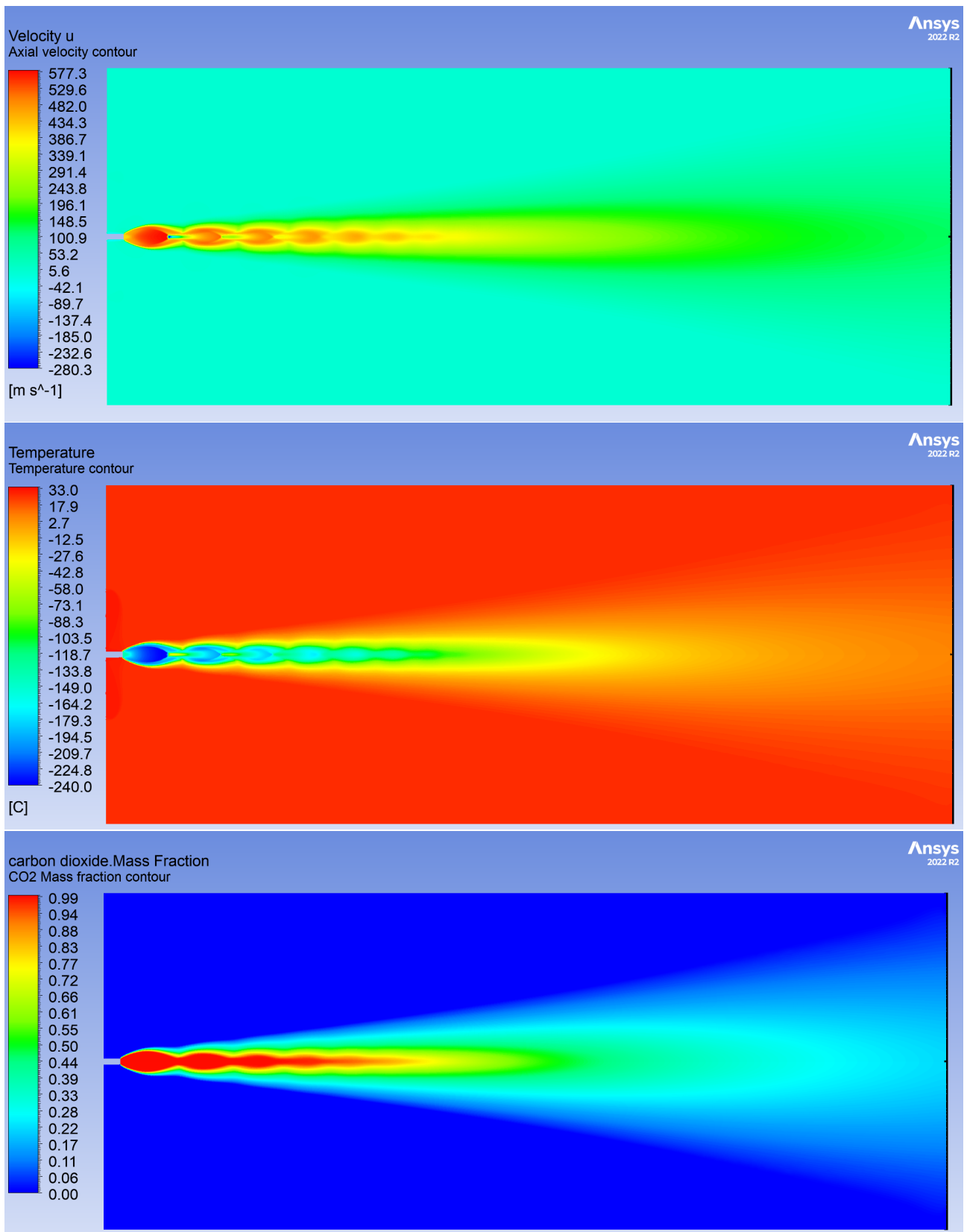


**Figure 5.9:** Contours of axial velocity, temperature and carbon dioxide mass fraction computed using mesh M3 in the cold overpressure leakage situation.

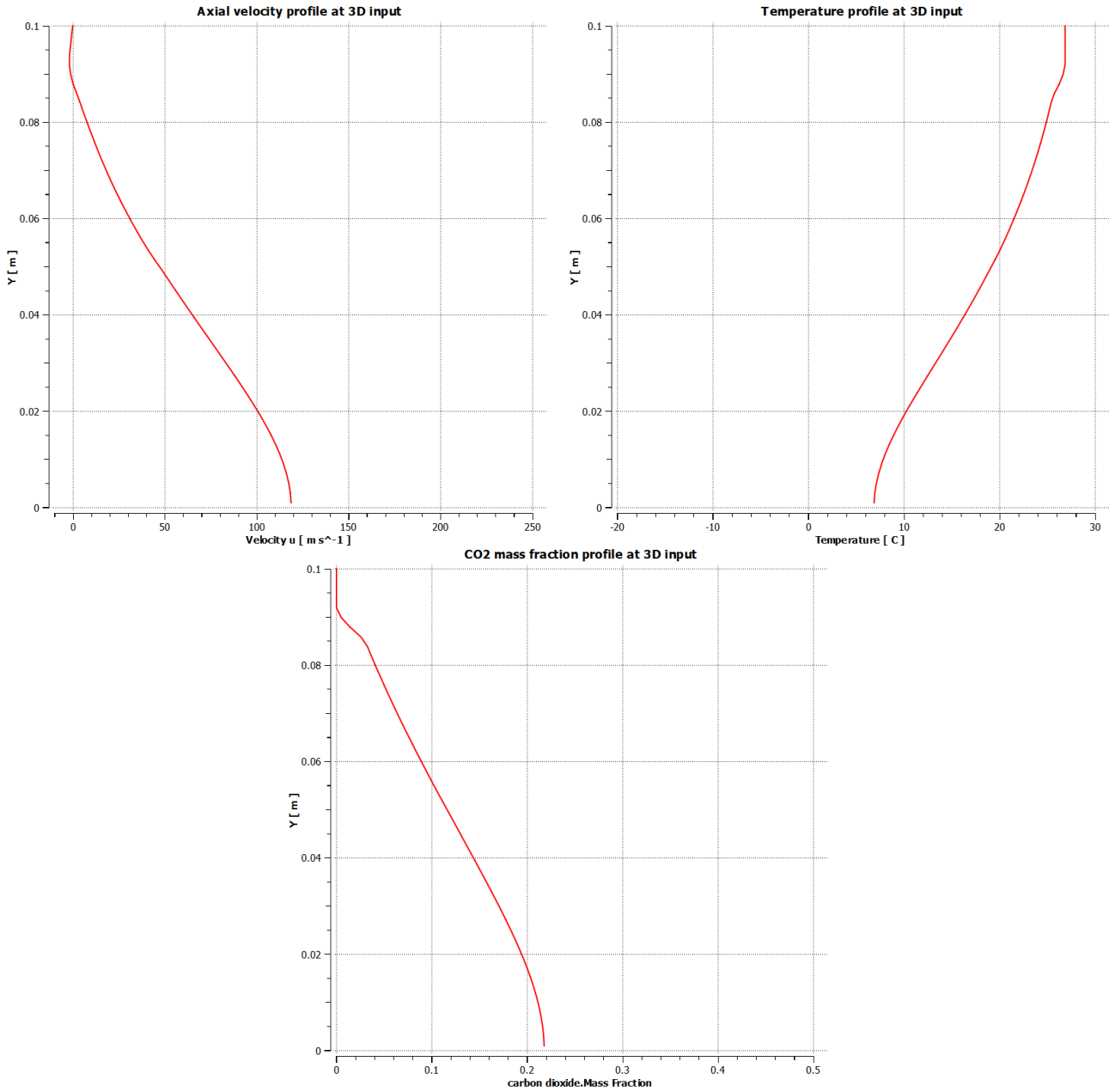


**Figure 5.10:** Profiles extracted for the 3D simulation as equivalently representing initial conditions proposed by CMS safety team in the cold overpressure leakage situation. Conditions are verified being within 1% margin of the mass-flow condition given.

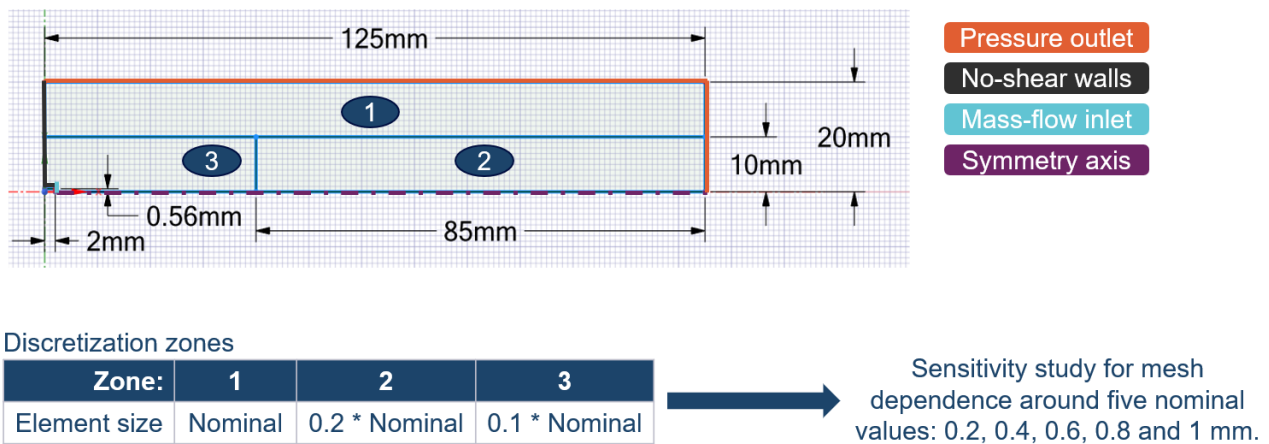
### 5.1.4. Case 3: Fitting leak

The fitting leak case is a special case for a leakage on the Vacuum tank on the inner part of the CMS detector with the conditions given in Table 5.4.

**Table 5.4:** Boundary conditions for the under-expanded choked flow in the fitting leak leakage condition, as provided by CMS safety team.

A (mm <sup>2</sup> )	$\dot{m}$ (g/s)	T (°C)	P (bar)
1	20.37	-9	27

Due to the extremely small dimensions of the leakage point, the discretizations used up to this point on the 2D geometry fail to properly resolve the 2D inlet under the conditions imposed (more than 10 cells in the characteristic length), except for M1, which leads to numerical error. To solve this issue, a smaller geometry is designed in the vicinity of the leakage point, allowing for further refinement and a similar analysis as the one performed for the above-presented cases. The geometry, discretization and setup used is depicted in Figure 5.11.



\* Growth rate 1.1 at zone boundary

**Figure 5.11:** Geometry, discretization and setup for the 2D local simulations in the leak point vicinity for the case of the fitting leak.

Finally, the case is resolved, showing in Figure 5.12, the profiles of the key variables at the end of the domain for each of the discretizations on the study. Now every mesh is able to properly resolve the 2D inlet. The two finer meshes, M0.2 and M0.4 lead to numerical instabilities. On the other hand, the rest of the meshes show a similar behavior. Output for the 3D simulation will be taken from the coarser mesh, M1.0. For M1.0, the contours of the three variables of interest can be computed and are presented in Figure 5.13, where again a black line at the end of the domain is shown, depicting where the conditions for the 3D simulations are taken. These conditions are presented in Figure 5.14, and will be further studied in the next section for its transition into boundary conditions to the 3D CFD model.

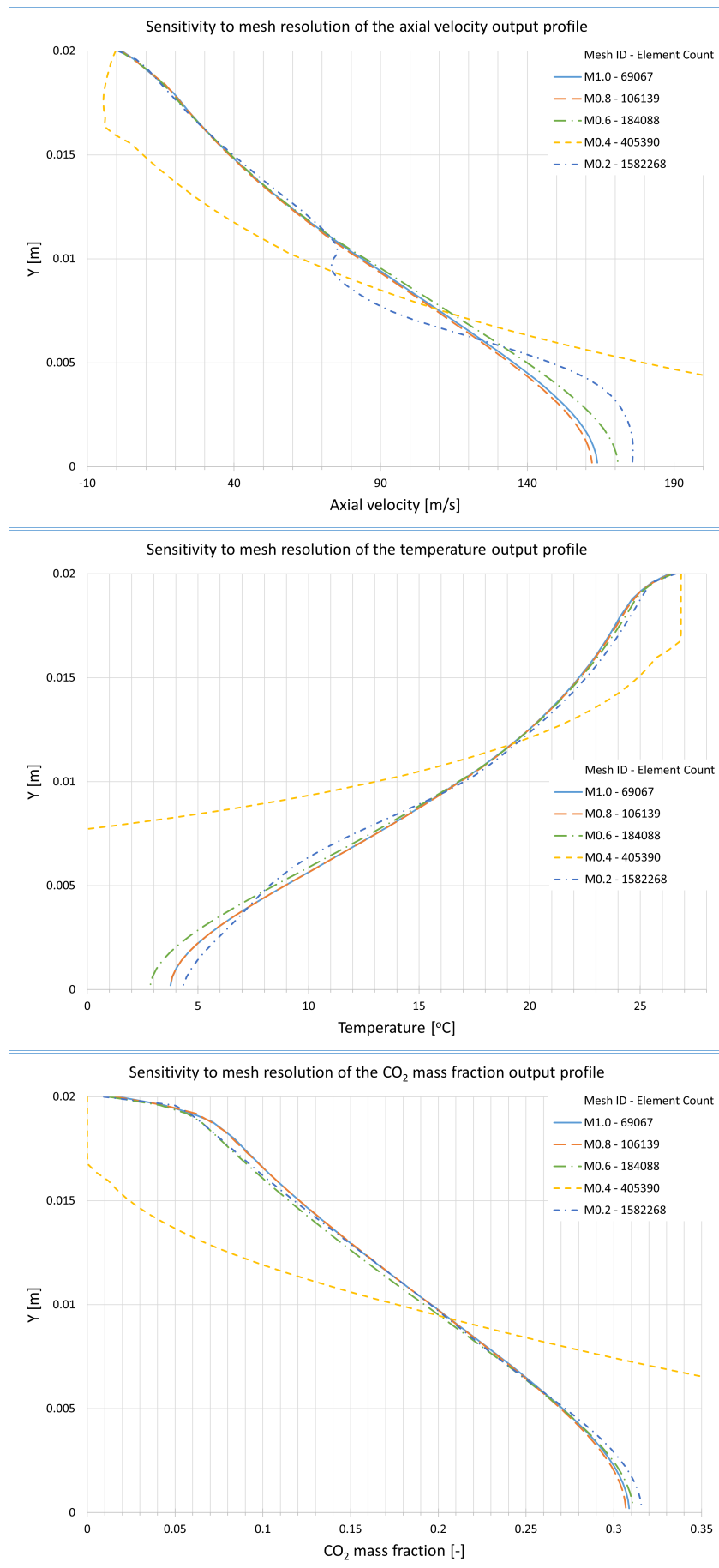


**Figure 5.12:** Fitting leak case: Output profiles of axial velocity, temperature and carbon dioxide mass fraction for the five different discretizations of the geometry used in the grid independence study. Every mesh resolves the 2D inlet, with the two finer meshes, M0.2 and M0.4 leading to numerical instabilities. M1.0 to M0.6 show a similar behavior in terms of output profiles for the 3D simulation.

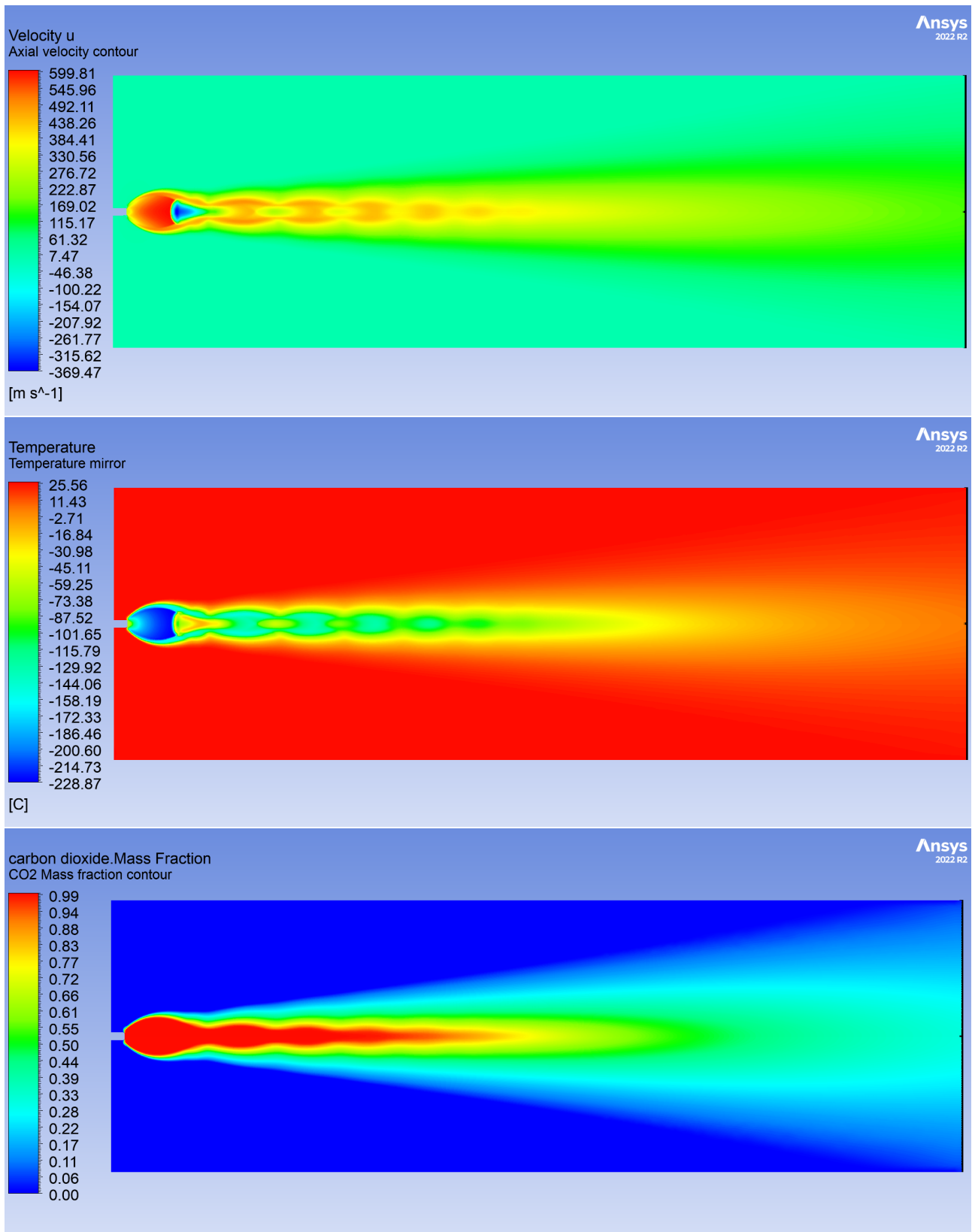


**Figure 5.13:** Contours of axial velocity, temperature and carbon dioxide mass fraction computed using mesh M1 in the fitting leak leakage situation.

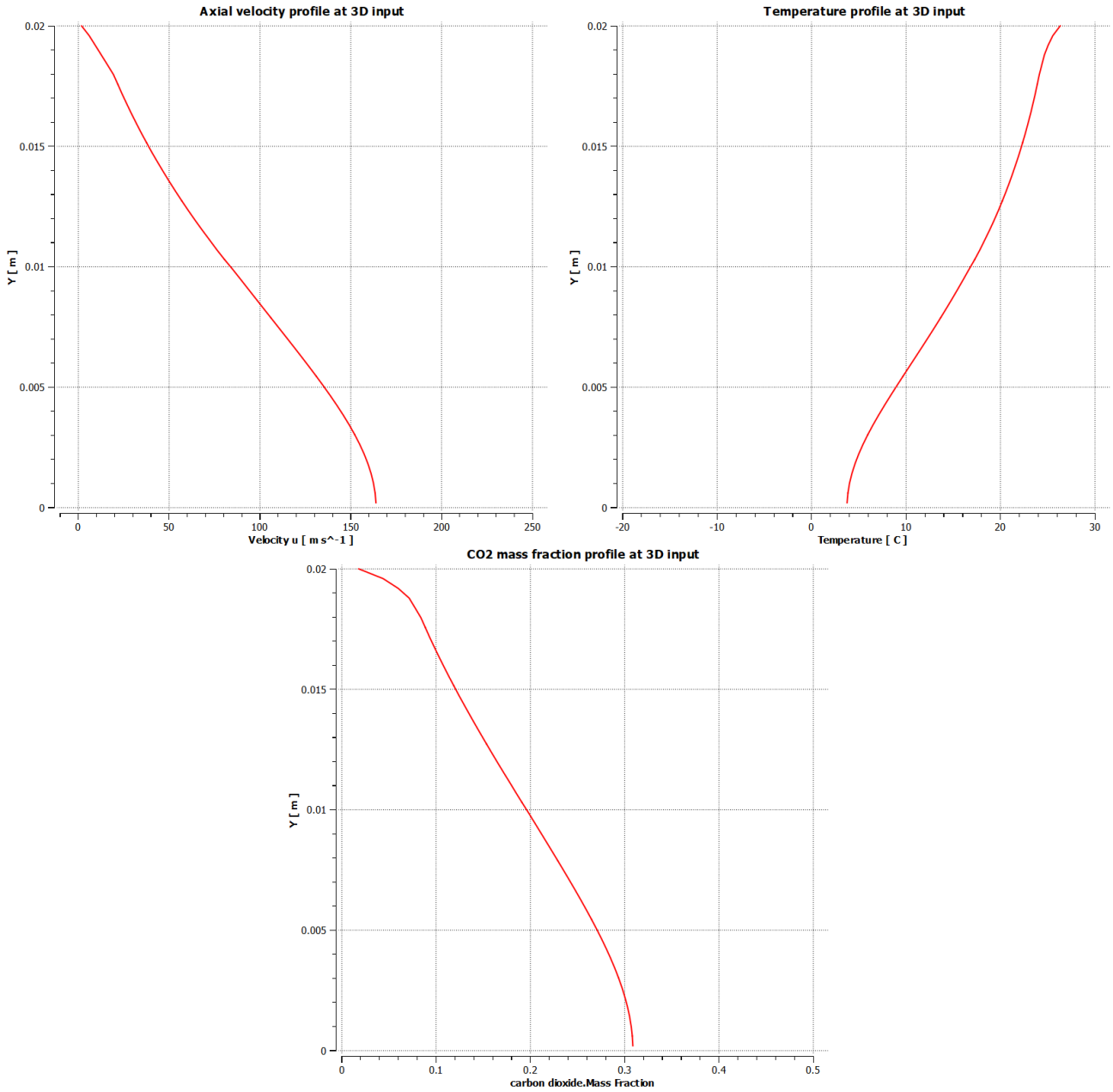


**Figure 5.14:** Profiles extracted for the 3D simulation as equivalently representing initial conditions proposed by CMS safety team in the cold overpressure leakage situation. Conditions are verified being within 1% margin of the mass-flow condition given.

## 5.2. CMS experimental cavern 3D model

In this section, the computational model of the CMS experimental cavern is shown. For that purpose, first the arguments for the simplification of several parts is given. Then, the setup of the boundary conditions and leakage points is depicted. After that, a summary of the different cases and methodology is explained. Finally, the discretization of the 3D model is shown.

### 5.2.1. Simplification of the geometry

The geometry of the experimental cavern had three major simplifications. The first one is related to the ventilation system on the cavern, as many different parts were present in the original geometry, a smother model resembling the original one was created allowing for a higher computational efficiency. This simplification will not compromise the CFD results as the characteristic lengths suppressed from the model are negligible when compared to the fluid flow within the cavern. Secondly, the most important simplification is the one related to the racks and platforms, as well as other smaller objects within the cavern. The racks and platforms situated away from the fluid flow are suppressed to improve computational efficiency. This simplification still provides accurate flow resolution in the locality of the leakage point as well as a reliable solution for the fluid flow within the cavern. Both simplifications are depicted in Figure 5.15.

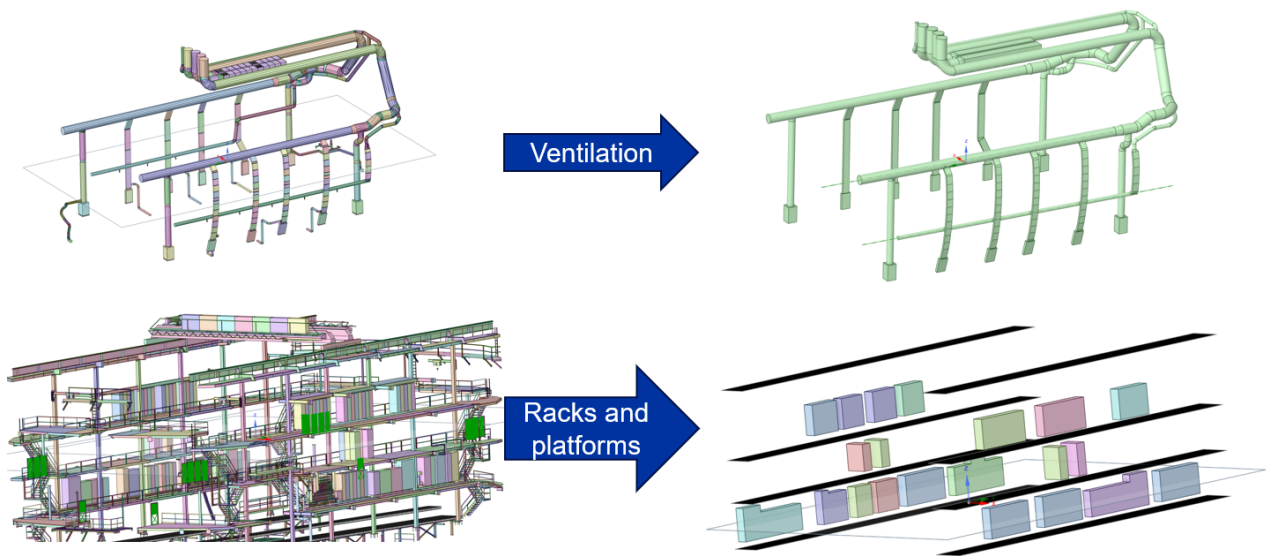


Figure 5.15: Major geometry simplifications on the CMS experimental cavern.

#### Porous platforms study

The third simplification included in the model implies transforming every platform into 2D "porous plates". This is motivated so that it can allow for a faster computation during the simulation. In order to properly characterize the 2D plate, the following study is proposed: an accurate model of the grided platform / baffle is introduced on a virtual wind tunnel designed in ANSYS Fluent. Pressure drop is measured for different fluid flow velocities ranging from 0.1 to 10 m/s (resembling all the different scales expected within the experimental cavern). Then, a 2D plate modeled as a porous jump is introduced on the same virtual wind tunnel, and the coefficients defining the porous jump [31] are computed to optimize the fit with the pressure drop measured on the grided platform / baffle. The study results in the computation of two coefficients that define a 2D porous plate resembling the pressure drop on the grided platforms and baffles within the cavern. The computation of the coefficients (permeability of the medium and pressure-jump coefficient) can be performed via least square method, knowing that the pressure drop is given by Equation 5.1 [31].

$$\Delta p = - \left( \frac{\mu}{\alpha} v + C_2 \frac{1}{2} \rho v^2 \right) \Delta m \quad (5.1)$$

where the Darcy's law was used in combination with an inertial loss term and  $\mu$  is the laminar fluid viscosity,  $\alpha$  is the permeability of the medium,  $C_2$  is the pressure-jump coefficient,  $v$  is the velocity normal to the porous face, and  $\Delta m$  is the thickness of the medium.

From this study it is concluded that platforms within the CMS experimental cavern can be modeled as 2D porous plates with a pressure-jump defined by the coefficients in Table 5.5.

**Table 5.5:** Coefficients defining the fitted porous-jump in the 2D plates resembling the grided platforms and baffles within the CMS experimental cavern. Thickness of the medium is taken as 1 mm. Error on pressure drop is kept within less than 1%.

$C_2$ (1/m)	$\alpha$ (m <sup>2</sup> )
32.606	5.219E-05

### 5.2.2. Complete 3D CAD model

In addition to the model for the experimental cavern shown (named at CERN as UXC55), to complete the model, two underground floors beneath the cavern need to be added. These floors are kept in a separated model and they are connected via input/output faces that are shown in Figure 5.17 and in Figure 5.18. The underground floors contain simplified cabled trays, as well as racks and ventilation inlets coming from the ventilation system in the experimental cavern. The aim of separating the geometries has the purpose of allowing higher computational efficiencies, due to the fact that some leakage points will be above the underground floors and therefore these will not take part on the simulation. When the leakage point is located within the underground floors, two simulations will be computed. First on the underground, then the output profile will be collected and inputted if needed on the rest of the cavern. The complete model can be seen in Figure 5.16.

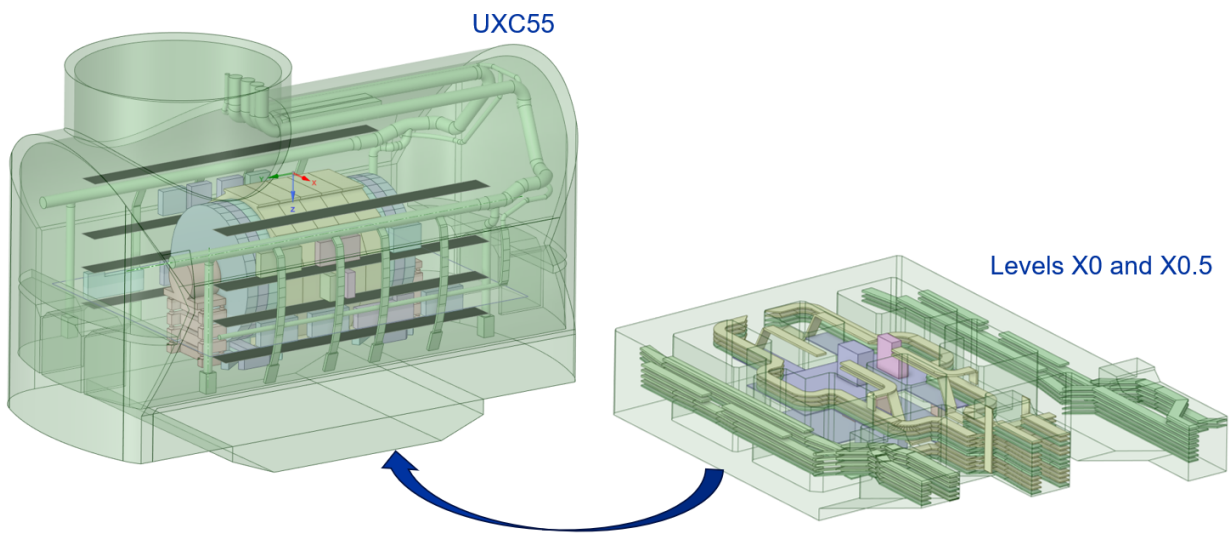


**Figure 5.16:** Complete 3D CAD geometrical models of the CMS experimental cavern, separating the X0 and X0.5 floors (beneath the detector) from the main UXC55 model.

#### Leakage points and boundary conditions

Here, the configurations and setup of the different models are explained. First, the underground floors boundaries configuration can be seen at Figure 5.17. Next, the configuration of the rest of the cavern is shown at Figure 5.18. Finally, the leakage point for the fitting leak special case is shown at Figure 5.19. The ventilation system blows 45000 m<sup>3</sup>/h of fresh air at 17°C and the racks within the cavern have a heat loss of 50 kW in total. On the underground floors, each of the ventilation fans blow 800 m<sup>3</sup>/h of fresh air at 17°C and the racks have a global heat loss of 500 W. Leakage locations have been carefully selected in collaboration with CMS safety team by considering worst case scenarios at different places within the cavern. The simulations conducted provide a complete overview of the coolant leakage phenomena.

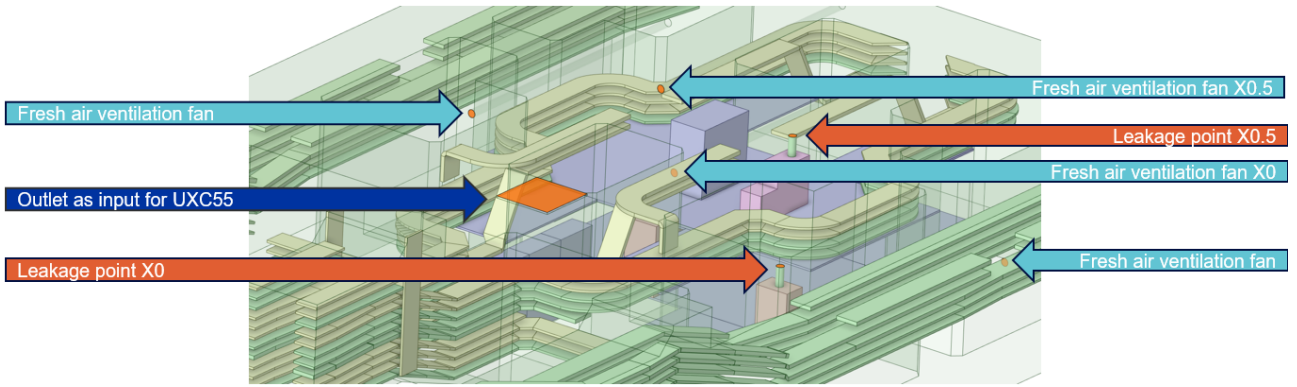


Figure 5.17: Boundaries configuration on the underground floors model, floors X0 and X0.5.

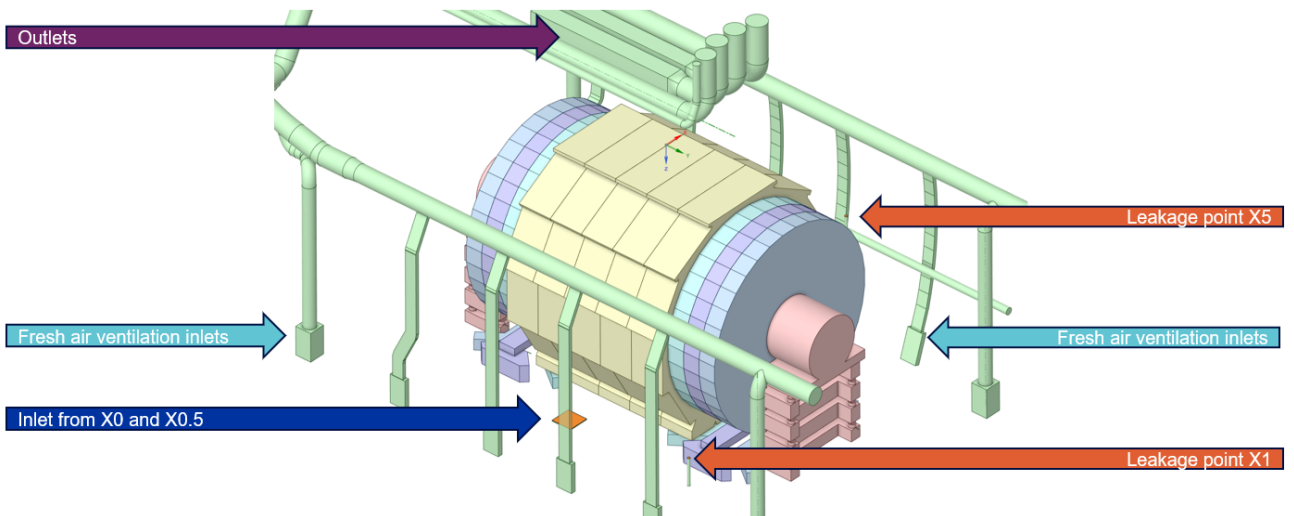


Figure 5.18: Boundaries configuration on the experimental cavern, floors X1 to X5.

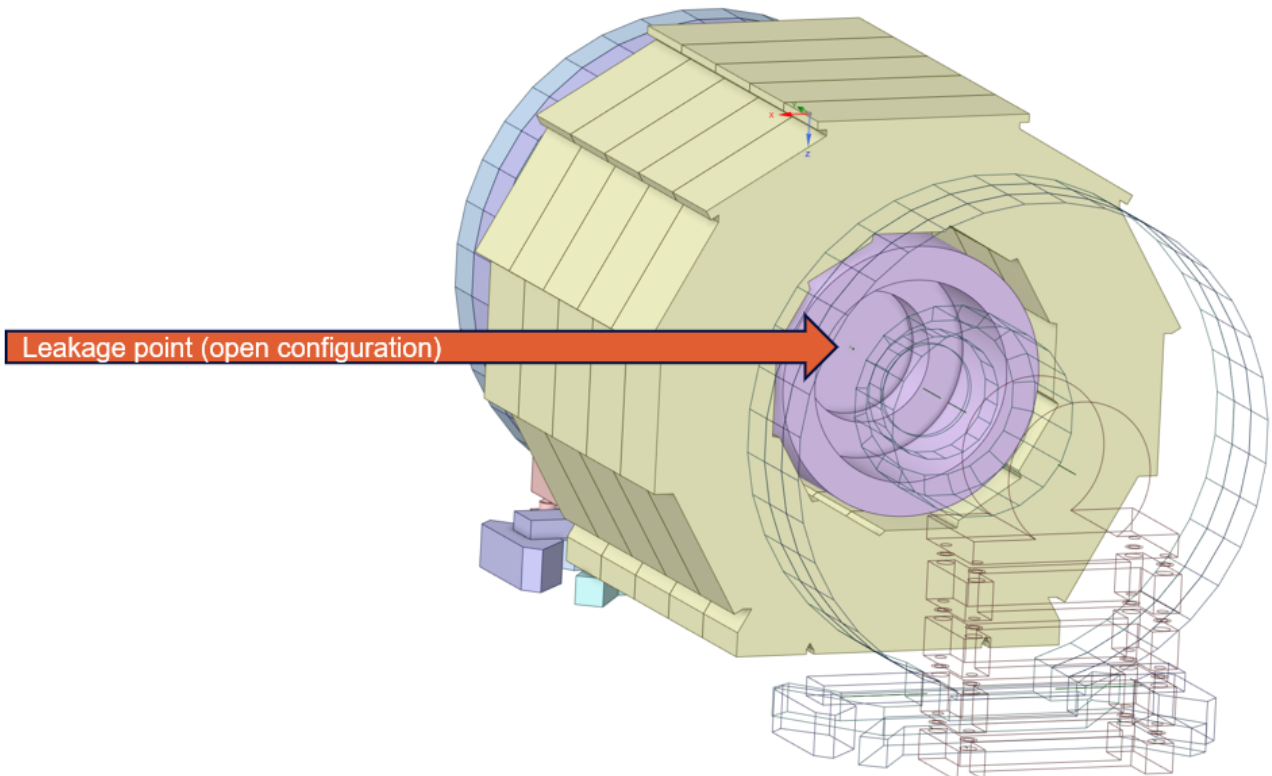


Figure 5.19: Boundaries configuration for the fitting leak leakage scenario.

### 5.2.3. Summary of simulation cases

Once every leakage point and boundary condition have been discussed, in this subsection a summary of the different simulation cases and their location is shown in Table 5.6. Where the leakage time has been computed from the mass flows provided by CMS safety team and the reserves of carbon dioxide that are subject to leak. The fitting leak at the vacuum tank represents a special case with an extremely small mass flow and reserves in the order of tonnes of carbon dioxide, a steady-state simulation is considered for this leakage condition. The transient simulations will be resolved for ten times the amount of time of the leakage or up to the point in which there are no health risks in the cavern anymore due to low carbon dioxide concentrations.

**Table 5.6:** Summary of the different cases to be resolved and their location and type of simulation.

	Location	Type
Maintenance	X0	3.38 s leak
Warm Overpressure	X0, X0.5	49.3 s leak
Cold Overpressure	X5	141 s leak
Fitting Leak	Vacuum tank	Steady State

### 5.2.4. Discretization of the 3D model

A polyhedral mesh was created using ANSYS Meshing to ensure detailed resolution of the different scales within the cavern. Local sizing was applied to achieve at least 20 cells across the diameter of leakage inlets, ensuring a proper resolution. Boundary layers were refined on the walls. This setup enhances the accuracy of the simulation by capturing essential flow details and characteristic gradients. Figure 5.20 shows the mesh model and its configuration. For the basement of the experimental cavern, the same approach was taken. Figure 5.21 shows the discretization obtained.

It is worth noting that in this case, verification via grid independence study will not be repeated. Previous validation studies conducted internally at CERN showed that CFD simulation in a similarly modelled cavern performs optimally for a discretization sized as the one obtained. This mesh configuration has been proven to deliver accurate results for similar flow behaviors.

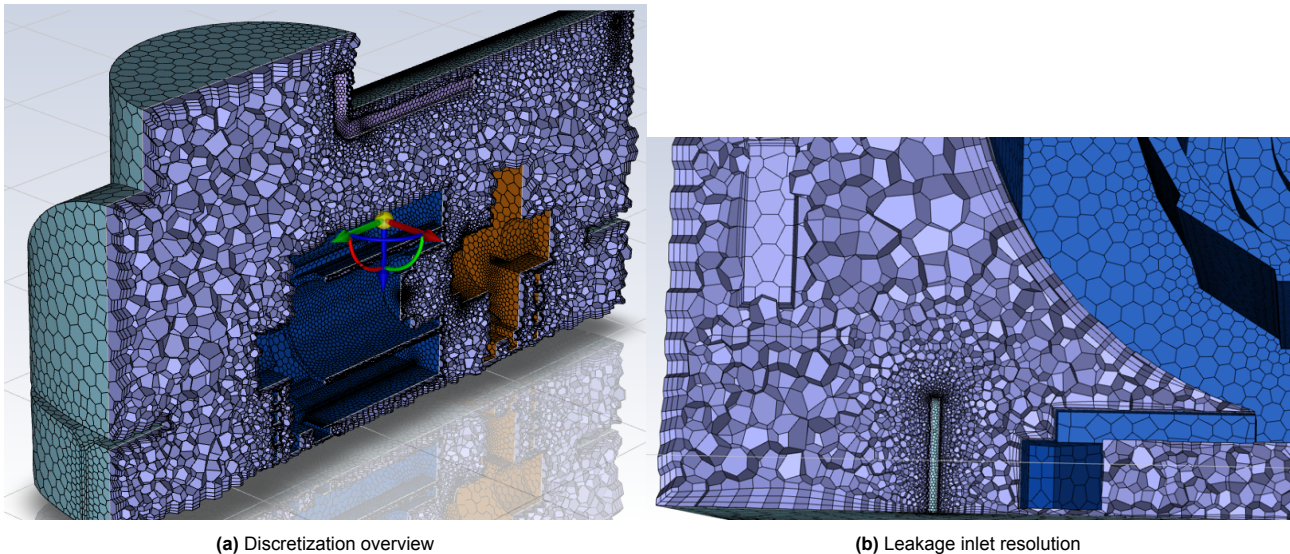
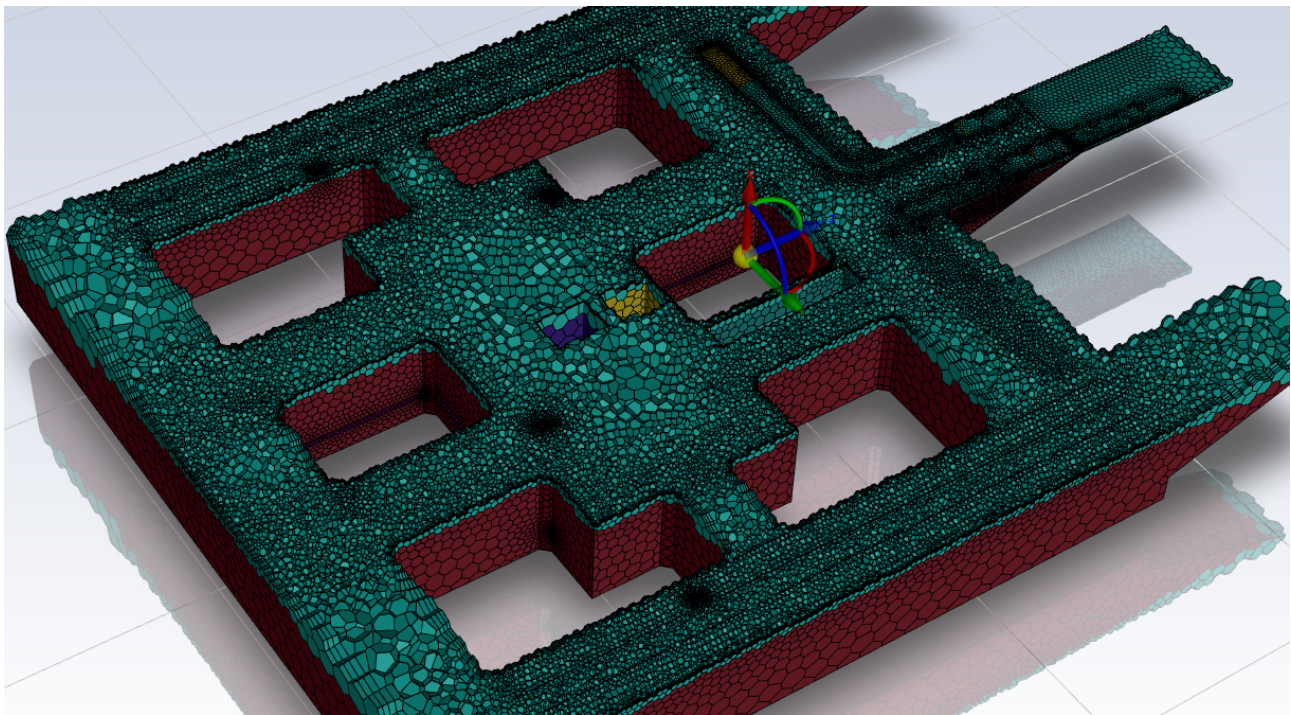


**Figure 5.20:** Discretization of the 3D CAD model using ANSYS Meshing applied to the main area of the experimental cavern.



(a) Discretization overview



(b) Detailed resolution

**Figure 5.21:** Discretization of the 3D CAD model using ANSYS Meshing applied to the basement of the experimental cavern.

## 5.3. Results of the 3D CFD simulations

### 5.3.1. 2D profiles adapted to the 3D simulations

The first step to resolve the 3D simulations is to adapt the results obtained from the 2D simulations so that they can be used as their initial/boundary conditions. This adaptation in a two step process:

1. The profiles obtained for axial velocity, carbon dioxide mass fraction, and temperature, are fitted to a polynomial of high order via the minimum squared method, minimizing the error introduced on this step.
2. A user-defined function is written in C language to express the initial and boundary conditions for the leakage points, as well as time conditions (such as closing of the inlet at carbon dioxide run-out) for transient simulations.

On the graphics below (Figure 5.22 to Figure 5.25), the 2D profiles fitting analysis is shown.

The source code listings written in C language that were inputted in ANSYS Fluent Solver can be found in Appendix A. These User-Defined Functions (UDFs) contain the necessary details to define the initial conditions stemming from the 2D simulations as well as the time dependencies of the boundary conditions if any.

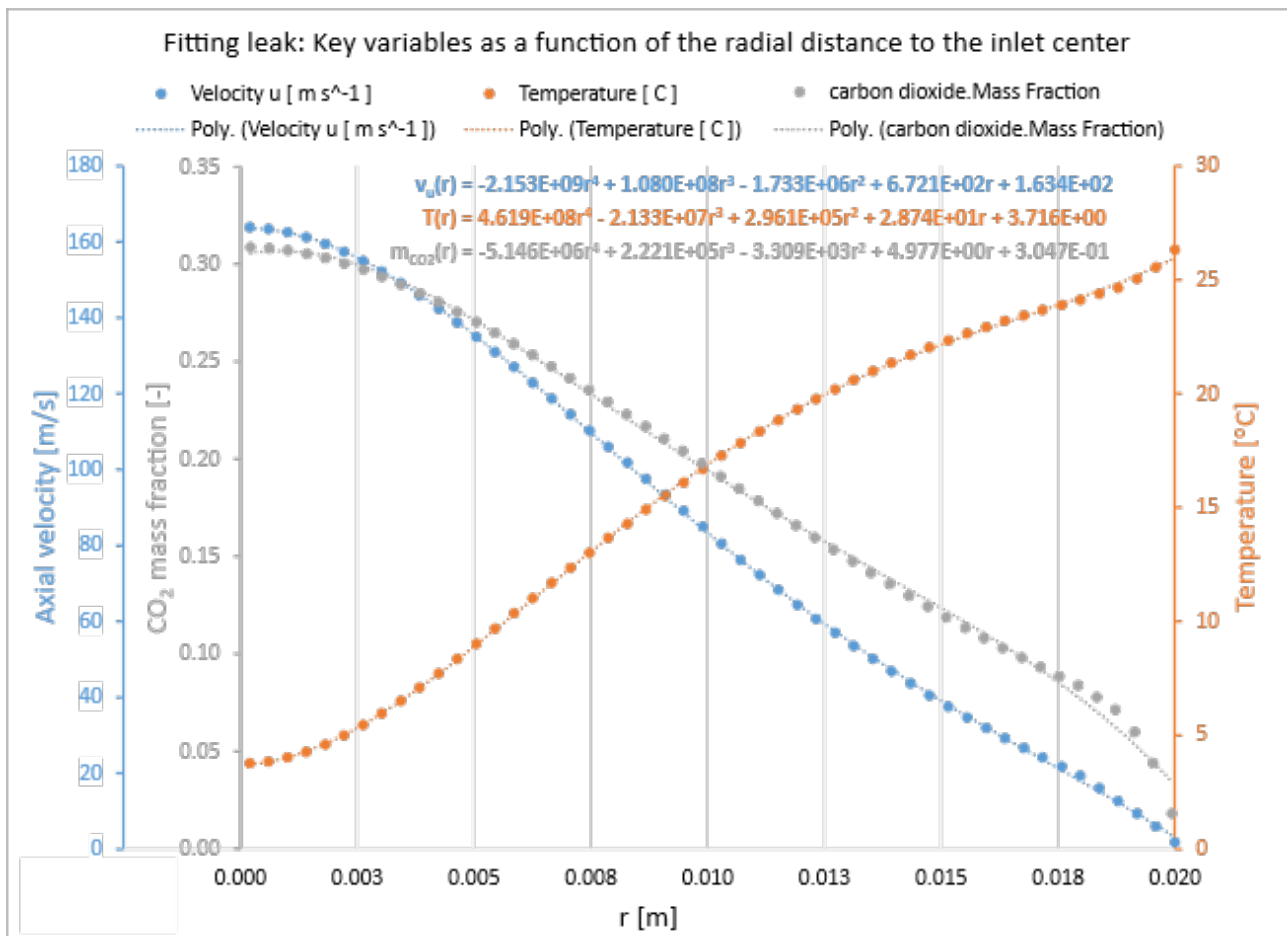
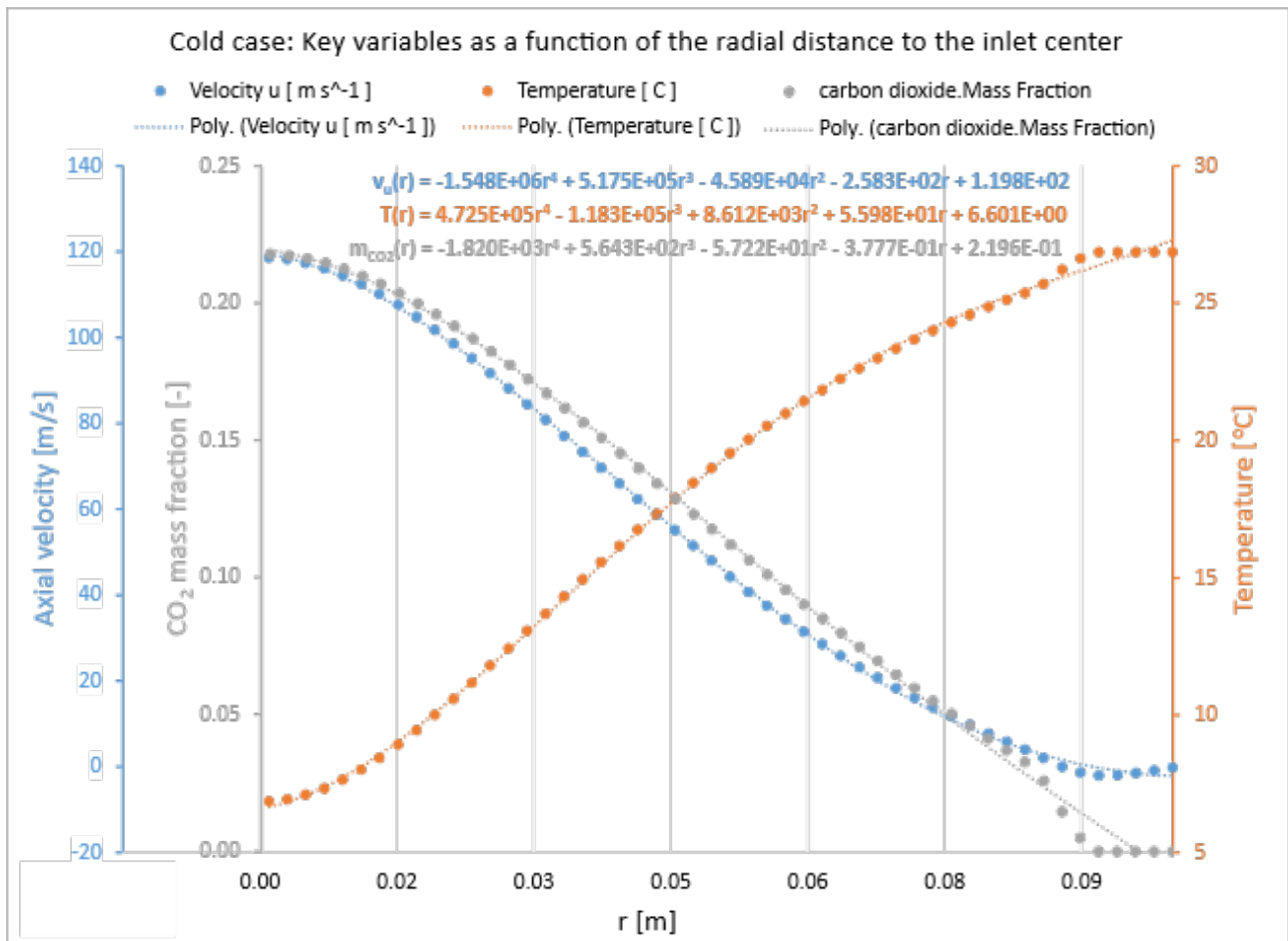


Figure 5.22: Fitted 2D profiles via minimum squared method for the fitting leak case.



**Figure 5.23:** Fitted 2D profiles via minimum squared method for the cold overpressure case.

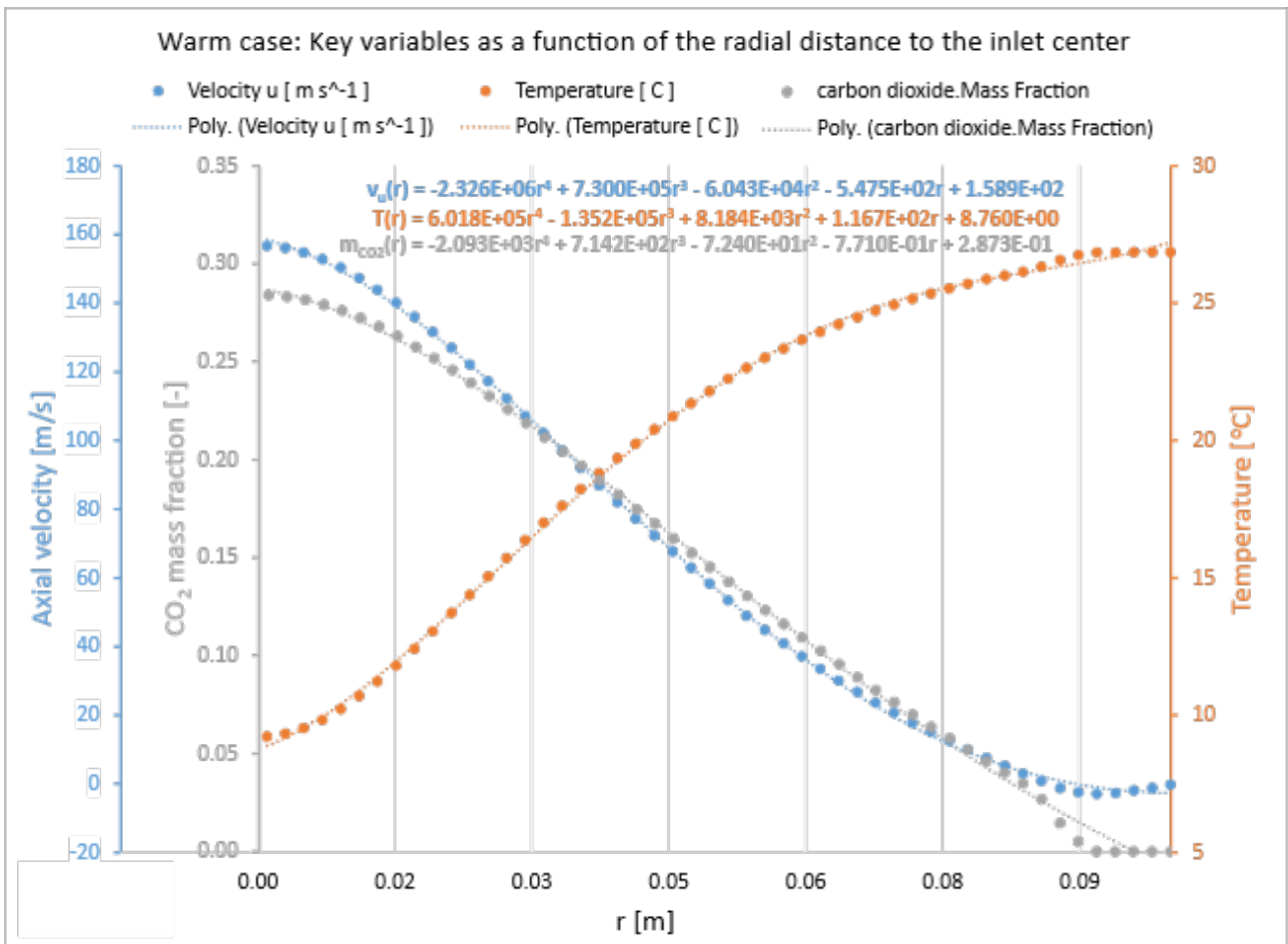


Figure 5.24: Fitted 2D profiles via minimum squared method for the warm overpressure case.

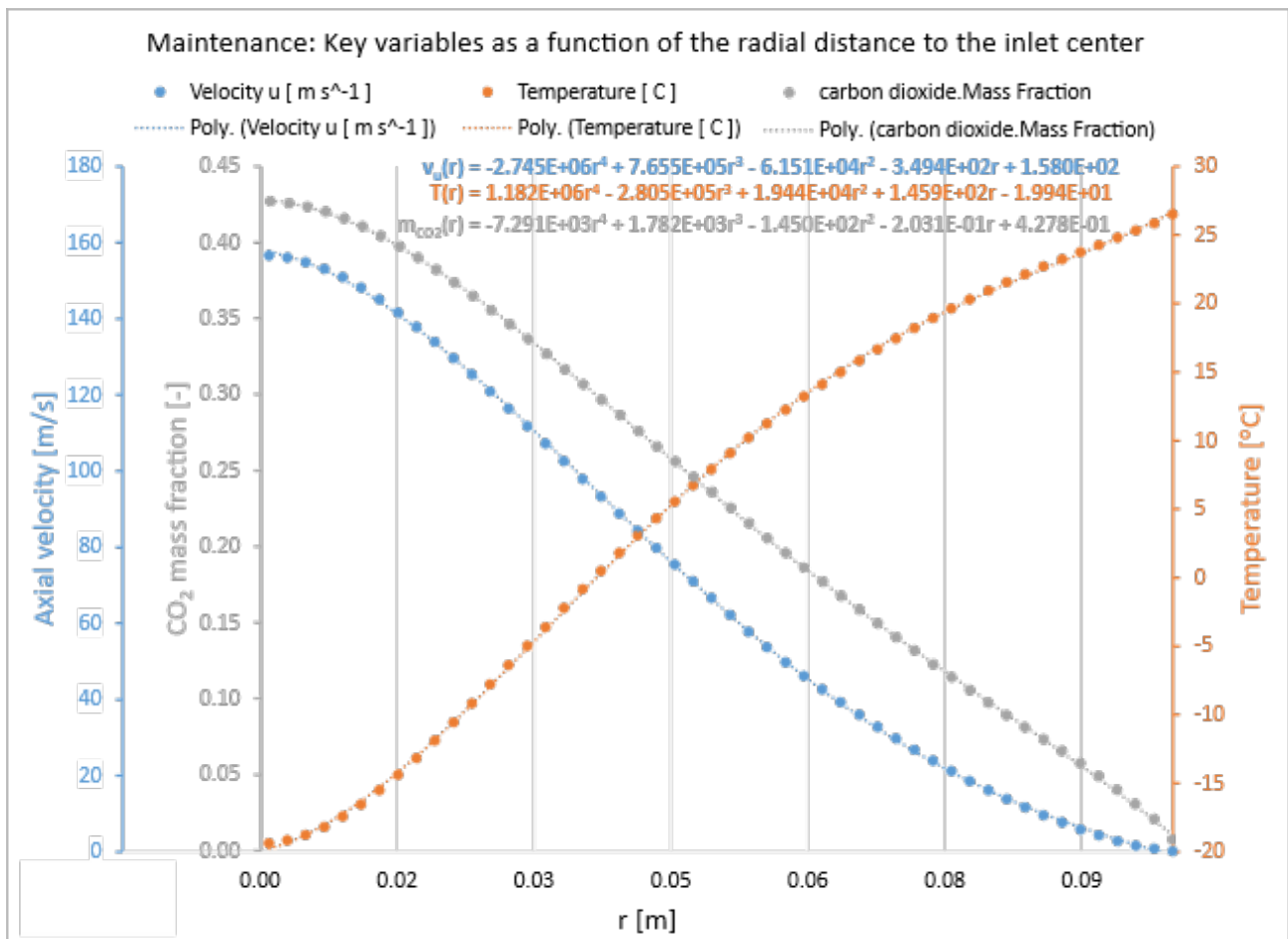


Figure 5.25: Fitted 2D profiles via minimum squared method for the maintenance case.

### 5.3.2. Sim. 1: Fitting leak at Vacuum Tank

The fitting leak is a type of leak that could happen at the Vacuum Tank, as studied by CMS Safety Team. This type of leak is triggered due to an inappropriate fitting, meaning that normally, no worker would be standing at the vicinity of the leak point.

The amount of carbon dioxide present that can be potentially released is much higher than the release rate in this leakage scenario, meaning that the depletion and end of leak will happen at around two weeks after the initial release. Due to the reaction time of the safety team being much quicker (usually minutes), the steady-state case will be considered. In case of important threats, which are not expected, a transient simulation for the first minutes of the release will be performed.

Figure 5.26 shows a contour of the carbon dioxide concentration within a vertical section of the cavern intersecting the entire longitude of the detector. As it was expected the fitting leak, due to the small release rate, does not pose a threat to any workers in the rest of the underground cavern.



**Figure 5.26:** Contour of carbon dioxide concentration in the vicinity of the vacuum tank of CMS in its open configuration (fitting leak case). There is no threat to workers in the cavern, with the leakage spreading about a meter from the leakage point.

Important to notice here is that, due to the fact of the release not spreading to the rest of the cavern, the leakage can stay undetected. The results of this simulation show a clear direction: either a monitoring device shall be placed in the vicinity of the vacuum tank, or a close monitoring of the carbon dioxide reserves shall be made, or both. Only this way can ensure that this type of leakage can stay under control.

### 5.3.3. Sim. 2: Cold overpressure at X5

The cold overpressure is a type of leak that could happen in the case of an overpressure at the cold part of the cryogenic carbon dioxide line of the 2PACL system, as assessed by CMS Safety Team. Again, and as it will be the case for the warm overpressure, no worker is considered to be standing at the immediate vicinity of the release point.

In this case, a transient simulation will be performed to assess the release, as understanding the rapidity of the dissipation of the carbon dioxide plume after the stop of the release will be key to assessing the performance of the current ventilation system on the cavern.

In the graphics that follow (Figure 5.27 up to Figure 5.31) the transient behavior is described. It can be seen how the carbon dioxide plume rapidly spreads over the vertical column around 2 meters in diameter from the

leak point. From there, the behavior is stationary until the cut-off of the release. After the carbon dioxide inflow stops, the ventilation system of the cavern is able to dissipate the potentially threatening concentrations of carbon dioxide in a matter of less than 5 seconds.

For the workers that could be in the immediate vicinity of a leakage point of this category, the following security measures need to be imposed:

- Every worker must carry his/her own Oxygen Deficiency Hazard (ODH) detector. In addition to the ones that are strategically placed at different locations in the cavern.
- Every worker must be trained in terms of evacuation pathways. In case of a release, the worker shall immediately evacuate.
- If works are to be done in a place where the evacuation pathways could become compromised. The worker must be trained in the usage of a self-rescue mask. In case of a release, the worker shall move away from the danger, put on the self-rescue mask, and evacuate immediately.

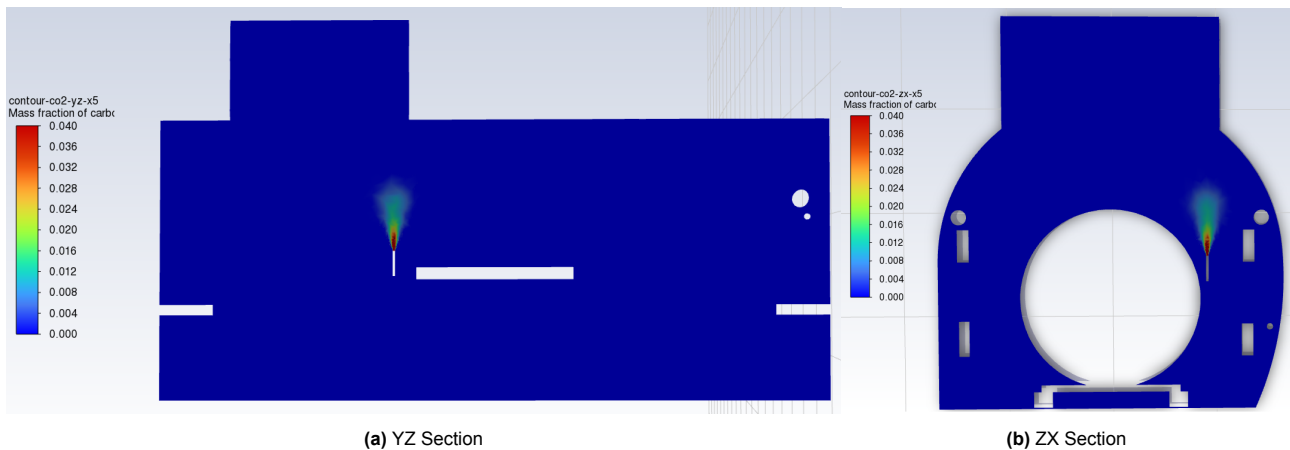


**Figure 5.27:** Carbon dioxide concentration contour in the CMS underground cavern: 1 s after the leak is initiated (cold overpressure case). Plume reaches about 2 meters height.

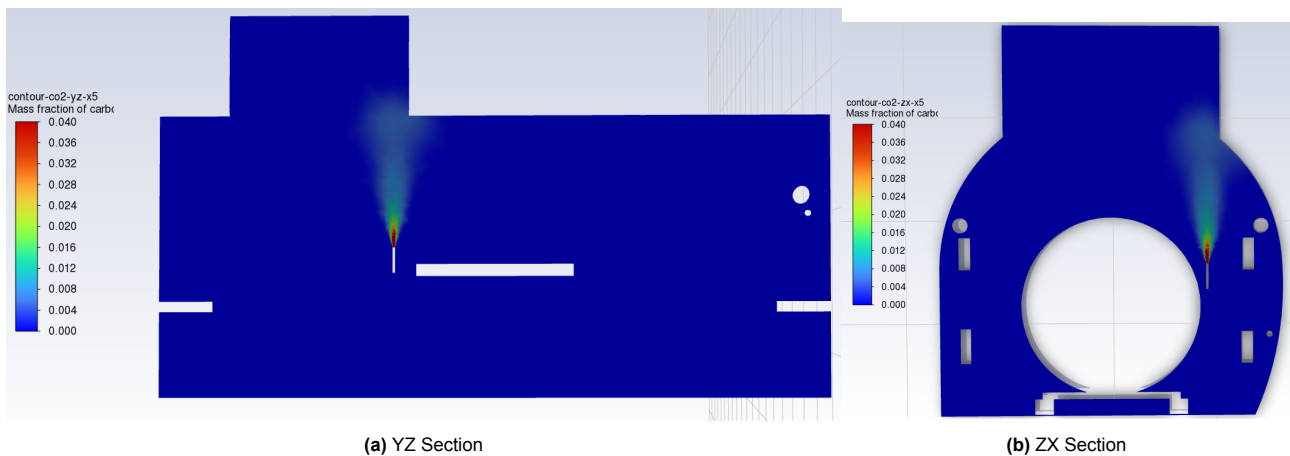


**Figure 5.28:** Carbon dioxide concentration contour in the CMS underground cavern: 5 s after the leak is initiated (cold overpressure case). Plume spreads up to ceiling of the cavern.

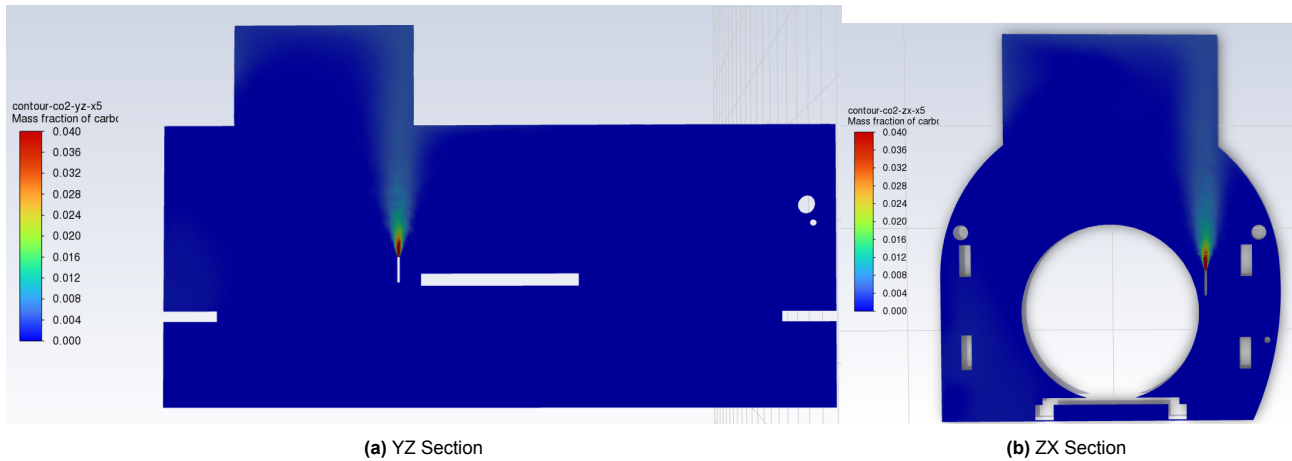


**Figure 5.29:** Carbon dioxide concentration contour in the CMS underground cavern: Steady-state behavior after the leak is initiated (cold overpressure case). Plume is spread up to ceiling of the cavern.

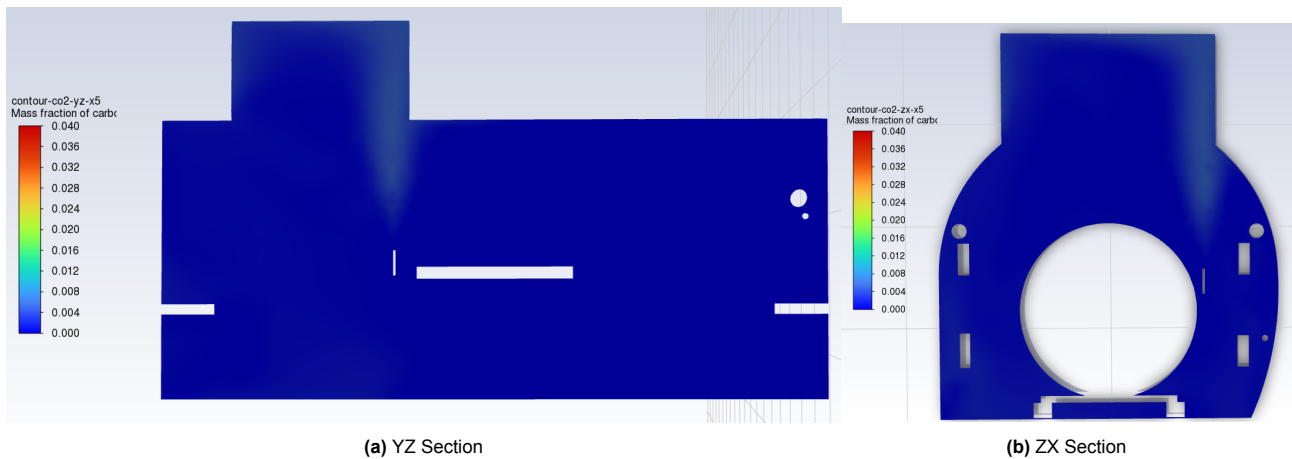


**Figure 5.30:** Carbon dioxide concentration contour in the CMS underground cavern: 1 s after the closure of the leak point (142 s) (cold overpressure case). Vicinity of the leak point is quickly dissipated.

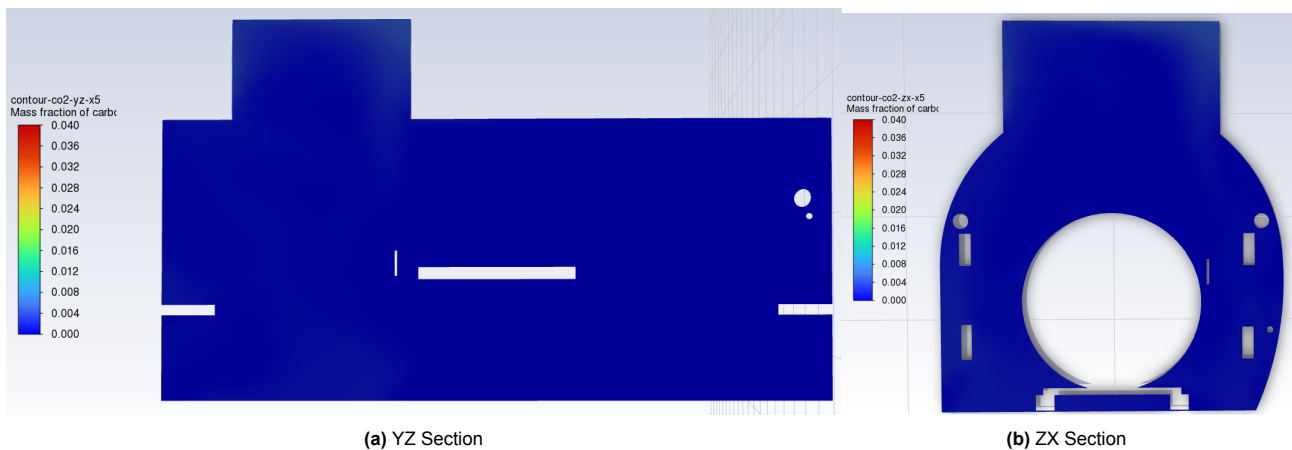


**Figure 5.31:** Carbon dioxide concentration contour in the CMS underground cavern: 5 s after the closure of the leak point (146 s) (cold overpressure case). Carbon dioxide has been appropriately dissipated from the cavern thanks to the ventilation system.

#### 5.3.4. Sim. 3: Warm overpressure at X0

After the assessment of the leakage cases in the upper part of the cavern, the floors under it are assessed. This part of the underground cavern consists of two semi-floors (X0 and X0.5) with fewer fresh-air inflow from the ventilation system. In addition, the buoyancy effect on the carbon dioxide, which will sink due to its higher molecular weight, is expected to hinder the evacuation of it, as the extraction outlets are situated at the top of the floors. Therefore, in this area there is a major threat to be expected.

The first case to be analysed is the warm overpressure at X0. This overpressure is to be triggered at the part of the carbon dioxide cryogenic cooling line that already extracted heat from the electronics, thus being warmer. However, as seen by the 2D simulations, the release remains to be aggressive. Again a transient simulation is to be done to properly assess the spread of carbon dioxide through the underground floors.

In the following graphics (Figure 5.32 up to Figure 5.36) the transient behavior is depicted. The contours of carbon dioxide concentration are shown in perpendicular vertical planes at the leakage point plus an additional horizontal plane that is located at the average nose-mouth height of a worker so that the threat is meaningfully addressed. It can be seen how in a matter of less than 10 seconds, the central part of the floor reaches potentially dangerous carbon dioxide concentrations. The case keeps getting worse up to the point that before the leak turning off, the main part of the underground floor has life-threatening concentrations of carbon dioxide all around. After the leakage running out of carbon dioxide, the concentration diminishes rapidly. However, even 1 minute after the leak cutting off, the concentrations remain potentially dangerous for any worker in the area.

These results evidence a clear need for safety measures for any works to be done. In particular, the following security measures shall be imposed:

- Every worker must carry his/her own Oxygen Deficiency Hazard (ODH) detector. In addition to the ones that are strategically placed at different locations in the cavern.
- Every worker must be trained to follow clear evacuation pathways.
- Every worker must be trained to properly use a self-rescue mask. It must be easily accessible in all situations.
- In case of leakage, two different evacuations plans will happen in parallel depending on the position of the worker in relation to the leak point:
  - If the worker is in the vicinity of the leak point, that is: the central room and/or within 3 meters of the leakage point. He/she will notice the leak, either by own awareness or by his/her personal ODH alarm being triggered. He must immediately evacuate triggering as well the ODH alarm if it was not yet the case.
  - If the worker is not in the vicinity of the leak point, he/she will notice the leak thanks to the ODH alarm being triggered. Being further away gives ample time to react by using the self-rescue mask. Once the mask is on, he/she must immediately evacuate the area.

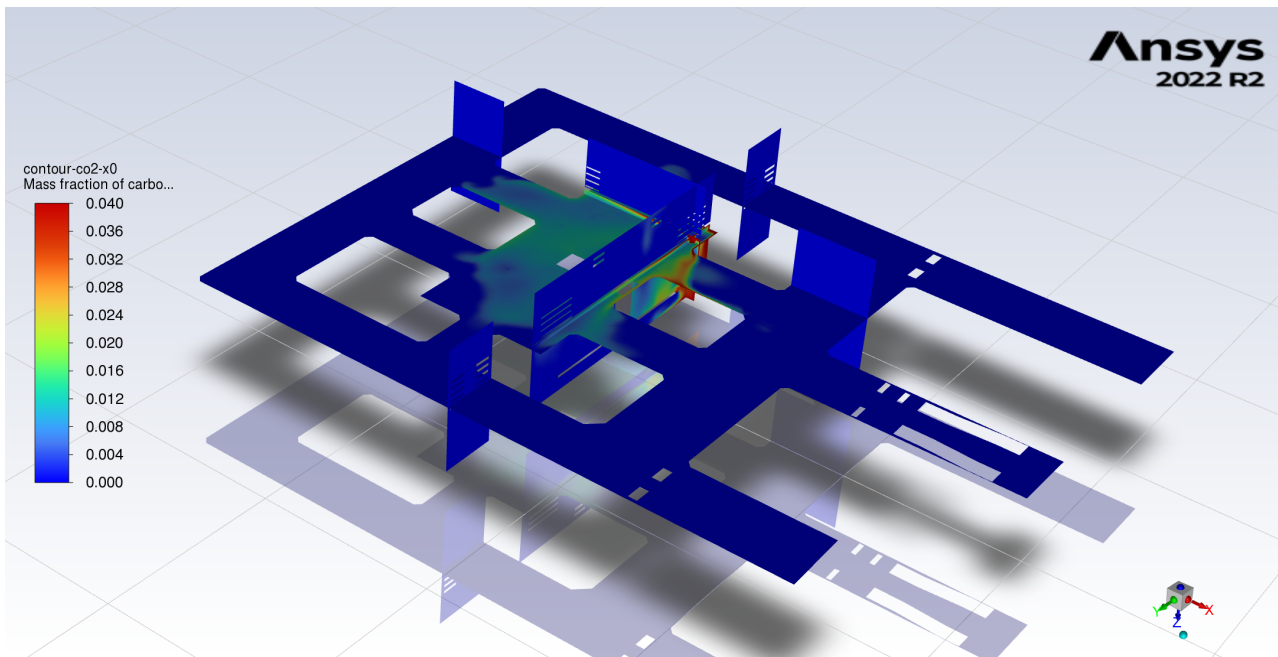


**Figure 5.32:** Contour of carbon dioxide concentration in the underground floors of the CMS cavern (X0 and X0.5): 5 s after the leak is initiated in the X0 floor (warm overpressure case). Carbon dioxide spreads over the central space.

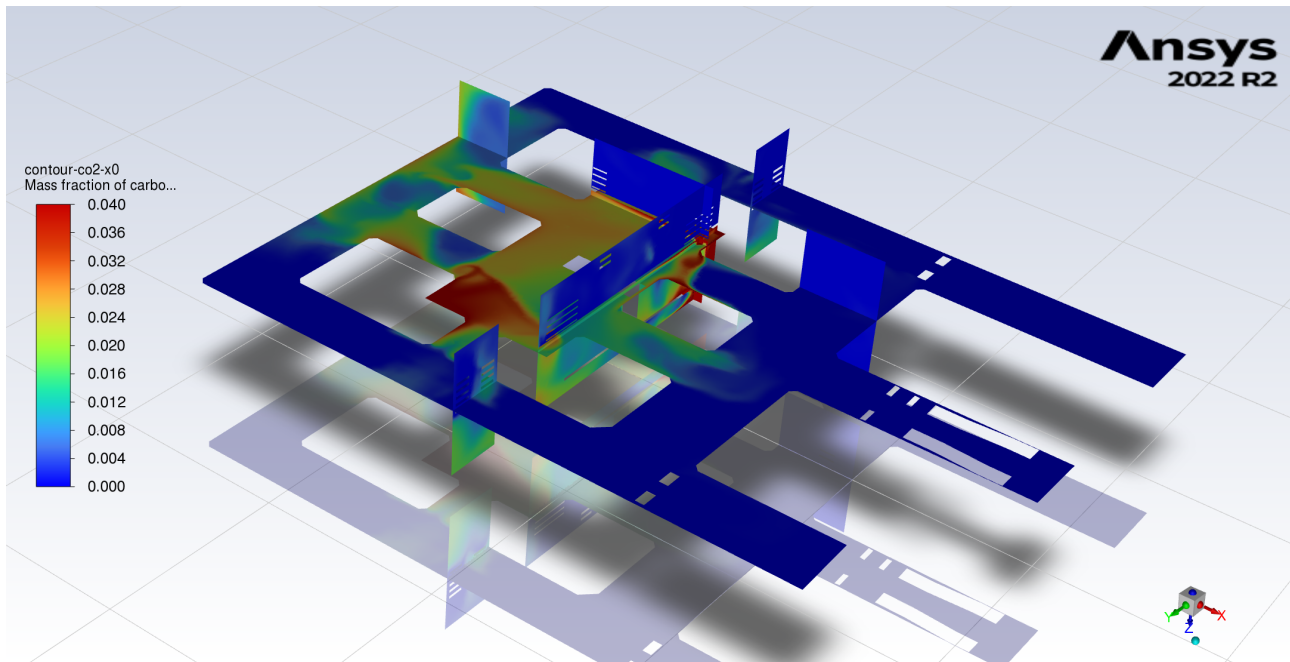


**Figure 5.33:** Contour of carbon dioxide concentration in the underground floors of the CMS cavern (X0 and X0.5): 30 s after the leak is initiated in the X0 floor (warm overpressure case). Carbon dioxide is fully spread over the central space.

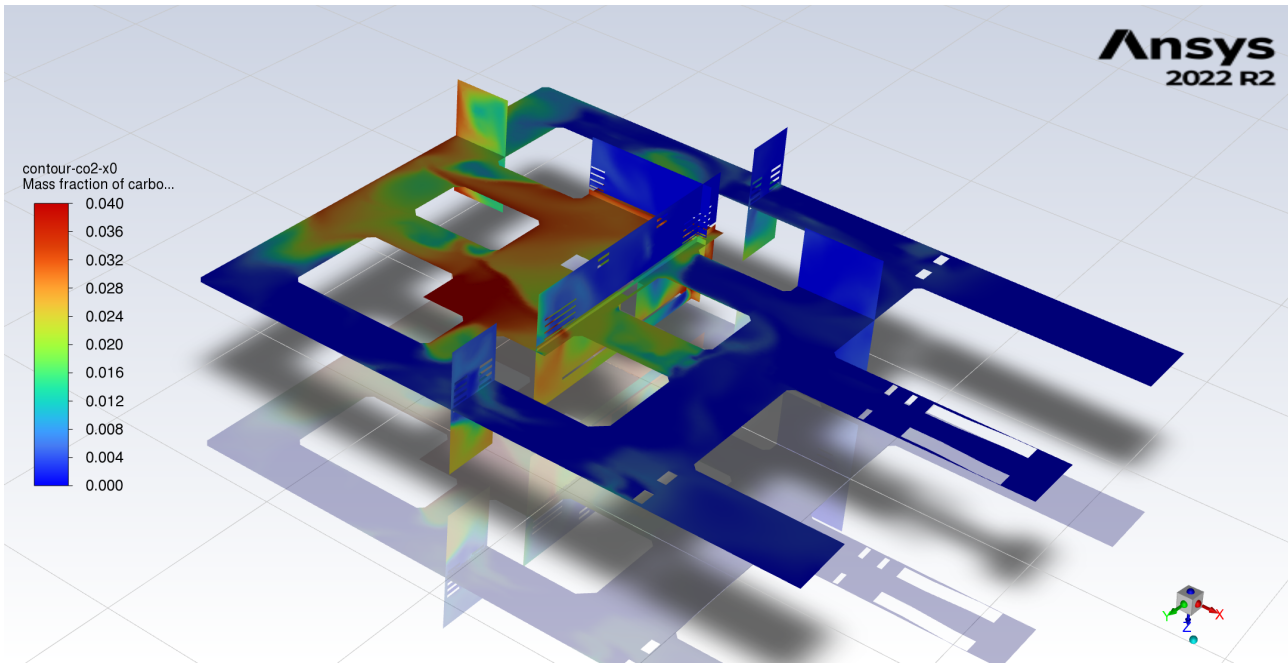


**Figure 5.34:** Contour of carbon dioxide concentration in the underground floors of the CMS cavern (X0 and X0.5): 1 s after the leak is closed in the X0 floor (warm overpressure case). Worst event, carbon dioxide reaches life-threatening concentrations in the entire central area.

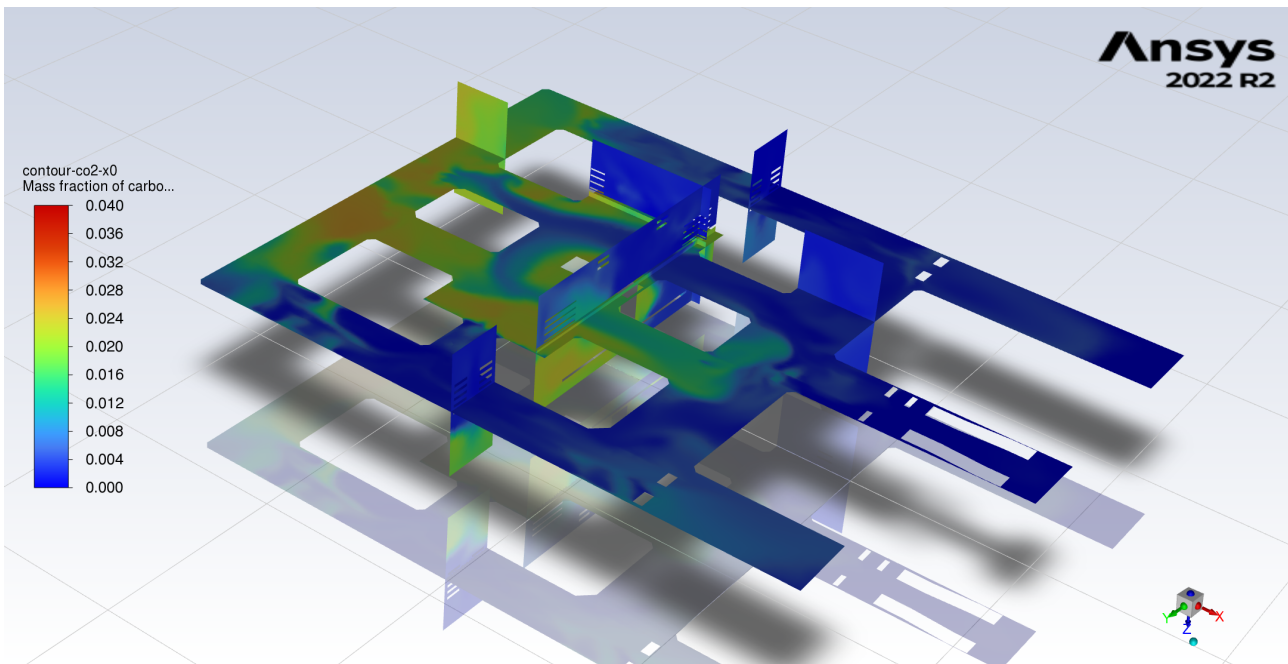


**Figure 5.35:** Contour of carbon dioxide concentration in the underground floors of the CMS cavern (X0 and X0.5): 30 s after the leak is closed in the X0 floor (warm overpressure case). Carbon dioxide has dissipated but the concentrations remain dangerous.

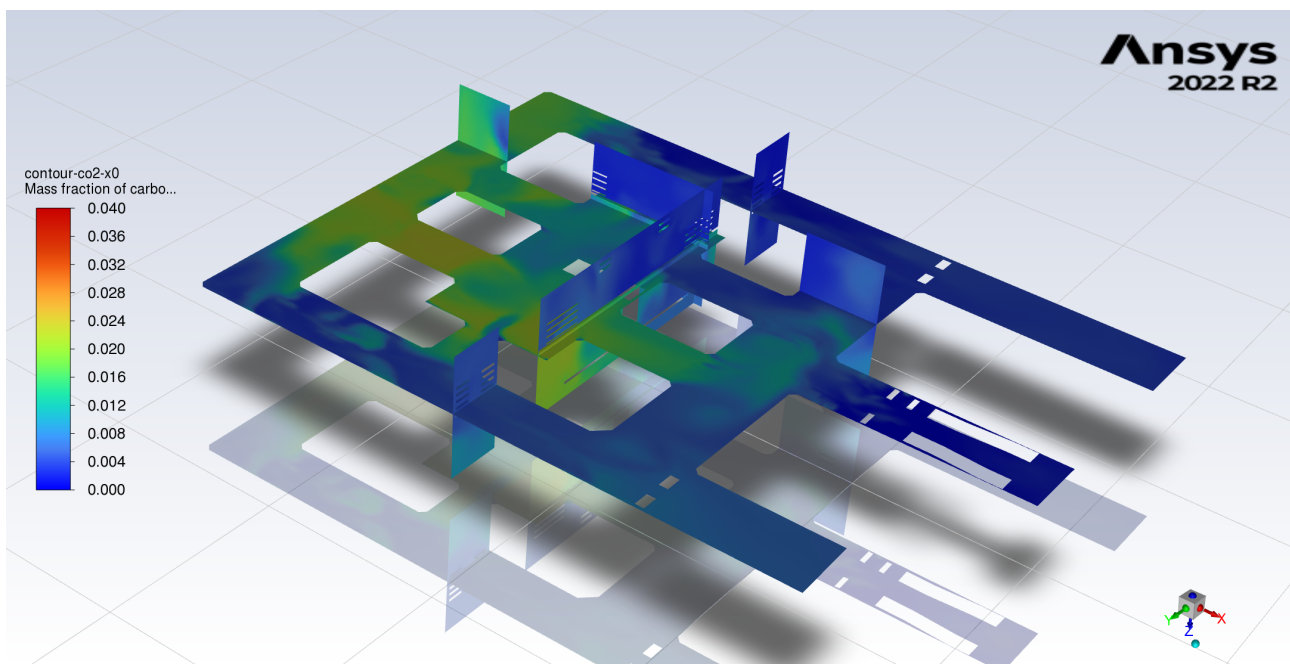


**Figure 5.36:** Contour of carbon dioxide concentration in the underground floors of the CMS cavern (X0 and X0.5): 60 s after the leak is closed in the X0 floor (warm overpressure case). Carbon dioxide dissipation occurs at a low rate, the concentrations remain dangerous.

### 5.3.5. Sim. 4: Warm overpressure at X0.5

As it has been shown, the warm overpressure case poses an imminent threat to life in the underground cavern. The same leakage case is analysed now in the X0.5 floor, in order to assess the threat and verify that the danger is not spreading to the rest of the cavern.

In the graphics below (Figure 5.37 up to Figure 5.41) the transient behavior is shown. The contours of carbon dioxide concentration are once again shown in perpendicular vertical planes at the leakage point plus an additional horizontal plane that is located at the average nose-mouth height of a worker so that the threat is meaningfully addressed. The observed behavior is similar to the previous case: in a matter of less than 10 seconds, the central part of the floor reaches potentially dangerous carbon dioxide concentrations. The case keeps getting worse up to the point that before the leak turning off, the main part of the underground floor has life-threatening concentrations of carbon dioxide all around. After the leakage running out of carbon dioxide, the concentration diminishes rapidly. However, even 1 minute after the leak cutting off, the concentrations remain potentially dangerous for any worker in the area.

In this case, the results again emphasized the importance for safety measures for any works to be done. In particular, the same safety measures explained for the works to be carried at X0 apply for the works at X0.5.

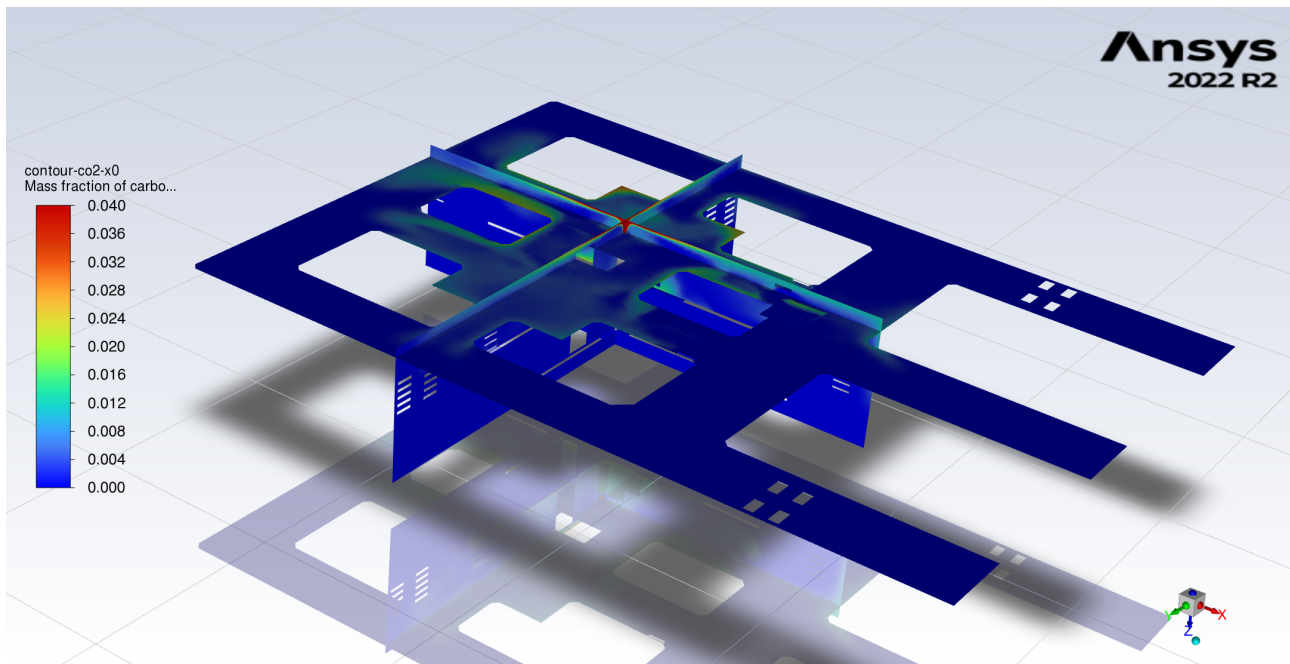


**Figure 5.37:** Contour of carbon dioxide concentration in the underground floors of the CMS cavern (X0 and X0.5): 5 s after the leak is initiated in the X0.5 floor (warm overpressure case). Carbon dioxide spreads over the central space.

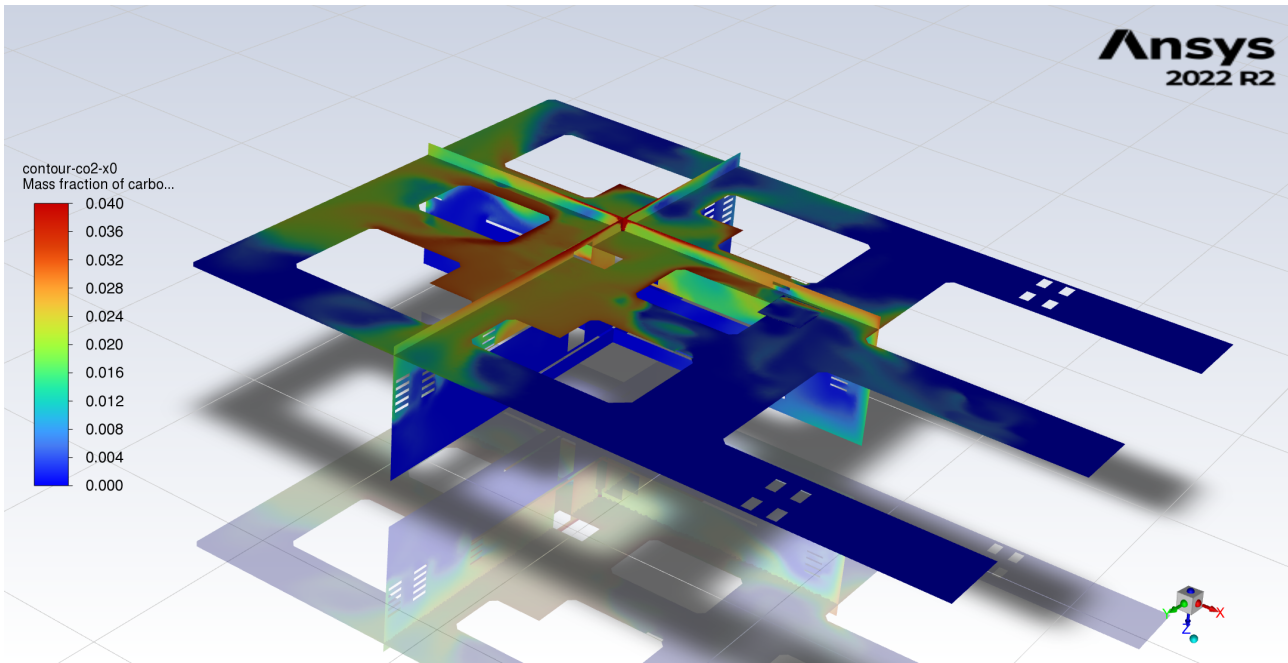


**Figure 5.38:** Contour of carbon dioxide concentration in the underground floors of the CMS cavern (X0 and X0.5): 30 s after the leak is initiated in the X0.5 floor (warm overpressure case). Carbon dioxide is fully spread over the central space.

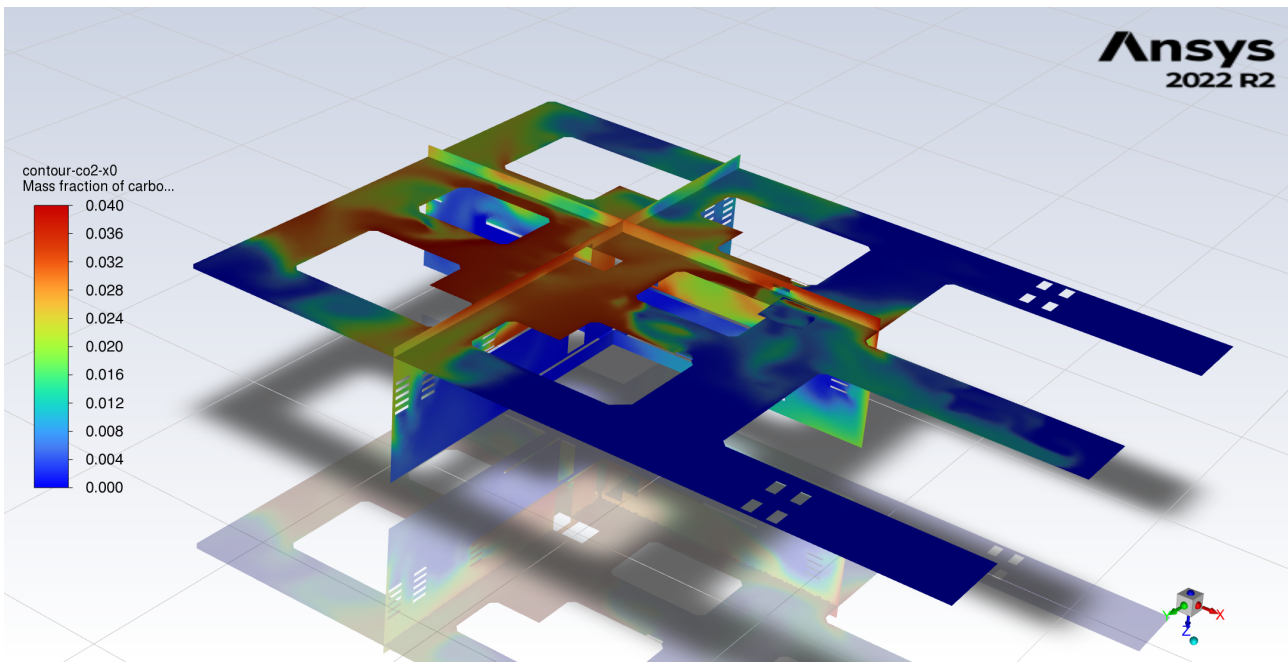


**Figure 5.39:** Contour of carbon dioxide concentration in the underground floors of the CMS cavern (X0 and X0.5): 1 s after the leak is closed in the X0.5 floor (warm overpressure case). Worst event, carbon dioxide reaches life-threatening concentrations in the entire central area.

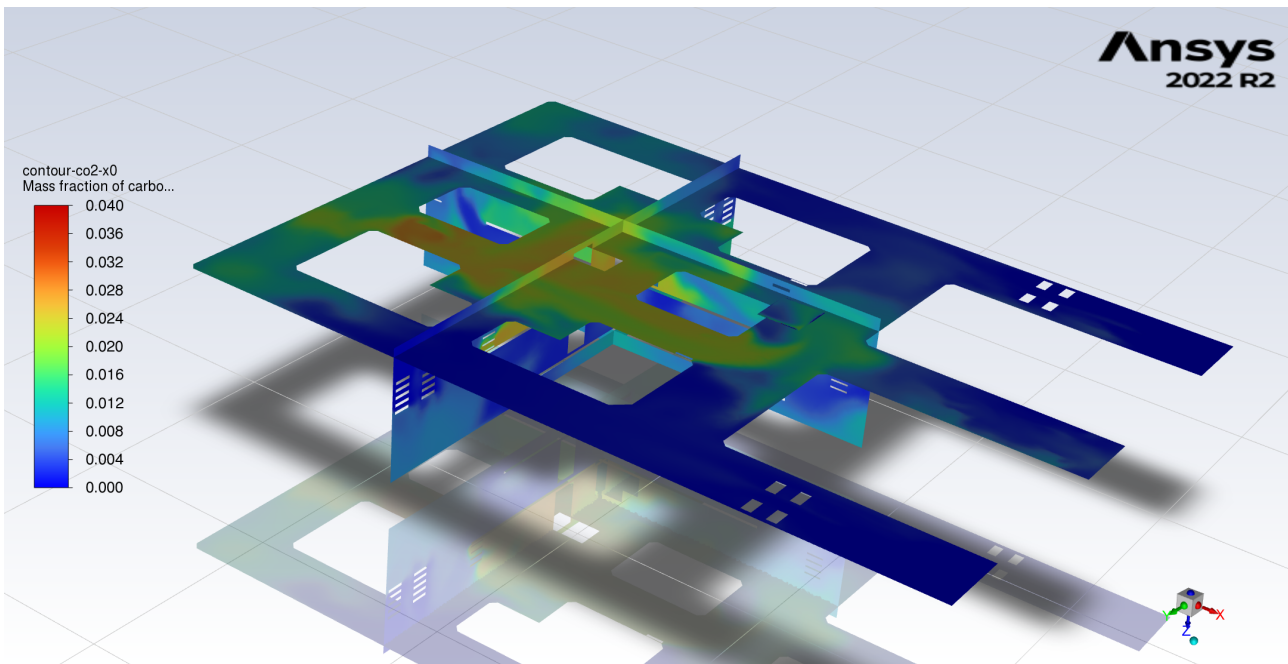


**Figure 5.40:** Contour of carbon dioxide concentration in the underground floors of the CMS cavern (X0 and X0.5): 30 s after the leak is closed in the X0.5 floor (warm overpressure case). Carbon dioxide has dissipated but the concentrations remain dangerous.

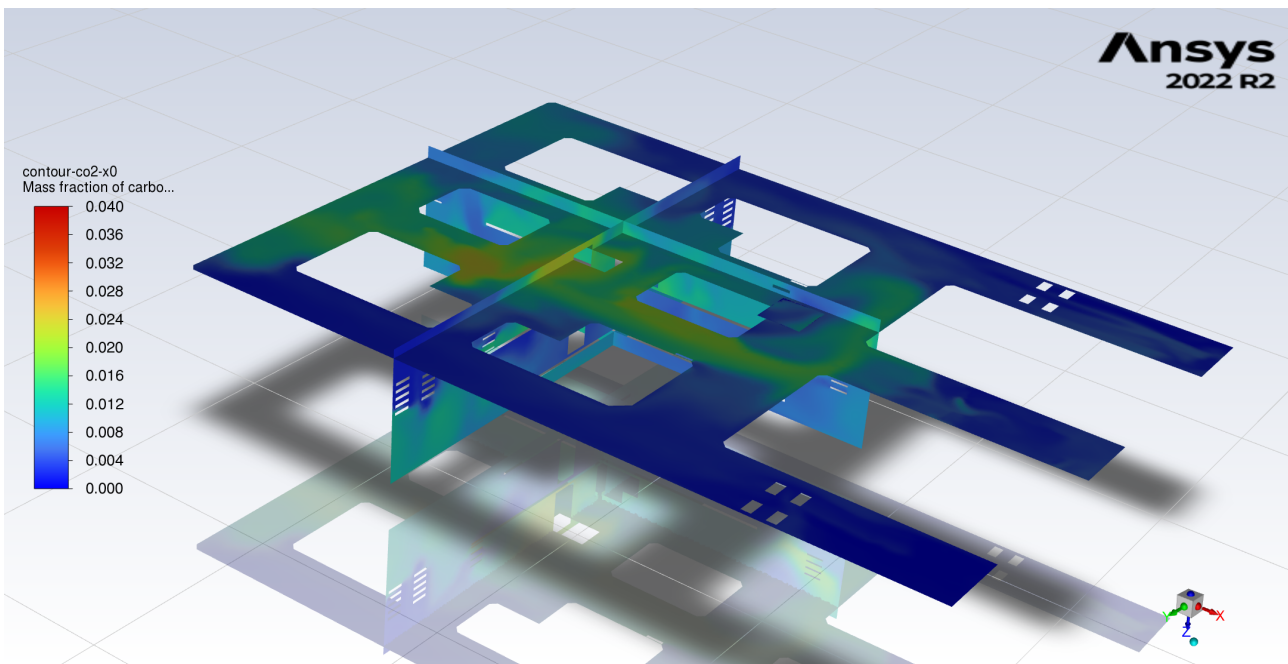


**Figure 5.41:** Contour of carbon dioxide concentration in the underground floors of the CMS cavern (X0 and X0.5): 60 s after the leak is closed in the X0.5 floor (warm overpressure case). Carbon dioxide dissipation occurs at a low rate, the concentrations remain dangerous.

### 5.3.6. Sim. 5: Maintenance at X0

Finally, the maintenance case is studied at the most threatening location. This case is particularly dangerous, as this type of leak is thought to be caused directly by a worker, meaning that he/she would be exposed to the threat from the very beginning and would need to be able to react, which implies that a standardised procedure must be in place in order to keep the safety of the individuals working in the area.

Following this description, the transient behavior is graphically depicted (Figure 5.42 up to Figure 5.46). Once again, the contours of carbon dioxide concentration are shown in perpendicular vertical planes at the leakage point plus an additional horizontal plane that is located at the average nose-mouth height of a worker. It is shown how this condition is really aggressive, resulting in spreading, in threatening concentrations, in a diameter of 4 meters, in just the first 3 seconds. Fortunately, the leak quickly stops and the dissipation reaches safe levels in around 10 seconds after the cut off (less than 15 seconds of total time).

Even though this case is classified as less dangerous than the warm overpressure, it still carries a powerful threat. In this case, there is not enough reaction time to use a self-rescue mask. The leak will immediately be noticed by the worker, and the his/her response shall be to evacuate as soon as possible, instinctively holding breath for a few seconds. Other workers in the area must evacuate the place following the most convenient pathways, following a previously developed evacuation plan.

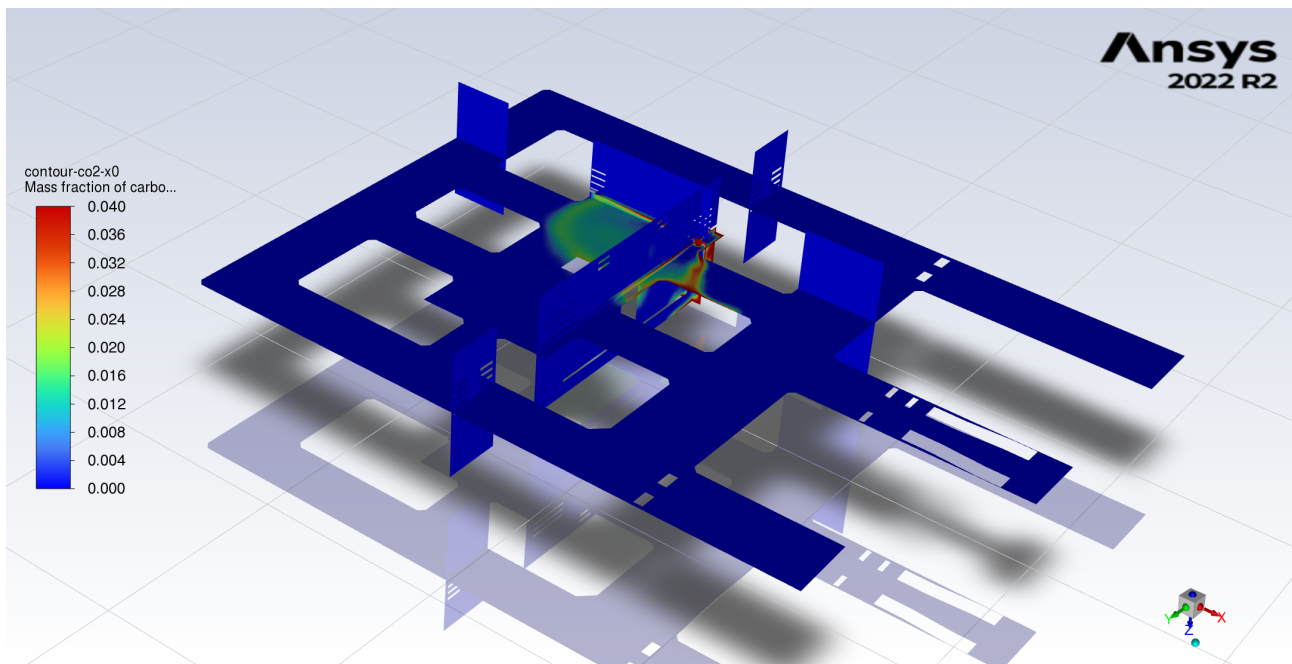


**Figure 5.42:** Contour of carbon dioxide concentration in the underground floors of the CMS cavern (X0 and X0.5): 1 s after the leak is initiated in the X0 floor (maintenance case). Carbon dioxide aggressively spreads.

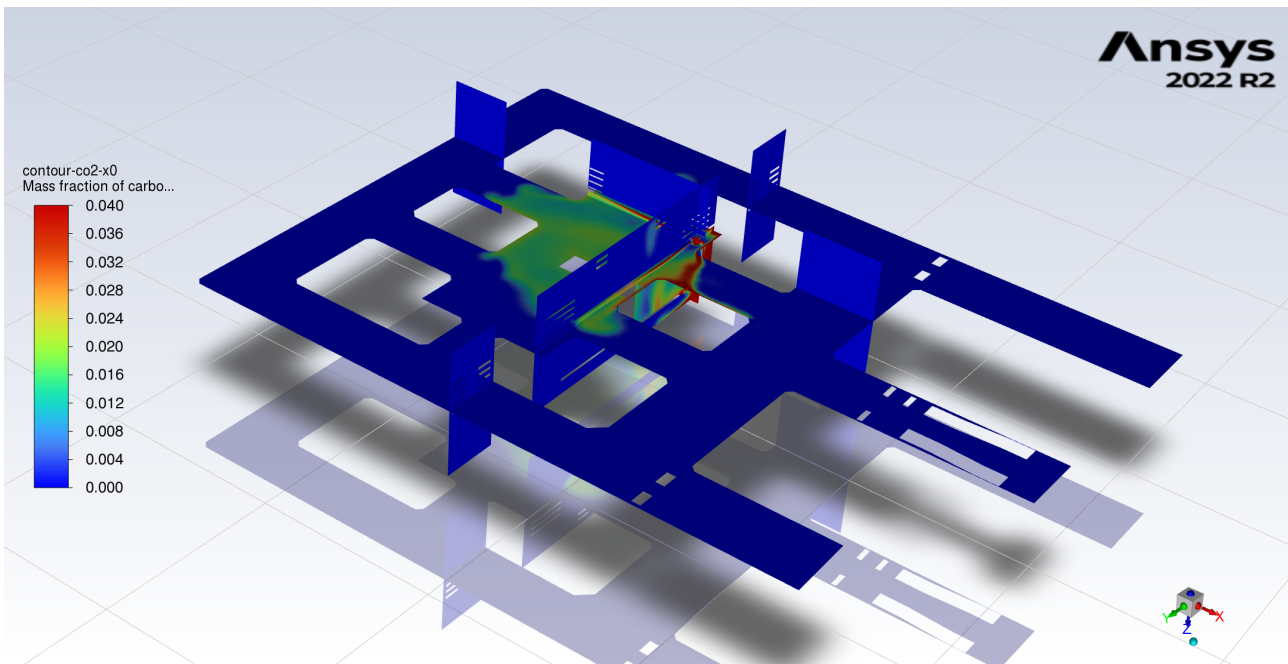


**Figure 5.43:** Contour of carbon dioxide concentration in the underground floors of the CMS cavern (X0 and X0.5): 3 s after the leak is initiated in the X0 floor (maintenance case). Carbon dioxide reaches its maximum spread.

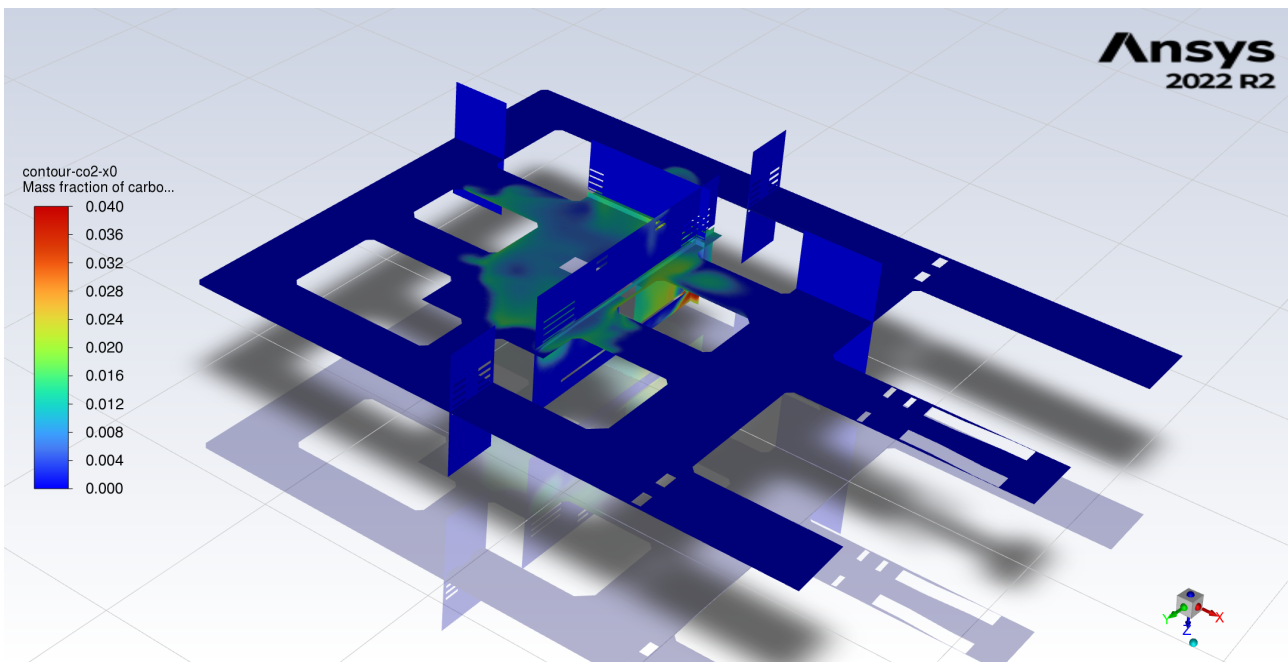


**Figure 5.44:** Contour of carbon dioxide concentration in the underground floors of the CMS cavern (X0 and X0.5): 2 s after the leak is closed in the X0 floor (maintenance case). Concentrations diminish quickly from the peak event.

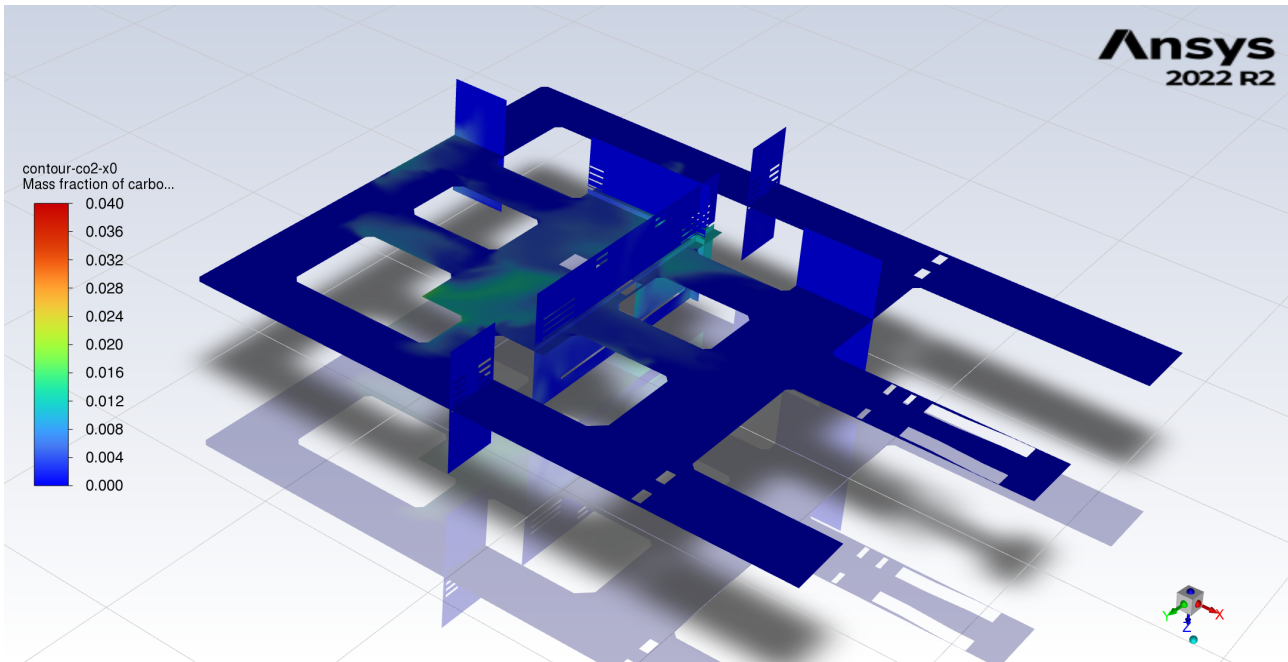


**Figure 5.45:** Contour of carbon dioxide concentration in the underground floors of the CMS cavern (X0 and X0.5): 10 s after the leak is closed in the X0 floor (maintenance case). Carbon dioxide has dissipated and the concentrations are less dangerous.

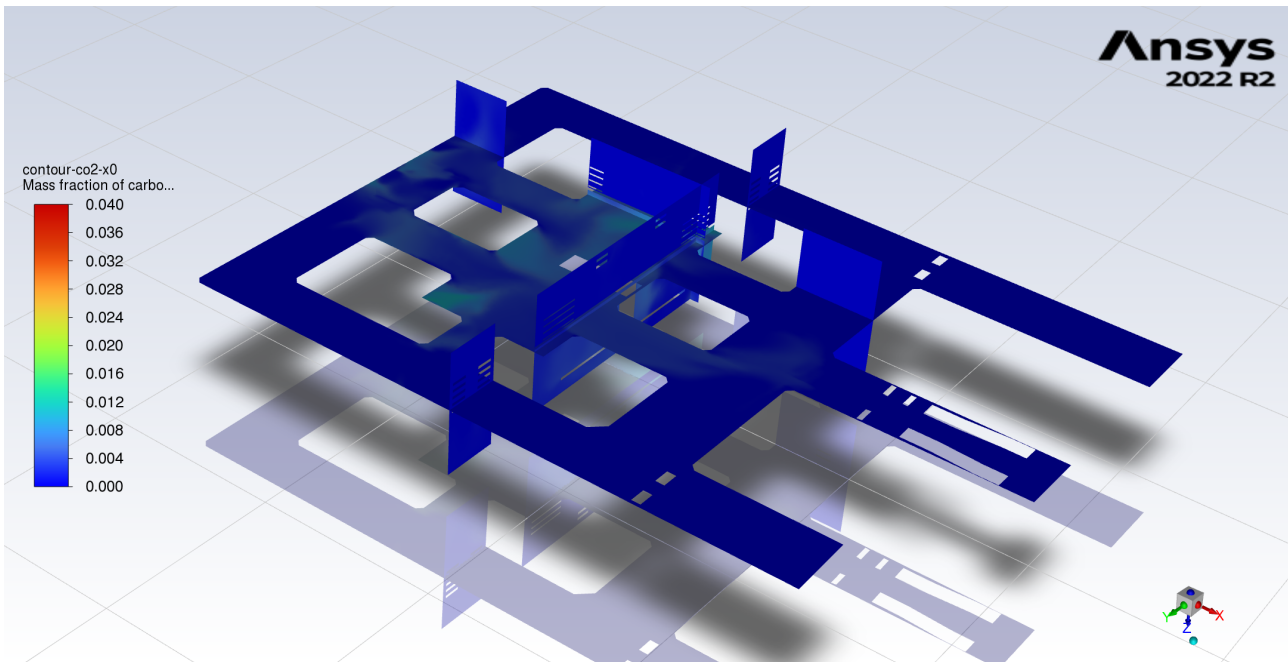


**Figure 5.46:** Contour of carbon dioxide concentration in the underground floors of the CMS cavern (X0 and X0.5): 30 s after the leak is closed in the X0 floor (maintenance case). Carbon dioxide is almost fully dissipated and there is no danger in the area.

# 6

## Discussion

The goals of this thesis were to:

- Understand leakage dynamics in two-phase cooling systems.
- Assess the effectiveness of current ventilation systems in the CMS experimental cavern.
- Study any potential health and safety risks for workers in the area after a coolant leakage.

The results presented have successfully addressed the research questions that were presented in chapter 3.

Firstly, with regards of the leakage dynamics in two-phase cooling systems, it has been demonstrated that the shock expansion has an extremely aggressive behavior, that is confined to a maximum of 30 centimeters from the leak point. The initial conditions of the leaked coolant are of lesser importance, given that after the shock expansion, the state of the fluid will be much milder in comparison, smoothing the differences in initial leak conditions coming from different leak scenarios. Additionally, it has been verified that the expansion is extremely fast at the beginning, leaving just a short reaction time, showing the need for a thorough evacuation plan plus safety measures to be imposed. Direct answers to the research questions:

- RQ1: The shock expansion manifests as an aggressive burst confined to the closest region (in the order of decimeters from the leakage point). Immediate physical effects include the possible formation of dry ice due to the extremely low temperature.
- RQ2: Initial conditions show little correlation with the expansion of the vapor cloud. Different conditions leading to shock expansions show a similar shock wave even though initial conditions can differ by a larger amount.
- RQ3: In open areas, coolant dispersion is achieved within seconds. However, in smaller areas such as the underground floors, coolant dispersion needs several minutes to reach safe levels.

Secondly, with respect to the effectiveness of the ventilation system to deal with the different scenarios, it has been shown how the fresh-air inflow is sufficient to keep a safe atmosphere within the main part of the cavern (floors X1 to X5) for every leak scenario in different locations. The very high volume of air present in the cavern, compared to the amount of carbon dioxide release, contributes to diminishing the oxygen deficiency hazard. Besides, the ventilation system allows for a quick dissipation of the leaked coolant within the first 30 seconds. Direct answers to research questions:

- RQ4: Within the main floors of the cavern (X1 to X5), the coolant can be evacuated by the current ventilation system in the order of tens of seconds. The underground (floors X0 and X0.5) show worse effectiveness of the current ventilation system, with several minutes needed to reach a safe local atmosphere.
- RQ5: The ventilation on the cavern is setup so that the air is moved from the bottom to be extracted at the top. This is made by having fresh air inlets at the bottom. Fresh air gets warmer and buoyancy effects lead this mass to the top of the cavern, where the outlets are located. Carbon dioxide has a higher density when compared to air, meaning that it will tend to go to the bottom of the cavern. This favours mixing with air, and coolant concentration drops rapidly. The highest concentrations of carbon dioxide are within the torrent coming from the leakage point.

The ventilation on the underground floors comes from the primary ventilation, and it is introduced in the cavern at a height of 2 meters from X0. There is only one extraction point that goes to the main cavern, the same place from where workers can access the underground. This situation explains the difficulties

in coolant dispersion. Fresh air is not coming from the bottom and lacks a clear direction, mixing is not enhanced and carbon dioxide plumes can establish rapidly and endure longer times.

- RQ6: The location and initial conditions of the leakage have little influence on the effectiveness of the ventilation. There are two differentiated parts within the cavern, X1 to X5 and X0 to X0.5 that are well and badly ventilated, respectively. The location of a leak show similar plumes if simulations are conducted in different zones of the same (well or badly ventilated) part of the cavern.
- RQ7: Ventilation on the main part of the cavern does not need any modifications. It delivers appropriate conditions in terms of temperature, pressure and humidity. Besides, it has been shown in this study that is well designed to protect against accidental releases of carbon dioxide. The lower part of the cavern however has a worse ventilation, that can keep appropriate environmental conditions, but cannot deal effectively with accidental releases. Specific modifications need to be studied if there is a need to reduce dispersion times and/or to facilitate the performance of workers in the area. Some modifications that can be studied are: higher airflow rates, more fresh air inlets, different positioning of inlets, more outlets, or using fans in strategic points.

Thirdly, in relation with the health and safety risk, the basement of the cavern (floors X0 and X0.5) has been demonstrated to be life-threatening in different leakage scenarios, if safety measures are not imposed. In particular, the worst case, a warm overpressure leak, will spread in less than 15 seconds through the entire main part of the basement. Clear safety measures are imposed to every worker who needs to perform any kind of works in floors X0 and X0.5. Direct answers to the research questions:

- RQ8: 4% of carbon dioxide in air is considered the threshold above which the average person will become unconscious. The oxygen deficiency monitors being used at CERN trigger an alarm at 1.6%, in accordance to safety regulations. In the event of an accidental release, peak concentrations reach occupational safety thresholds easily. Therefore, additional measures to eradicate risks are mandatory.
- RQ9: In the basement floors, hazardous conditions develop in just 15 seconds, which is the time that the plume needs to advance through most of the zones in the basements. In the local vicinity of the leakage, this time gets even smaller, so that trusting on a decent reaction time of a worker is not safe at all.
- RQ10: The only areas with the current ventilation that are susceptible to health and safety risks due to coolant accumulation are the basement floors. There is no sensitive equipment there, however, works are frequent during maintenance operations. Safety procedures will be imposed.
- RQ11: Evacuation can take place easily anywhere on the cavern, if only the safety measures recommended are imposed.

Finally, given the results obtained, the measures that need to be taken can be summarized as:

1. For every worker who is going to carry works at any place within the experimental cavern:
  - Every worker must carry his/her own Oxygen Deficiency Hazard (ODH) detector (being trained to do so). In addition to the ones that are strategically placed at different locations in the cavern.
  - Every worker must be trained to follow clear evacuation pathways depending on its position within the floors.
2. Additionally, for workers to be allowed to enter X0 and X0.5 floors, or specific locations within X1 to X5 with potentially compromised evacuation pathways:
  - Every worker must be trained to properly use a self-rescue mask. And, it must be easily accessible in all situations.
3. Lastly, for the fitting leak case:
  - A monitoring device for the amount of coolant shall raise an alarm for increased rate of depletion, giving notice that a fitting leak has likely happened at the vacuum tank.

Thanks to this study, in the framework of Hostlab Phase 2 updates, the safety measures in the CMS Experimental Cavern at CERN will be updated prior to its next phase, based on informed decisions coming from rigorous CFD analysis coming as a result of the collaboration between CERN and TU Delft via this master thesis.

## 6.1. Recommendations and Future Work

After the study conducted, there are three main areas that have been identified for future work to be performed. In this section, these research lines are explained and their priority and effort are discussed. Table 6.1 shows the different research lines to be followed.

**Table 6.1:** Recommendations and future work to be performed on the line of this study.

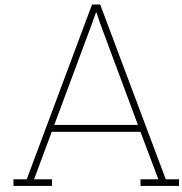
Research line	Given priority	Required effort
<b>Validation of CFD simulations via experimentation</b>	<b>Highest:</b> The conclusions extracted from the CFD simulations depend directly on the validation of the results. The highest priority for future work is thus to validate experimentally the results of the CFD simulations. This validation will allow as well for further experimentation to be performed. As explained in the next line of research, modifications of the current ventilation system shall be made to improve effectiveness. However, those simulations need a validated base. For this reason, validating the results obtained in this study is the highest priority.	<b>Highest:</b> Experimentation of this kind in the cavern is extremely restricted and complex. The most cost-effective way to perform this validation is through the development of a scaled model containing the regions of interest for the validation. Using a controlled environment with carbon dioxide detectors in strategic positions and performing a release will result in an analogous situation. This could be designed so that the simulations can be validated against experimental measurements.
<b>R&amp;D of modifications within the ventilation system in the basement of the cavern</b>	<b>Mid-priority:</b> The basement of the cavern remains to be the most hazardous place in UXC55. Workers need to follow strict health and safety rules so that risk is diminished. Improving the ventilation system there could enhance the ventilation in a way such that health and safety measures could be relaxed and an accidental release could be a less stressful situation specially for workers in the area. This research line has relevance as it will simplify the safety procedures and it will impact directly the maintenance work performed in the basement.	<b>Mid-effort:</b> Under a validated base of simulations, such as the ones performed on this study, more simulations shall be conducted varying different parameters of the ventilation system such as locations and flow-rates, as well as the addition of alternative ventilation system such as strategically positioned fans. The computational cost of performing this kind of simulations is high due to the amount of combinations that shall be tested over a complex computational model such as the one under study.
<b>Analysis of structural stresses and thermal effects in the leakage point</b>	<b>Lowest:</b> The violent burst occasioned after an accidental release of carbon dioxide in any of the scenarios studied can cause structural and thermal stresses to the equipment involved that have not been considered in this study. Understanding these stresses has some relevance, as even though it will not affect the health and safety measures, it will help to understand how to better protect the equipment and services provided to the detector so that they can withstand these kind of events.	<b>Lowest:</b> In order to perform these studies, experiments with cryogenic releases of carbon dioxide shall be made in a controlled environment and machinery.



# References

- [1] D. G. Gilmore. "Spacecraft Thermal Control Handbook, Volume I: Fundamental Technologies". In: 2002. URL: <https://api.semanticscholar.org/CorpusID:125023491>.
- [2] A. Colijn and B. Verlaat. "Evaporative CO<sub>2</sub> heat transfer measurements for cooling systems of particle physics detectors". In: 2010. URL: <https://api.semanticscholar.org/CorpusID:55655142>.
- [3] P. Zhang et al. "Review of recent developments on pump-assisted two-phase flow cooling technology". In: *Applied Thermal Engineering* (2019). DOI: 10.1016/J.APPLTHERMALENG.2018.12.169.
- [4] A. Delfini et al. "Development of a Two-Phase Flow Cooling System for Space Systems: design and ground research activity of Baridi-Sana Project". In: *2023 IEEE 10th International Workshop on Metrology for AeroSpace (MetroAeroSpace)* (2023), pp. 104–108. DOI: 10.1109/MetroAeroSpace57412.2023.10190009.
- [5] P. Tropea et al. "Advancements and plans for the LHC upgrade detector thermal management with CO<sub>2</sub> evaporative cooling". In: *Nuclear Instruments and Methods in Physics Research Section A: Accelerators, Spectrometers, Detectors and Associated Equipment* (2019). DOI: 10.1016/J.NIMA.2018.10.083.
- [6] P. Tropea et al. "CO<sub>2</sub> evaporative cooling: The future for tracking detector thermal management". In: *Nuclear Instruments & Methods in Physics Research Section A-accelerators Spectrometers Detectors and Associated Equipment* 824 (2016), pp. 473–475. DOI: 10.1016/J.NIMA.2015.08.052.
- [7] Z. Ling et al. "A hybrid thermal management system for lithium ion batteries combining phase change materials with forced-air cooling". In: *Applied Energy* 148 (2015), pp. 403–409. DOI: 10.1016/J.APENERGY.2015.03.080.
- [8] T. Zhang et al. "Two-phase refrigerant flow instability analysis and active control in transient electronics cooling systems". In: *International Journal of Multiphase Flow* 37 (2011), pp. 84–97. DOI: 10.1016/J.IJMULTIPHASEFLOW.2010.07.003.
- [9] D. T. Pollock, Z. Yang, and J. Wen. "Dryout avoidance control for multi-evaporator vapor compression cycle cooling". In: *Applied Energy* 160 (2015), pp. 266–285. DOI: 10.1016/J.APENERGY.2015.08.113.
- [10] T. Fielden. "Corrosion monitoring of cooling systems". In: *Anti-corrosion Methods and Materials* 22 (1975), pp. 12–15. DOI: 10.1108/EB006982.
- [11] E. Beynon, N. Cooper, and H. Hannigan. "Cooling System Corrosion in Relation to Design and Materials". In: *Corrosion* (1978). DOI: 10.4271/780919.
- [12] M. Shaeri, R. Bonner, and M. Ellis. "Thin hybrid capillary two-phase cooling system". In: *International Communications in Heat and Mass Transfer* 112 (2020), p. 104490. DOI: 10.1016/j.icheatmasstransfer.2020.104490.
- [13] C. Xiao et al. "Numerical simulation of liquid CO<sub>2</sub> accidental release at atmospheric environment". In: *IOP Conference Series: Earth and Environmental Science* 675 (2021). URL: <https://api.semanticscholar.org/CorpusID:234051394>.
- [14] K. Li et al. "An experimental investigation of supercritical CO<sub>2</sub> accidental release from a pressurized pipeline". In: *Journal of Supercritical Fluids* 107 (2016), pp. 298–306. URL: <https://api.semanticscholar.org/CorpusID:53689592>.
- [15] T. Guansa. "Simulating the Leakage Processes of Flammable Refrigerants from Cooling Systems". In: *Journal of Engineering Thermophysics* (2000).
- [16] A. Yatim et al. "Risk Assessment of Flammable Natural Refrigerant Application in Air Conditioning Systems". In: *2022 IEEE International Conference on Industrial Engineering and Engineering Management (IEEM)* (2022), pp. 1078–1082. DOI: 10.1109/IEEM55944.2022.9989964.
- [17] R. W. James. "Safe use of refrigerants for process applications". In: *Journal of Loss Prevention in The Process Industries* 7 (1994), pp. 492–500. DOI: 10.1016/0950-4230(94)80007-3.
- [18] Nigel J. Langford. "Carbon Dioxide Poisoning". In: *Toxicological Reviews* 24 (2005), pp. 229–235. URL: <https://api.semanticscholar.org/CorpusID:22508841>.
- [19] J. M. Calm. "Emissions and environmental impacts from air-conditioning and refrigeration systems". In: *International Journal of Refrigeration-revue Internationale Du Froid* 25 (2002), pp. 293–305. DOI: 10.1016/S0140-7007(01)00067-6.

- [20] N. Abas et al. "Natural and synthetic refrigerants, global warming: A review". In: *Renewable and Sustainable Energy Reviews* (2018). DOI: 10.1016/J.RSER.2018.03.099.
- [21] C. R. Prakash et al. "CFD simulation of HC-290 leakage from a split type room air conditioner". In: *Proceedings of the Institution of Mechanical Engineers, Part E: Journal of Process Mechanical Engineering* 235 (2021), pp. 1847–1857. URL: <https://api.semanticscholar.org/CorpusID:236400948>.
- [22] G. Ambrosi et al. "Upgrade of the mechanically pumped CO<sub>2</sub> two-phase cooling system for the alpha magnetic spectrometer on the international space station". In: *Applied Thermal Engineering* (2023). URL: <https://api.semanticscholar.org/CorpusID:258673329>.
- [23] N. Borshchev, A. E. Sorokin, and A. E. Belyavskii. "Mutual Influence of Capillary Pumps in Heat-Pipe Systems with Different Evaporator Loads". In: *Russian Engineering Research* 39 (2019), pp. 782–784. URL: <https://api.semanticscholar.org/CorpusID:204159352>.
- [24] ANSYS. *ANSYS Fluent 12.0 Theory Guide*. ANSYS.
- [25] K. Li et al. "Experimental Investigation of CO<sub>2</sub> Accidental Release from a Pressurised Pipeline". In: *Energy Procedia* 75 (2015), pp. 2221–2226. URL: <https://api.semanticscholar.org/CorpusID:114509923>.
- [26] Chenghuan Xiao et al. "Effects of Flow Velocity on Transient Behaviour of Liquid CO<sub>2</sub> Decompression during Pipeline Transportation". In: *Processes* 9.2 (2021). ISSN: 2227-9717. DOI: 10.3390/pr9020192. URL: <https://www.mdpi.com/2227-9717/9/2/192>.
- [27] Krishna Zore et al. "ANSYS CFD Simulations of Supersonic and Hypersonic Flows". In: Feb. 2020.
- [28] Christopher J. Wareing et al. "Numerical Simulation of CO<sub>2</sub> Dispersion From Punctures and Ruptures of Buried High-pressure Dense Phase CO<sub>2</sub> Pipelines with Experimental Validation". In: *Energy Procedia* 63 (2014). 12th International Conference on Greenhouse Gas Control Technologies, GHGT-12, pp. 2500–2509. ISSN: 1876-6102. DOI: <https://doi.org/10.1016/j.egypro.2014.11.273>. URL: <https://www.sciencedirect.com/science/article/pii/S1876610214020888>.
- [29] J. Franke et al. "Best practice guideline for the CFD simulation of flows in the urban environment". In: 2007. URL: <https://api.semanticscholar.org/CorpusID:18735721>.
- [30] Y. Tominaga et al. "AIJ guidelines for practical applications of CFD to pedestrian wind environment around buildings". In: *Journal of Wind Engineering and Industrial Aerodynamics* 96 (2008), pp. 1749–1761. URL: <https://api.semanticscholar.org/CorpusID:55896311>.
- [31] ANSYS. *ANSYS Fluent 12.0 User's Guide*. URL: <https://www.afs.enea.it/project/neptunius/docs/fluent/html/ug/node256.htm> (visited on 05/12/2024).



# Source Code User-Defined Functions

In this appendix, the source code on C language, utilized to craft the User-Defined Functions (UDFs) are shown. This UDFs capture the details of the outputs from the 2D simulations as well as the time dependencies of the boundary conditions of the simulation, if any.

**Listing A.1:** Fitting leak case source code.

```
1 #include "udf.h"
2
3 #define R_MAX 0.02 // Maximum radius of the inlet
4
5 #define X_CENTER -0.75502291 // Define based on model geometry
6
7 #define Z_CENTER 6.1840913 // Define based on model geometry
8
9 DEFINE_PROFILE(axial_velocity_profile, thread, position)
10 {
11     real x[ND_ND]; // ND_ND is the number of dimensions
12     real r, axial_velocity;
13     face_t f;
14
15     begin_f_loop(f, thread)
16     {
17         F_CENTROID(x, f, thread);
18         r = sqrt((x[0] - X_CENTER)*(x[0] - X_CENTER) + (x[2] - Z_CENTER)*(x[2] - Z_CENTER)); //
19             Compute radial distance
20         if (r <= R_MAX)
21         {
22             // Polynomial for axial_velocity
23             axial_velocity = (-2.153e+09 * r*r*r*r) + (1.080e+08 * r*r*r) + (-1.733e+06 * r*r) +
24                 (6.721e+02 * r) + (1.634e+02);
25             // Just for debugging: Message("Face %d, r = %f, axial_velocity = %f\n", f, r,
26                 axial_velocity);
27             F_PROFILE(f, thread, position) = axial_velocity;
28         }
29         else
30         {
31             F_PROFILE(f, thread, position) = 0.0; // Outside the defined radius
32             // Just for debugging: Message("Face %d, r = %f, axial_velocity set to 0.0\n", f, r);
33         }
34     }
35     end_f_loop(f, thread)
36 }
37
38 DEFINE_PROFILE(temperature_profile, thread, position)
39 {
40     real x[ND_ND];
41     real r, temperature;
42     face_t f;
43
44     begin_f_loop(f, thread)
45     {
46         F_CENTROID(x, f, thread);
47         r = sqrt((x[0] - X_CENTER)*(x[0] - X_CENTER) + (x[2] - Z_CENTER)*(x[2] - Z_CENTER)); //
48             Compute radial distance
49         if (r <= R_MAX)
```

```

46     {
47         // Polynomial for temperature
48         temperature = (4.619e+08 * r*r*r*r) + (-2.133e+07 * r*r*r) + (2.961e+05 * r*r) + (2.874e
49             +01 * r) + (3.716e+00);
50         F_PROFILE(f, thread, position) = temperature + 273.15; // Convert to Kelvin scale
51     }
52     else
53     {
54         F_PROFILE(f, thread, position) = 300.0; // Outside the defined radius
55     }
56 }
57 end_f_loop(f, thread)
58 }
59 DEFINE_PROFILE(mass_fraction_profile, thread, position)
60 {
61     real x[ND_ND];
62     real r, mass_fraction;
63     face_t f;
64
65     begin_f_loop(f, thread)
66     {
67         F_CENTROID(x, f, thread);
68         r = sqrt((x[0] - X_CENTER)*(x[0] - X_CENTER) + (x[2] - Z_CENTER)*(x[2] - Z_CENTER)); //
69             Compute radial distance
70         if (r <= R_MAX)
71         {
72             // Polynomial for mass fraction
73             mass_fraction = ( (-5.146e+06 * r*r*r*r) + (2.221e+05 * r*r*r) + (-3.309e+03 * r*r) +
74                 (4.977e+00 * r) + (3.047e-01) ) * 1.1; // 10% mass flow correction
75             F_PROFILE(f, thread, position) = mass_fraction;
76         }
77         else
78         {
79             F_PROFILE(f, thread, position) = 0.0; // Outside the defined radius
80         }
81     }
82 end_f_loop(f, thread)
83 }

```

Listing A.2: Cold overpressure case source code.

```

1 #include "udf.h"
2
3 #define R_MAX 0.1 // Maximum radius of the inlet
4
5 #define OPEN_TIME 141 // Inlet is open for OPEN_TIME seconds
6
7 #define X_CENTER 7.4913828 // Define based on model geometry --- Current is for inlet X5
8
9 #define Y_CENTER 7.9841784 // Define based on model geometry --- Current is for inlet X5
10
11 DEFINE_PROFILE(axial_velocity_profile, thread, position)
12 {
13     real x[ND_ND]; // ND_ND is the number of dimensions
14     real r, axial_velocity;
15     face_t f;
16
17     begin_f_loop(f, thread)
18     {
19         F_CENTROID(x, f, thread);
20         r = sqrt((x[0] - X_CENTER)*(x[0] - X_CENTER) + (x[1] - Y_CENTER)*(x[1] - Y_CENTER)); //
21             Compute radial distance
22         if (r <= R_MAX && CURRENT_TIME <= OPEN_TIME)
23         {
24             // Polynomial for axial_velocity
25             axial_velocity = (-1.548e+06 * r*r*r*r) + (5.175e+05 * r*r*r) + (-4.589e+04 * r*r) +
26                 (-2.583e+02 * r) + (1.198e+02);
27             // Just for debugging: Message("Face %d, r = %f, axial_velocity = %f\n", f, r,
28                 axial_velocity);
29             F_PROFILE(f, thread, position) = -1 * axial_velocity; // Change pointing direction due
30                 to geometry
31         }
32         else
33         {
34             F_PROFILE(f, thread, position) = 0.0; // Outside the defined radius
35             // Just for debugging: Message("Face %d, r = %f, axial_velocity set to 0.0\n", f, r);
36         }
37     }
38 }

```

```

32     }
33 }
34 end_f_loop(f, thread)
35 }
36
37 DEFINE_PROFILE(temperature_profile, thread, position)
38 {
39     real x[ND_ND];
40     real r, temperature;
41     face_t f;
42
43     begin_f_loop(f, thread)
44     {
45         F_CENTROID(x, f, thread);
46         r = sqrt((x[0] - X_CENTER)*(x[0] - X_CENTER) + (x[1] - Y_CENTER)*(x[1] - Y_CENTER)); //
            Compute radial distance
47         if (r <= R_MAX && CURRENT_TIME <= OPEN_TIME)
48         {
49             // Polynomial for temperature
50             temperature = (4.725e+05 * r*r*r*r) + (-1.183e+05 * r*r*r) + (8.612e+03 * r*r) + (5.598e
                +01 * r) + (6.601e+00);
51             F_PROFILE(f, thread, position) = temperature + 273.15; // Convert to Kelvin scale
52         }
53         else
54         {
55             F_PROFILE(f, thread, position) = 300.0; // Outside the defined radius
56         }
57     }
58     end_f_loop(f, thread)
59 }
60
61 DEFINE_PROFILE(mass_fraction_profile, thread, position)
62 {
63     real x[ND_ND];
64     real r, mass_fraction;
65     face_t f;
66
67     begin_f_loop(f, thread)
68     {
69         F_CENTROID(x, f, thread);
70         r = sqrt((x[0] - X_CENTER)*(x[0] - X_CENTER) + (x[1] - Y_CENTER)*(x[1] - Y_CENTER)); //
            Compute radial distance
71         if (r <= R_MAX && CURRENT_TIME <= OPEN_TIME)
72         {
73             // Polynomial for mass fraction
74             mass_fraction = (-1.820e+03 * r*r*r*r) + (5.643e+02 * r*r*r) + (-5.722e+01 * r*r) +
                (-3.777e-01 * r) + (2.196e-01);
75             F_PROFILE(f, thread, position) = mass_fraction;
76         }
77         else
78         {
79             F_PROFILE(f, thread, position) = 0.0; // Outside the defined radius
80         }
81     }
82     end_f_loop(f, thread)
83 }

```

**Listing A.3:** Warm overpressure case source code for the leakage inlet located at X0.

```

1 #include "udf.h"
2
3 #define R_MAX 0.1 // Maximum radius of the inlet
4
5 #define OPEN_TIME 49.3 // Inlet is open for OPEN_TIME seconds
6
7 #define X_CENTER 2.1500056 // Define based on model geometry --- Current is valid for inlet at X0
8
9 #define Y_CENTER -2.1288878 // Define based on model geometry --- Current is valid for inlet at X0
10
11 DEFINE_PROFILE(axial_velocity_profile, thread, position)
12 {
13     real x[ND_ND]; // ND_ND is the number of dimensions
14     real r, axial_velocity;
15     face_t f;
16
17     begin_f_loop(f, thread)
18     {

```

```

19 F_CENTROID(x, f, thread);
20 r = sqrt((x[0] - X_CENTER)*(x[0] - X_CENTER) + (x[1] - Y_CENTER)*(x[1] - Y_CENTER)); //
    Compute radial distance
21 if (r <= R_MAX && CURRENT_TIME <= OPEN_TIME)
22 {
23     // Polynomial for axial_velocity
24     axial_velocity = (-2.326e+06 * r*r*r*r) + (7.300e+05 * r*r*r) + (-6.043e+04 * r*r) +
        (-5.475e+02 * r) + (1.589e+02);
25     // Just for debugging: Message("Face %d, r = %f, axial_velocity = %f\n", f, r,
        axial_velocity);
26     F_PROFILE(f, thread, position) = axial_velocity;
27 }
28 else
29 {
30     F_PROFILE(f, thread, position) = 0.0; // Outside the defined radius
31     // Just for debugging: Message("Face %d, r = %f, axial_velocity set to 0.0\n", f, r);
32 }
33 }
34 end_f_loop(f, thread)
35 }
36
37 DEFINE_PROFILE(temperature_profile, thread, position)
38 {
39     real x[ND_ND];
40     real r, temperature;
41     face_t f;
42
43     begin_f_loop(f, thread)
44     {
45         F_CENTROID(x, f, thread);
46         r = sqrt((x[0] - X_CENTER)*(x[0] - X_CENTER) + (x[1] - Y_CENTER)*(x[1] - Y_CENTER)); //
            Compute radial distance
47         if (r <= R_MAX && CURRENT_TIME <= OPEN_TIME)
48         {
49             // Polynomial for temperature
50             temperature = (6.018e+05 * r*r*r*r) + (-1.352e+05 * r*r*r) + (8.184e+03 * r*r) + (1.167e
                +02 * r) + (8.760e+00);
51             F_PROFILE(f, thread, position) = temperature + 273.15; // Convert to Kelvin scale
52         }
53         else
54         {
55             F_PROFILE(f, thread, position) = 300.0; // Outside the defined radius
56         }
57     }
58     end_f_loop(f, thread)
59 }
60
61 DEFINE_PROFILE(mass_fraction_profile, thread, position)
62 {
63     real x[ND_ND];
64     real r, mass_fraction;
65     face_t f;
66
67     begin_f_loop(f, thread)
68     {
69         F_CENTROID(x, f, thread);
70         r = sqrt((x[0] - X_CENTER)*(x[0] - X_CENTER) + (x[1] - Y_CENTER)*(x[1] - Y_CENTER)); //
            Compute radial distance
71         if (r <= R_MAX && CURRENT_TIME <= OPEN_TIME)
72         {
73             // Polynomial for mass fraction
74             mass_fraction = ( (-2.093e+03 * r*r*r*r) + (7.142e+02 * r*r*r) + (-7.240e+01 * r*r) +
                (-7.710e-01 * r) + (2.873e-01) ) * 1.1; // 10% mass flow correction
75             F_PROFILE(f, thread, position) = mass_fraction;
76         }
77         else
78         {
79             F_PROFILE(f, thread, position) = 0.0; // Outside the defined radius
80         }
81     }
82     end_f_loop(f, thread)
83 }

```

Listing A.4: Warm overpressure case source code for the leakage inlet located at X0.5.

```

1 #include "udf.h"
2

```

```

3 #define R_MAX 0.1 // Maximum radius of the inlet
4
5 #define OPEN_TIME 49.3 // Inlet is open for OPEN_TIME seconds
6
7 #define X_CENTER -0.37165494 // Define based on model geometry --- Current is valid for inlet at X0
  .5
8
9 #define Y_CENTER -0.39723881 // Define based on model geometry --- Current is valid for inlet at X0
  .5
10
11 DEFINE_PROFILE(axial_velocity_profile, thread, position)
12 {
13     real x[ND_ND]; // ND_ND is the number of dimensions
14     real r, axial_velocity;
15     face_t f;
16
17     begin_f_loop(f, thread)
18     {
19         F_CENTROID(x, f, thread);
20         r = sqrt((x[0] - X_CENTER)*(x[0] - X_CENTER) + (x[1] - Y_CENTER)*(x[1] - Y_CENTER)); //
          Compute radial distance
21         if (r <= R_MAX && CURRENT_TIME <= OPEN_TIME)
22         {
23             // Polynomial for axial_velocity
24             axial_velocity = (-2.326e+06 * r*r*r*r) + (7.300e+05 * r*r*r) + (-6.043e+04 * r*r) +
              (-5.475e+02 * r) + (1.589e+02);
25             // Just for debugging: Message("Face %d, r = %f, axial_velocity = %f\n", f, r,
              axial_velocity);
26             F_PROFILE(f, thread, position) = axial_velocity;
27         }
28         else
29         {
30             F_PROFILE(f, thread, position) = 0.0; // Outside the defined radius
31             // Just for debugging: Message("Face %d, r = %f, axial_velocity set to 0.0\n", f, r);
32         }
33     }
34     end_f_loop(f, thread)
35 }
36
37 DEFINE_PROFILE(temperature_profile, thread, position)
38 {
39     real x[ND_ND];
40     real r, temperature;
41     face_t f;
42
43     begin_f_loop(f, thread)
44     {
45         F_CENTROID(x, f, thread);
46         r = sqrt((x[0] - X_CENTER)*(x[0] - X_CENTER) + (x[1] - Y_CENTER)*(x[1] - Y_CENTER)); //
          Compute radial distance
47         if (r <= R_MAX && CURRENT_TIME <= OPEN_TIME)
48         {
49             // Polynomial for temperature
50             temperature = (6.018e+05 * r*r*r*r) + (-1.352e+05 * r*r*r) + (8.184e+03 * r*r) + (1.167e
              +02 * r) + (8.760e+00);
51             F_PROFILE(f, thread, position) = temperature + 273.15; // Convert to Kelvin scale
52         }
53         else
54         {
55             F_PROFILE(f, thread, position) = 300.0; // Outside the defined radius
56         }
57     }
58     end_f_loop(f, thread)
59 }
60
61 DEFINE_PROFILE(mass_fraction_profile, thread, position)
62 {
63     real x[ND_ND];
64     real r, mass_fraction;
65     face_t f;
66
67     begin_f_loop(f, thread)
68     {
69         F_CENTROID(x, f, thread);
70         r = sqrt((x[0] - X_CENTER)*(x[0] - X_CENTER) + (x[1] - Y_CENTER)*(x[1] - Y_CENTER)); //
          Compute radial distance

```

```

71     if (r <= R_MAX && CURRENT_TIME <= OPEN_TIME)
72     {
73         // Polynomial for mass fraction
74         mass_fraction = ( (-2.093e+03 * r*r*r*r) + (7.142e+02 * r*r*r) + (-7.240e+01 * r*r) +
75             (-7.710e-01 * r) + (2.873e-01) ) * 1.1; // 10% mass flow correction
76         F_PROFILE(f, thread, position) = mass_fraction;
77     }
78     else
79     {
80         F_PROFILE(f, thread, position) = 0.0; // Outside the defined radius
81     }
82 }
83 }

```

Listing A.5: Maintenance case source code.

```

1 #include "udf.h"
2
3 #define R_MAX 0.1 // Maximum radius of the inlet
4
5 #define OPEN_TIME 3.38 // Inlet is open for OPEN_TIME seconds
6
7 #define X_CENTER 2.1500056 // Define based on model geometry --- Current is valid for inlet at X0
8
9 #define Y_CENTER -2.1288878 // Define based on model geometry --- Current is valid for inlet at X0
10
11 DEFINE_PROFILE(axial_velocity_profile, thread, position)
12 {
13     real x[ND_ND]; // ND_ND is the number of dimensions
14     real r, axial_velocity;
15     face_t f;
16
17     begin_f_loop(f, thread)
18     {
19         F_CENTROID(x, f, thread);
20         r = sqrt((x[0] - X_CENTER)*(x[0] - X_CENTER) + (x[1] - Y_CENTER)*(x[1] - Y_CENTER)); //
21             Compute radial distance
22         if (r <= R_MAX && CURRENT_TIME <= OPEN_TIME)
23         {
24             // Polynomial for axial_velocity
25             axial_velocity = (-2.745e+06 * r*r*r*r) + (7.655e+05 * r*r*r) + (-6.151e+04 * r*r) +
26                 (-3.494e+02 * r) + (1.580e+02);
27             // Just for debugging: Message("Face %d, r = %f, axial_velocity = %f\n", f, r,
28                 axial_velocity);
29             F_PROFILE(f, thread, position) = axial_velocity;
30         }
31         else
32         {
33             F_PROFILE(f, thread, position) = 0.0; // Outside the defined radius
34             // Just for debugging: Message("Face %d, r = %f, axial_velocity set to 0.0\n", f, r);
35         }
36     }
37     end_f_loop(f, thread)
38 }
39
40 DEFINE_PROFILE(temperature_profile, thread, position)
41 {
42     real x[ND_ND];
43     real r, temperature;
44     face_t f;
45
46     begin_f_loop(f, thread)
47     {
48         F_CENTROID(x, f, thread);
49         r = sqrt((x[0] - X_CENTER)*(x[0] - X_CENTER) + (x[1] - Y_CENTER)*(x[1] - Y_CENTER)); //
50             Compute radial distance
51         if (r <= R_MAX && CURRENT_TIME <= OPEN_TIME)
52         {
53             // Polynomial for temperature
54             temperature = (1.182e+06 * r*r*r*r) + (-2.805e+05 * r*r*r) + (1.944e+04 * r*r) + (1.459e
55                 +02 * r) + (-1.994e+01);
56             F_PROFILE(f, thread, position) = temperature + 273.15; // Convert to Kelvin scale
57         }
58         else
59         {
60             F_PROFILE(f, thread, position) = 300.0; // Outside the defined radius

```

```
56     }
57   }
58   end_f_loop(f, thread)
59 }
60
61 DEFINE_PROFILE(mass_fraction_profile, thread, position)
62 {
63   real x[ND_ND];
64   real r, mass_fraction;
65   face_t f;
66
67   begin_f_loop(f, thread)
68   {
69     F_CENTROID(x, f, thread);
70     r = sqrt((x[0] - X_CENTER)*(x[0] - X_CENTER) + (x[1] - Y_CENTER)*(x[1] - Y_CENTER)); //
        Compute radial distance
71     if (r <= R_MAX && CURRENT_TIME <= OPEN_TIME)
72     {
73       // Polynomial for mass fraction
74       mass_fraction = ( (-7.291e+03 * r*r*r*r) + (1.782e+03 * r*r*r) + (-1.450e+02 * r*r) +
        (-2.031e-01 * r) + (4.278e-01) ) * 1.1; // 10% mass flow correction
75       F_PROFILE(f, thread, position) = mass_fraction;
76     }
77     else
78     {
79       F_PROFILE(f, thread, position) = 0.0; // Outside the defined radius
80     }
81   }
82   end_f_loop(f, thread)
83 }
```